IOWA STATE UNIVERSITY
Digital Repository

1978

Applications of solid state nuclear magnetic resonance techniques to the study of coals and polymers

Robert George Pembleton
Iowa State University

Recommended Citation

INFORMATION TO USERS

7900203

PEMBLETON, ROBERT GEORGE
APPLICATIONS OF SOLID STATE NUCLEAR MAGNETIC
RESONANCE TECHNIQUES TO THE STUDY OF COALS
AND POLYMERS.

IOWA STATE UNIVERSITY, PH.D., 1978

Applications of solid state nuclear magnetic resonance

techniques to the study of coals and polymers

by

Robert George Pembleton

A Dissertation Submitted to the

Graduate Faculty in Partial Fulfillment of

The Requirements for the Degree of

DOCTOR OF PHILOSOPHY

Department: Chemistry
Major: Physical Chemistry

Approved:

In Charge of Major Work

For the Major Department

For the Graduate College

Iowa State University
Ames, Iowa

1978

TABLE OF CONTENTS

LIST OF FIGURES

LIST OF TABLES

INTRODUCTION

Since the discovery of nuclear magnetic resonance (NMR)
by Purcell et al. (1) and Bloch et al. (2) in 1945, and the
subsequent realization by Proctor and Yu (3) and others (4-7)
that nuclear resonance in liquids was a source of chemical
fingerprinting of nuclei in molecules, NMR has enjoyed
great success as a chemical analytical tool. Resonant
frequencies (e.g., chemical shifts) and relaxation
characteristics have been used to study both structure and
dynamics of liquids and molecules in solution (5). Solid
state NMR has not, however, been a tool widely used by
chemists. The primary reason for this lack is the fact
that NMR is a relatively insensitive technique compared to,
e.g., IR or ESR, so most common applications of NMR
are to nuclei with high gyromagnetic ratios and high
natural abundance such as ^{1}H, ^{19}F and ^{31}P. With few
exceptions, the solid state NMR spectra of these nuclei
are characterized by broad featureless lines, void of much
chemically interesting information, and from which the
chemical shift, so dear to the hearts of chemists is
generally not extractable. There are two major sources of
this broadening. The first is that linewidths due to
dipolar interactions between like nuclei of high natural
abundance may be 30 KHz (500 ppm), whereas the differences
in chemically shifted resonances can be as small as one

ppm. The second is that a given nucleus such as ^{1}H in

H_2O (s) can have a chemical shift anisotropy as large as

34 ppm which spans the entire range of chemical shifts.

Compare this to a typical linewidth of less than 0.1 ppm

in a liquid NMR spectra.

Therefore, even if dipolar interactions in the solid

state were absent, the NMR spectrum of a randomly oriented

solid containing many chemically different nuclei would

yield severely overlapping lineshapes which would in general

be impossible to deconvolute.

The principal point of attack of the work reported in

this dissertation is achievement of high resolution NMR in

randomly oriented solids with strong homonuclear and

heteronuclear dipolar coupling, and a wide variety of

chemical shift anisotropies. In addition, applications of

recent advances in pulse and multiple pulse NMR are made to

systems important to an understanding of the chemistry and

physics of the solid state. Specific applications are made

to crystallinity in polymers, and to aromatic and aliphatic

content of vitrain portions of coals of varying carbon

content.

LITERATURE REVIEW

Due to the scope of the material covered in this dissertation, the literature review will be informally divided into two subsections. The first section will discuss recent advances in pulse and multiple pulse NMR in solids. The second will predominantly review work done in applying solid state NMR to the study of polymers and to coals.

One of the first reported NMR spectra was of the protons in solid paraffin (1). Despite this fact, the NMR of solids has not until recently been used by the chemist to the extent that high resolution NMR is used as an analytical tool to study the structure of molecules in solution. The reason for this lack of use is that the broad featureless lines, encountered in solid state NMR generally contain little information directly relatable to fine details of the chemical structure of the material being studied (5,7,8). The source of this broadening, in the case of a nucleus with high natural abundance, is predominantly the dipolar interaction between like nuclear spin pairs. In the absence of molecular motion the dipolar interaction, e.g., between protons in a hydrocarbon, may be tens of kilohertz. In instances when a dilute spin, e.g., ^{13}C, is being probed by NMR the dominant broadening mechanism is the heteronuclear dipolar interaction between

the dilute spin and abundant neighbor, e.g., ^{1}H. In recent years several techniques have been developed which successfully eliminate heteronuclear and homonuclear dipolar interactions. High resolution NMR in solids has therefore become a real possibility. Determinations not only of chemical shifts, but also their anisotropies then become a reality.

The first attempt to overcome the obstacle of homonuclear dipolar broadening in solids was made independently by E. R. Andrew et al. (9-15) and I. Lowe (16) by using "magic angle" sample spinning. This technique modulates the spatial part of the dipolar interaction given by $(1 - 3\cos^2\theta_{ij})r_{ij}^{-3}$, where θ_{ij} is the angle between the internuclear spin vector, $\vec{r}_{ij}$, and the external magnetic field (5). To circumvent the dipolar interaction it is necessary to spin the sample at a speed larger than the natural linewidth about an axis tilted by the "magic angle" (arc $\cos^{-1}(1/\sqrt{3})$) with respect to the static d.c. field, $\vec{H}_o$. Under these conditions the time average of the spatial part of the dipolar interaction is zero. In practice one need not spin at speeds exceeding the dipolar linewidth as illustrated by the proton spectrum of polystyrene obtained by Schnabel and Taplick (17) but even spinning rates of 10 KHz has obvious mechanical disadvantages.

Alternatively, one may attack the spin part of the dipolar Hamiltonian in an attempt to circumvent the natural line broadening in solids (18). These techniques require manipulating the time development of the nuclear spin system (which is the inverse Fourier transform of a "normal" NMR spectrum (19)) in such a manner that the system time develops under an "average" Hamiltonian (20). This is analogous to a situation in liquid NMR where a nucleus jumps between two sites of different electronic environment at a sufficiently rapid rate that the resulting chemical shift is an average of the chemical shift experienced by the nucleus at the two sites (6). J. S. Waugh et al. (20, 21) in 1968 were the first to realize that by applying a cycle of intense radiofrequency (rf) pulses it was possible to average the dipolar Hamiltonian to zero over the cycle time of the pulse sequence (22). The rf pulse cycle used by Waugh consisted of four 90° pulses of various phases and has come to be known as the WAHUHA cycle. The WAHUHA multiple pulse cycle suffers in resolution due to rf in- homogeneity effects. Following the lead of Waugh, W.-K. Rhim et al. (23-25) and P. Mansfield (26) independently proposed a more complex eight pulse cycle (MREV-8) (27). The MREV-8 multiple pulse sequence reduced the cross terms between the dipolar interaction and the rf inhomogeneity, reducing the ^{19}F linewidth in CaF_2 from

120 Hz obtained using the WAHUHA multiple pulse cycle to 17 Hz using the MREV-8.

Nature has provided still another means of suppressing dipolar broadening in the form of naturally dilute spin systems ^{13}C, ^{15}N. (This is not to say that man has not tried to imitate nature by isotopically doping samples to form dilute systems (28,29)). In an environment of an abundant spin system like ^{1}H or ^{19}F, NMR of ^{13}C is now accepted as a powerful tool for the study of liquids (30). The absence of magnetic coupling between ^{13}C nuclei and wide range of chemical shifts are particular advantages of observing ^{13}C nuclei rather than nuclei such as ^{1}H. In contrast, the usefulness of ^{13}C NMR in solids has not been outstanding. There are two reasons for this, poor sensitivity due to low natural abundance, and poor resolution due to dipolar broadening between the dilute ^{13}C spins and neighboring abundant spins. In order to obtain high resolution ^{13}C NMR spectra with maximum signal-to-noise ratio the techniques of double resonance and decoupling are combined. The double resonance technique established by Hartman and Hahn (31) alleviates the problem of sensitivity. By this technique, dilute spins are first polarized by the abundant spin system (32,33). The dilute spins are subsequently observed while the abundant spins are decoupled in order to suppress the heteronuclear

dipolar broadening (34-36). This technique was initially utilized by Pines et al. (37-39) and is referred to as Proton Enhanced Nuclear Induction Spectroscopy, PENIS.

In many solids, residual linewidths under the application of one of these multiple pulse sequences are dominated by chemical shift anisotropies which contain a wealth of information pertaining to molecular structure, molecular motion and local geometry (40,41). These anisotropies can be large compared to the entire range of chemical shifts observed for a nucleus in a liquid, e.g., 20 ppm for protons (40) and 200 ppm for ^{19}F and ^{13}C (41). When different chemical species of a nucleus are present in a polycrystalline material, however, it may be impossible to separately resolve their individual chemical shifts. To obtain chemical shift information on such materials in randomly oriented solids, it is necessary to remove both the dipolar broadening and the chemical shift anisotropies. Such an experiment has been shown feasible by Schaefer et al. (42-44) by a combination of dipolar decoupling and magic angle spinning in cases where the $^{13}C-^{1}H$ heteronuclear dipolar interaction is the dominant broadening mechanism. To date, aside from the work to be reported in this dissertation, no such combined experiment has been attempted on systems experiencing homonuclear dipolar broadening. The prospects of a Combined Rotation

and Multiple Pulse Spectroscopy, CRAMPS, has been considered
briefly in the past (18). It is the application of
these techniques to a variety of problems that constitutes
a portion of this dissertation.

The recent interest in supplemental fuels from coal
has provided new impetus to study the chemical structure of
coal. Of prime importance is the knowledge of the hydrogen
and carbon content and distribution among aromatic and non-
aromatic regions in the coal. High resolution NMR would be
a particularly powerful technique for such a study provided
the coal were soluble. Rather brutal treatment (heating in
pyridine at 400°C) can lead to extracts representing 20 to
30% of the parent material. These fractions are readily
examined by high resolution NMR and along with broadline
NMR of solids, have formed the basis for much of the work
being done to elucidate chemical structures in coal.
Retcofsky and Friedel (45-47), Brown et al. (48), and others
(49-52) have been responsible for much of the work in this
field. In many of the early proton NMR studies, the
proton data were treated using an aromacity equation
developed by Brown and Ladner (49). One of the major
concerns in using this equation is the choice of values
for H_{ali}/C_{ali} where H_{ali} is the number of aliphatic protons
and C_{ali} is the number of aliphatic carbons. Over the past
several years the full potential of ^{13}C NMR in coal

research has been realized (45, 53-60). With the ability
to obtain high resolution ^{13}C NMR spectra this ratio could
easily be determined, making the calculation of aromatici-
ties from complementary ^{13}C and ^{1}H NMR a reality. The most
recent of these papers deal primarily with the ability of
high resolution solid state ^{13}C NMR to determine
aromaticities in coals (57-60). This subject will be
treated in greater detail in a later section of this
dissertation.

The use of NMR to study polymers has been explored in
detail in the past (61-63). Of a more specific nature to
the present work are the NMR studies devoted to polymer
crystallinity (64-69). The problem is that the measured
variable in these methods, e.g., the NMR linewidth,
contains contributions from both phases of the polymer,
making an unambiguous separation of the contribution of
the crystalline and noncrystalline regions difficult to
obtain. The method discussed in this dissertation provides
for a unique separation of these two regions.

THEORY

Basic Theory

A magnetic moment placed in a magnetic field has an interaction described by the Zeeman spin Hamiltonian (5)

$$H = -\bar{\mu}\cdot\bar{H} = -\gamma\bar{I}\cdot\bar{H} = -\gamma I_z H_o \tag{1}$$

where μ is the magnetic moment, I is the angular momentum, $\hbar$ equal unity, and H_o is the static magnetic field which we choose to be along the Z-axis. The eigenvalues of this system are:

$$E = -\gamma H_o m_I \tag{2}$$

since m_I ranges from $-I$ to $+I$ the energy separation between levels is

$$\Delta E = \gamma H_o = \omega_o \tag{3}$$

the Larmour precession frequency.

At equilibrium, the nuclei are distributed among the energy levels according to a Boltzman distribution resulting in a net magnetization along the Z axis, $M_z = M_o$. Following any perturbation which disturbs this equilibrium, for example, an rf pulse which leaves $M_y = M_o$ and $M_x = M_z = 0$, the system returns to equilibrium via at least two exponential relaxation rates. The characteristic times

T_1 and T_2 were initially used by Bloch to describe the decay of the magnetization (70,71). The longitudinal relaxation time T_1, describes the repolarization of the magnetization along the Z axis as it comes to equilibrium with its surroundings ("lattice"). To a solid state NMR spectroscopist T_1 governs how fast an experiment may be repeated. The transverse spin relaxation time T_2, describes the dephasing of the magnetization in the X,Y plane. In liquids one usually finds that $T_1 = T_2$ while in solids $T_2 << T_1$. The linewidth of a Lorentzian NMR spectrum is given by

$$2\delta f = \frac{1}{\pi T_2} \tag{4}$$

where $2\delta f$ is the full width at half intensity. Most rigid solids, however, exhibit free induction decays which decay exponentially as t^2 (5,72,73). The solid state NMR spectrum of such a decay is gaussian with full width at half height

$$2\delta f = \frac{(2 \ln 2)^{\frac{1}{2}}}{\pi T_2} \tag{5}$$

Multiple Pulse Theory

Recent experimental and theoretical advances have greatly expanded the utility of NMR as an experimental technique for the study of physical and chemical phenomena in solids. Developments in both heteronuclear and homonuclear coupling and decoupling schemes through 1975 have

been reviewed in a recent monograph (41), while a second
deals exclusively with homonuclear systems (40). In
addition, other aspects of solid state NMR have been
reviewed; particularly sample spinning (74). It is the
purpose here to briefly review the theory necessary to the
understanding of high resolution NMR in solids.

In general, the NMR spectrum of a nucleus is determined
by a series of interaction Hamiltonians. Those which
concern us are given by

$$H(t) = H_z + H_D^{II} + H_D^{IS} + H_\sigma + H_{rf}(t) \tag{6}$$

with

$$H_z = -\sum_i \gamma_i I_{zi} H_o \equiv -\sum \omega_o^i I_{zi}$$

(the Zeeman interaction between the static magnetic field
H_o which is along the Z axis and the nuclear spin system)

$$H_{rf} = -\omega_1 I_x \cos wt + \omega_1 I_y \sin wt$$

(the interaction between the spin system and the rf pulse)

$$H_D^{II} = \sum_{i<j} (1 - 3\cos^2 \theta_{ij}) \frac{r_{ij}^{-3}}{2} (\bar{I}_i \bar{I}_j - 3I_{zi} I_{zj})$$

(the secular portion of the homonuclear dipolar interaction)

$$H_D^{IS} = \sum_{i<j} (1 - 3\cos^2 \theta_{ij}) \frac{r_{ij}^{-3}}{2} (I_{zi} S_{zj})$$

(the secular portion of the heteronuclear interaction)

$$H_\sigma = \sum_i (\partial\omega + \omega_o \sigma_{zzi}) I_{zi}$$

(the chemical shift and resonance offset)

θ_{ij} is the angle formed between the magnetic field $\bar{H}_o$ and the internuclear vector $\bar{r}_{ij}$.

Each of these Hamiltonians contains information about the chemical system under study. Past problems have involved cases where one interaction was so large that it completely masked the potentially valuable information obtainable from one of the smaller terms (5,7). The most important example to us is that of the orientational information available from the components of the chemical shift tensor being obscured by the dipolar interaction.

Some of these difficulties have been resolved with the realization that one need not accept the set of interaction Hamiltonians in Eqn. (6) as unalterable but can devise perturbations which will suppress the effects of a particular Hamiltonian to allow the characterization of another inter-action. It was the realization that the time development of a many body interaction, e.g., the dipolar interaction, could be refocused (21) which has led to high resolution NMR in solids.

To understand the theory behind the Homonuclear Decoupling Experiment we examine the time evolution of a nuclear spin system as determined by the behavior of the density matrix ρ. The equation of motion which governs the evolution of the density matrix is given by the Liouville-Von Neuman equation (75). With $\hbar = 1$, this equation is

$$i \frac{d\rho}{dt} = [H, \rho] \tag{7}$$

In discussing the homonuclear decoupling experiment the spin Hamiltonian is given by Eqn. (6). The heteronuclear dipolar Hamiltonian, H_D^{IS}, is taken to be absent in this case. A formal solution to Eqn. (7) is

$$\rho(t) = e^{-iHt} \rho(o) e^{+iHt} \tag{8}$$

It is convenient to discuss the results of a multiple pulse NMR experiment in a frame of reference rotating about the Z axis at the Larmour precession frequency of the nuclei. The equation of motion of the density operator in this frame is

$$i \frac{d\tilde{\rho}}{dt} = [\tilde{H}, \tilde{\rho}] \tag{9}$$

where

$$\tilde{\rho}(t) = e^{iH_o t} \rho(t) e^{-iH_o t} \tag{10}$$

and

$$\tilde{H} = \tilde{H}_\sigma + \tilde{H}_D + \tilde{H}_{rf} = H_D + H_\sigma - \omega_1 I_x \tag{11}$$

To describe the effect of an NMR pulse sequence on the time development of a spin system we transform to an interaction representation described by the unitary operator, $U(t)$:

$$U(t) = U_{rf}(t) \, U_{int}(t) \tag{12}$$

where $U_i(t)$ is determined by the solution of

$$i \frac{dU_i(t)}{dt} = H_i U_i(t) \tag{13}$$

The solution to Eqn. (13) is the Dyson expression (76).

$$U_{rf}(t) = T \exp\{-i \int_o^t H_{rf}(t')dt'\} \qquad (14)$$

$$U_{int}(t) = T \exp\{-i \int_o^t \tilde{H}_{int}(t')dt'\} \qquad (15)$$

where

$$\tilde{H}_{int} = U_{rf}^+(t) \, H_{int} \, U_{rf}(t) \qquad (16)$$

and T is the Dyson time ordering operator. To simplify the formalism, the rf perturbation, H_{rf}, is arranged to satisfy two conditions (25):

1. the periodic condition

$$H_{rf}(t + nt_c) = H_{rf}(t) \qquad (17)$$

2. the cyclic condition

$$H_{rf} = \int_o^{t_c} H_{rf}(t)dt = 0 \qquad (18)$$

As a result, U_{int} becomes periodic through Eqn. (16) and the calculation of $U_{int}(t)$ for a single cycle is sufficient to predict the time development of the system at multiples of the cycle time, t_c. In this interaction representation the time development of the density operator is

$$\rho(t_c) = U_{int}(t_c)\rho(o)U_{int}^+(t_c) \qquad (19)$$

$U_{int}(t_c)$ can be expanded using the Magnus formula (77).

$$U_{int}(t_c) = \exp[-it_c(\bar{H}_{int}^{(o)} + \bar{H}_{int}^{(1)} + \bar{H}_{int}^{(2)} + \cdots)] \qquad (20)$$

where

$$\bar{H}_{int}^{(o)} = \frac{1}{t_c} \int_0^{t_c} \tilde{H}_{int}(t')dt' \tag{21}$$

$$H_{int}^{(1)} = \frac{-i}{2t_c} \int_0^{t_c} dt' \int_0^{t'} dt''[\tilde{H}_{int}(t'),\tilde{H}_{int}(t'')] \tag{22}$$

$$\bar{H}_{int}^{(2)} = \frac{1}{6t_c} \int_0^{t_c} dt' \int_0^{t'} dt'' \int_0^{t''} dt'''\{[[\tilde{H}_{int}(t'),$$

$$\tilde{H}_{int}(t'')],\tilde{H}_{int}(t''')] + [[\tilde{H}_{int}(t'''),$$

$$\tilde{H}_{int}(t'')],\tilde{H}_{nt}(t')]\} \tag{23}$$

The strong convergence condition in Eqn. (20) is

$$t_c||\tilde{H}_{int}(t)|| << 1 \tag{24}$$

where $||\tilde{H}_{int}(t)||$ is the magnitude of the internal inter-
action which is attacked by the particular rf cycle in
question.

The important interpretation to be derived from Eqns.
(19-23) is that the multiple pulsed NMR experiment measures
the time evolution of the system at integral multiples of
the cycle time, e.g., $t = nt_c$, as caused by an average
Hamiltonian prescribed by $U_{int}(t_c)$. This understanding has
led to a family of multiple pulse schemes designed to
effectively remove certain interactions while leaving others
unchanged. For purposes of the present discussion, the most
important of these are those designed to remove homonuclear

dipolar broadening while preserving the chemical shift anisotropy (78-80). The MREV-8 multiple pulse sequence (23,26) for the removal of homonuclear dipolar broadening is shown in Figure 1. The sequence consists of a series of eight rf pulses of various phases as indicated. The sequence is repeated with cycle time, t_c, and meets both the cyclic and periodic conditions. It can be shown that the homonuclear dipolar interaction over the cycle is zero to first order. The chemical shift interaction is scaled by a factor of approximately $\sqrt{2}/3$ and has the form

$$\bar{H}_\sigma^{(o)} = \frac{1}{3} \sum_i (\delta\omega + \omega_o \sigma_{zzi})(1 + 2\{\frac{3tw}{t_c} (\frac{4}{\pi} - 1)\})$$
$$(I_{xi} + I_{zi}) \tag{25}$$

where

$$\sigma_{zzi} = \sigma_{11} \cos^2 \alpha \sin^2 \beta$$
$$+ \sigma_{22} \sin^2 \alpha \sin^2 \beta + \sigma_{33} \cos^2 \beta \tag{26}$$

and tw is the pulse width.

In randomly oriented solids chemical shift anisotropies may span the entire range of chemical shifts for a given nucleus. In samples containing many chemically shifted nuclei of a given species, multiple pulse techniques alone are, generally, insufficient to allow the determination of the components of all of the chemical shift tensors. In these cases one might wish to remove both the homonuclear dipolar broadening and chemical shift anisotropies in order

PREPARING PULSE
SAMPLING WINDOW

t_C

τ_ω

2τ τ 2τ τ 2τ τ 2τ τ 2τ

P_x P_x P_y P_{-y} P_{-x} P_{-x} P_y P_{-y} P_x P_x
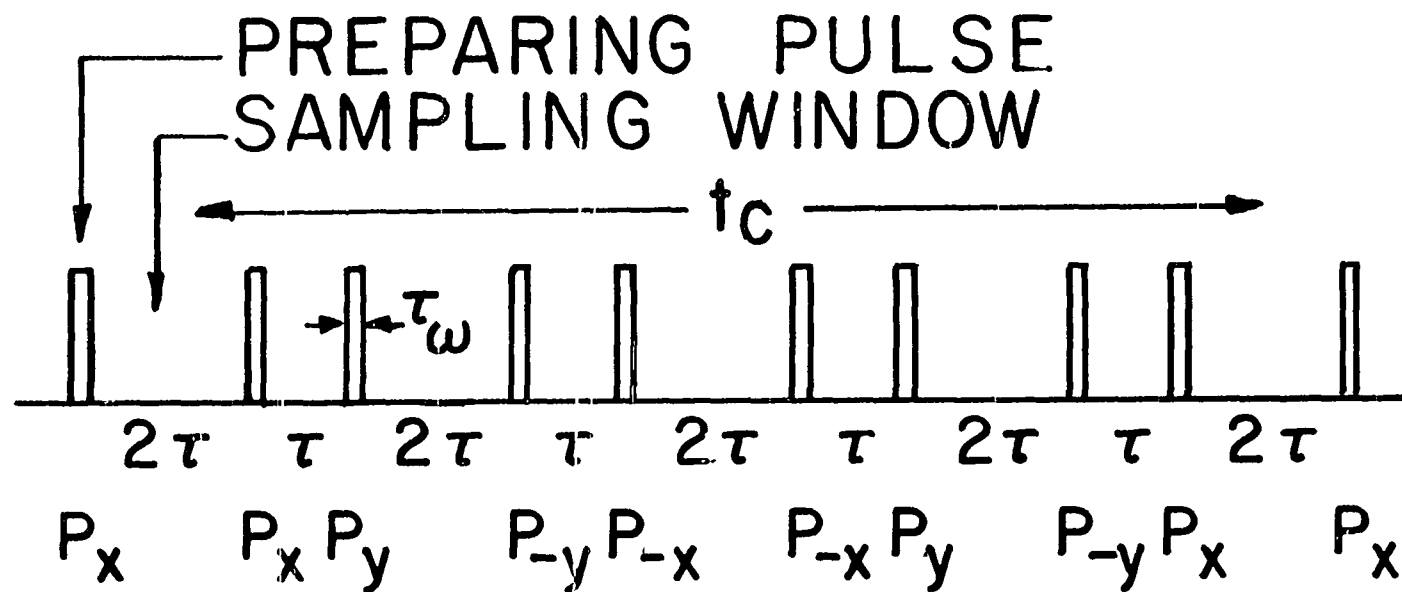
Figure 1. The REV-8 multiple pulse sequence used for removal of homonuclear
dipolar broadening. The cycle time of the sequence is t_c and the
pulse width is t_ω.

to obtain chemical shift information concerning the nuclei under study. Combining multiple pulse techniques and magic angle spinning techniques has been suggested as a means of obtaining chemical shift information in systems containing a number of nuclei with different chemical shifts (18). The theory of CRAMPS will be discussed as it pertains to the MREV-8 multiple pulse sequence.

CRAMPS Theory

Under magic angle spinning, the θ_{ij} term of the dipolar interaction becomes time dependent resulting in a Hamiltonian with the form (18)

$$H_D = \sum_{i<j} \frac{\gamma^2}{2r_{ij}^3} b_{ij}(t)(\bar{I}_i\bar{I}_j - 3I_{zi}I_{zj}) \tag{27}$$

where

$$b_{ij}(t) = A \cos \omega_r t - B \sin \omega_r t$$
$$+ (\cos 2\omega_r t - 1)\sin 2\omega_r t \tag{28}$$

The $b_{ij}(t)$ represents the time dependent form of $(3\cos^2\theta_{ij}-1)$ and is derived in the Appendix. One must now calculate the one cycle propogator for an MREV-8 sequence for which $t_c \ll t_r$. All of the initial conditions ($\sin \alpha$, $\cos \beta$ $\cdots$) are included in the A's, B's, C's and D's. These will change from cycle to cycle, because the starting point of one cycle will not have the same initial conditions as another, e.g.,

the individual cycles start at different times in the rotation cycle.

The effect of an eight pulse sequence on the spin part of the homonuclear dipolar Hamiltonian is shown in Figure 2 where for example $Z = (\bar{I}_i \bar{I}_j - 3I_{zi}I_{zj})$. To calculate the zero order average Hamiltonian Eqn. (21) is rewritten as

$$\bar{H}_D^{(o)} = \frac{1}{12\tau} \int_0^{12\tau} \tilde{H}_0(t)d(t) = \frac{\gamma^2 r^{-3}}{12\tau}[x\{\int_{2\tau}^{4\tau} b_{ij}(t)dt + \int_{8\tau}^{10\tau} b_{ij}(t)dt\}$$

$$+ Y\{\int_\tau^{2\tau} b_{ij}(t)dt + \int_{4\tau}^{5\tau} b_{ij}(t)dt + \int_{7\tau}^{8\tau} b_{ij}(t)dt$$

$$+ \int_{10\tau}^{11\tau} b_{ij}(t)dt\}$$

$$+ Z\{\int_0^\tau b_{ij}(t)dt + \int_{5\tau}^{7\tau} b_{ij}(t)dt + \int_{11\tau}^{12\tau} b_{ij}(t)dt\}] \qquad (29)$$

For simplicity of notation, only a two spin interaction is considered; here $\bar{r} = \bar{r}_{1,2}$. These integrals have the form for $\omega_r = \frac{1}{t_r}$

$$\int_{a\tau}^{b\tau} \sin \omega_r t \, dt = -t_r\{\cos \frac{b\tau}{t_r} - \cos \frac{a\tau}{t_r}\}$$

$$\int_{a\tau}^{b\tau} \cos \omega_r t = t_r\{\sin \frac{b\tau}{t_r} - \sin \frac{a\tau}{t_r}\} \qquad (30)$$
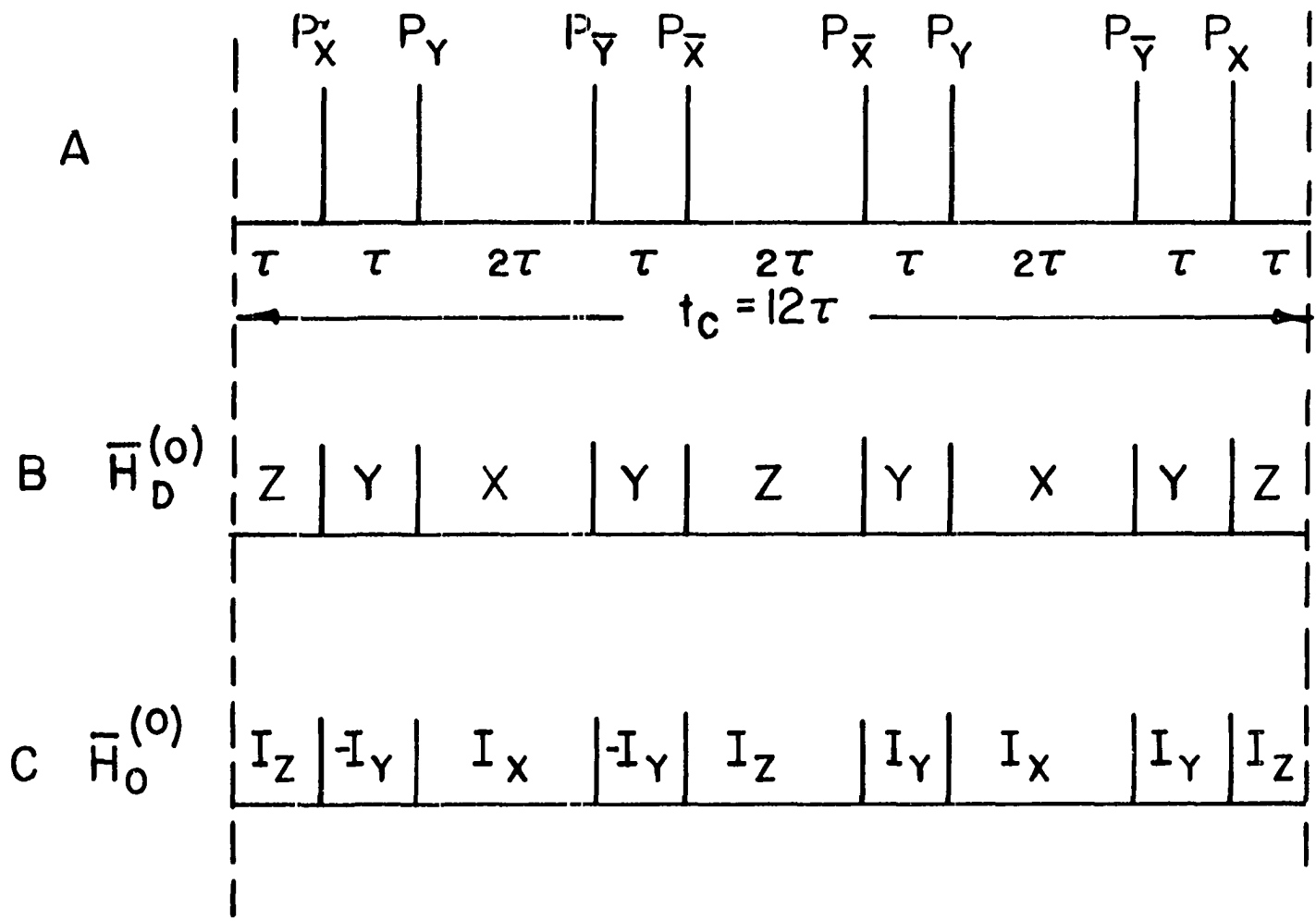
Figure 2. The values of the average dipolar and chemical shift interaction during the MREV-8 multiple pulse sequence are given on lines B and C, respectively.

Substitution of Eqn. (30) into Eqn. (29) yields

$$\bar{H}_D^{(o)} = \gamma^2 r^{-3} \frac{t_r}{12\tau} \ [X\{B(\cos \frac{4\tau}{t_r} - \cos \frac{2\tau}{t_r} + \cos \frac{10\tau}{t_r} - \cos \frac{8\tau}{t_r})$$

$$+ A(\sin \frac{4\tau}{t_r} - \sin \frac{2\tau}{t_r} + \sin \frac{10\tau}{t_r} - \sin \frac{8\tau}{t_r}$$

$$+ D(\cos \frac{8\tau}{t_r} - \cos \frac{4\tau}{t_r} + \cos \frac{20\tau}{t_r} - \cos \frac{16\tau}{t_r})$$

$$+ C(\sin \frac{8\tau}{t_r} - \sin \frac{4\tau}{t_r} + \sin \frac{20\tau}{t_r} - \sin \frac{16\tau}{t_r})\}$$

$$+ Y\{B(\cos \frac{2\tau}{t_r} - \cos \frac{\tau}{t_r} + \cos \frac{5\tau}{t_r} - \cos \frac{4\tau}{t_r})$$

$$+ \cos \frac{8\tau}{t_r} - \cos \frac{7\tau}{t_r} + \cos \frac{11\tau}{t_r} - \cos \frac{10\tau}{t_r})$$

$$+ A(\sin \frac{2\tau}{t_r} - \sin \frac{\tau}{t_r} + \sin \frac{5\tau}{t_r} - \sin \frac{4\tau}{t_r}$$

$$+ \sin \frac{8\tau}{t_r} - \sin \frac{7\tau}{t_r} + \sin \frac{11\tau}{t_r} - \sin \frac{10\tau}{t_r}$$

$$+ D(\cos \frac{4\tau}{t_r} - \cos \frac{2\tau}{t_r} + \cos \frac{10\tau}{t_r} - \cos \frac{8\tau}{t_r}$$

$$+ \cos \frac{16\tau}{t_r} - \cos \frac{14\tau}{t_r} + \cos \frac{22\tau}{t_r} - \cos \frac{20\tau}{t_r})$$

$$+ C(\sin \frac{4\tau}{t_r} - \sin \frac{2\tau}{t_r} + \sin \frac{10\tau}{t_r} - \sin \frac{8\tau}{t_r}$$

$$+ \sin \frac{16\tau}{t_r} - \sin \frac{14\tau}{t_r} + \sin \frac{22\tau}{t_r} - \sin \frac{20\tau}{t_r}\}$$

$$+ Z\{B(\cos \frac{\tau}{t_r} - \cos 0 + \cos \frac{7\tau}{t_r} - \cos \frac{5\tau}{t_r} + \cos \frac{12\tau}{t_r}$$

$$- \cos \frac{11\tau}{t_r})$$

$$+ A(\sin \frac{\tau}{t_r} - \sin 0 + \sin \frac{7\tau}{t_r} - \sin \frac{5\tau}{t_r}$$

$$+ \sin \frac{12\tau}{t_r} - \sin \frac{11\tau}{t_r})$$

$$+ D(\cos \frac{2\tau}{t_r} - \cos 0 + \cos \frac{14\tau}{t_r} - \cos \frac{10\tau}{t_r}$$

$$+ \cos \frac{24\tau}{t_r} - \cos \frac{22\tau}{t_r})$$

$$+ C(\sin \frac{2\tau}{t_r} - \sin 0 + \sin \frac{14\tau}{t_r} - \sin \frac{10\tau}{t_r}$$

$$+ \sin \frac{24\tau}{t_r} - \sin \frac{22\tau}{t_r})\}] \tag{31}$$

Fortunately, Eqn. (31) may be reduced considerably. Under typical experimental conditions τ will be approximately 3 μsec and t_r will be approximately 500 μsec (spinning frequency of 2 kHz) making the ratio $\tau/t_r \ll 1$. Under these conditions Eqn. (31) reduces to

$$\bar{H}_D^{(o)} = \gamma^2 r^{-3} \frac{t_r}{12\tau} (\frac{4A\tau}{t_r} + \frac{8C\tau}{t_r})(X+Y+Z) \tag{32}$$

but

$$X + Y + Z = 0 \tag{33}$$

We therefore have that the zero order average Hamiltonian is zero at multiple pulse cycle times, t_c, provided $\tau \ll t_r/12$. Under these conditions the A's, B's, C's and D's will not affect the results from one multiple pulse cycle to another.

To determine the effects of sample spinning on the chemical shift shielding parameters, it becomes useful to use irreducible spherical tensors (40,41). The shielding Hamiltonian for a given nucleus has the form (40)

$$H_\sigma = \gamma \sum_{\ell=0,2} \sum_{m=-\ell}^{\ell} (-1)^m T_{\ell,m}\sigma_{\ell,-m} \tag{34}$$

where $T_{\ell,m}$ describes the spin variables and the $\sigma_{\ell,-m}$'s are the components of a symmetric second rank tensor. In the tensor's principal axis system (PAS) only components with $m = 0,\pm2$ are nonzero. We denote these components by $\rho_{\ell,m}$. They are related to the PAS $\sigma_{\alpha\alpha}$'s by

$$\rho_{00} = \frac{1}{3} T_r\underline{\underline{\sigma}}$$

$$\rho_{2,0} = \sqrt{\frac{3}{2}}(\sigma_{33} - \frac{1}{3}T_r\underline{\underline{\sigma}}) = \sqrt{\frac{3}{2}}\delta \tag{35}$$

$$\rho_{2\pm2} = \frac{1}{2}(\sigma_{22} - \sigma_{11}) = \frac{1}{2}\eta\delta$$

The $\rho_{\ell,m}$'s can be expressed in the laboratory coordinate system (c.s.) in which all measurements are related, by the transformation

$$\sigma_{\ell,-m}(\text{LAB}) = \sum_{m'} \mathcal{D}^\ell_{m',-m}(\alpha\beta\gamma)\rho_{\ell m'} \tag{36}$$

The triple, α,β,γ, are the Euler angles by which the lab c.s. may be brought in coincidence with the PAS. Using the appropriate values of $\mathcal{D}^\ell_{m'm}$ and $T_{\ell,m}$ and substituting Eqn. (35) and (36) into Eqn. (34) yields

$$H_\sigma = \omega_0 I_z\{\frac{1}{3} T_r\underline{\underline{\sigma}} + \frac{\delta}{2}((3\cos^2\beta-1)$$

$$+ \eta \sin^2\beta \cos 2\gamma)\} \tag{37}$$

This is the normal powder pattern shielding Hamiltonian given in Ref. (40).

The question to be answered now is what happens to Eqn. (34) when the sample is rotated with frequency ω_r about an axis inclined at an angle θ away from the static fields H_o. Two transformations are required to relate the PAS components of $\underline{g}$ to the laboratory c.s. With this in mind Eqn. (36) becomes

$$\sigma_{\ell,-m}(\text{LAB}) = \sum_{m'} \mathcal{D}^\ell_{m',-m}(0,\theta,\omega_r t) \sum_{m''} \mathcal{D}^\ell_{m''m'}(\Omega')\rho_{\ell,m''} \quad (38)$$

where Ω' represents the Euler angles which bring the PAS in coincidence with the sample spinning c.s. Using Eqn. (38), Eqn. (34) now is given by

$$H_\sigma = \omega_o I_z \frac{1}{3} T_r \underline{g} + \omega_o I_z \{ \frac{(3\cos^2\theta-1)}{2} \cdot \frac{\delta}{2}[(3\cos^2\beta-1)$$

$$+ \eta \sin^2\beta\cos2\gamma]$$

$$- \frac{\sin2\theta e^{-i\omega_r t}}{2} \cdot \delta[\sqrt{\frac{3}{2}} \mathcal{D}^2_{0,-1}(\Omega')$$

$$+ \frac{\eta}{2} (\mathcal{D}^2_{-2,-1}(\Omega') + \mathcal{D}^2_{2,-1}(\Omega'))]$$

$$+ \frac{\sin2\theta e^{i\omega_r t}}{2} \cdot \delta[\sqrt{\frac{3}{2}} \mathcal{D}^2_{0,1}(\Omega')$$

$$+ \frac{\eta}{2} (\mathcal{D}^2_{-2,1}(\Omega') + \mathcal{D}^2_{2,1}(\Omega'))]$$

$$+ \frac{\sin^2\theta e^{i2\omega_r t}}{2} \cdot \delta[\frac{\sqrt{3}}{2} \mathcal{D}^2_{0,2}(\Omega')$$

$$+ \frac{\eta}{2} (\mathcal{D}^2_{-2,2}(\Omega') + \mathcal{D}^2_{2,2}(\Omega'))]$$

$$+ \frac{\sin^2\theta e^{-i2\omega_r t}}{2} \cdot \delta[\frac{\sqrt{3}}{2} \mathcal{D}_{0-2}(\Omega')$$

$$(39)$$

$$+ \frac{\eta}{2} (\mathcal{D}_{-2,-2}(\Omega') + \mathcal{D}_{2,-2}(\Omega'))]$$

Eqn. (39) may be rewritten in a simplified form as

$$H_{cs} = I_z\{A + Be^{-i\omega_r t} + Ce^{i\omega_r t} + De^{-i2\omega_r t}$$

$$+ Ee^{i2\omega_r t}\} \qquad (40)$$

To predict the effect of the interaction Hamiltonian on the magnetization, the expectation value of I_y is calculated. The normalized expectation value is given by

$$<I_y> = \frac{Tr\rho(t)I_y}{TrI_y^2} \qquad (41)$$

where

$$\rho(t) = U(t)\rho(o)U^+(t) \qquad (42)$$

U(t) is given by the Dyson expression

$$U(t) = T \exp\{-iI_z \int_o^t (A + Be^{-i\omega_r t'} + Ce^{i\omega_r t'}$$

$$+ De^{-i2\omega_r t'} + Ee^{i2\omega_r t'})dt'\} \qquad (43)$$

To illustrate how the final result is obtained, only the A
and B terms will be considered in the remaining discussion.
Eqn. (43) then becomes

$$\langle I_y \rangle = \frac{Tr\{[\exp\{-iI_z \int_0^t Be^{-i\omega_r t'} dt'\} e^{-iI_z t} I_y e^{iI_z t}}{TrI_y^2}$$

$$\cdot \frac{\exp\{iI_z \int_0^t Be^{-i\omega_r t'} dt'\}] I_y\}}{} \qquad (44)$$

which reduces to

$$\langle I_y \rangle = \frac{Tr\{[\exp\{-iI_z \int_0^t Be^{-i\omega_r t'} dt'(I_y \cos At + I_x \sin At)}{TrI_y^2}$$

$$\cdot \frac{\exp\{iI_z \int_0^t Be^{-i\omega_r t'} dt'] I_y\}}{} \qquad (45)$$

Now $TrI_x I_y = 0$ and $\dfrac{TrI_y^2}{TrI_y^2} = 1$, Eqn. (45) reduces to

$$\langle I_y \rangle = \cos(At + \frac{e^{-i\omega_r t}}{\omega_r} B) \qquad (46)$$

substituting for A and B gives

$$\langle I_y \rangle = \cos \omega_o \{t[\tfrac{1}{3}\text{Tr}\underline{\sigma} - \frac{(3\cos^2\theta - 1)}{2} \frac{\delta}{2}((3\cos^2\beta - 1)$$

$$+ \eta \sin^2\beta \cos 2\gamma)$$

$$+ \frac{e^{-i\omega_r t}}{\omega_r} [(\sigma_{33} - \tfrac{1}{3}\text{Tr}\underline{\sigma}) \frac{\sin 2\theta}{2} [\sqrt{\tfrac{3}{2}} \mathcal{D}^2_{0,-1}(\Omega')$$

$$+ \frac{\eta}{2} (\mathcal{D}^2_{-2,-1} + \mathcal{D}_{2-1})]]\} \qquad (47)$$

Under the condition of "fast" spinning (e.g., $\omega_r > (\sigma_{33} - \tfrac{1}{3}\text{Tr}\underline{\sigma})$ at the magic angle Eqn. (47) reduces to

$$\langle I_y \rangle = \cos \omega_o (t \cdot \tfrac{1}{3}\text{Tr}\underline{\sigma}) \qquad (48)$$

That is to say that the chemical shift lineshape collapses to its isotropic value. In addition, under the combined sample spinning multiple pulse experiment the zero order chemical shift Hamiltonian for a given nucleus becomes

$$\bar{H}^{(o)}_{cs} = \omega_o \tfrac{1}{3}\text{Tr}\underline{\sigma}(I_x + I_z) \qquad (49)$$

where the offset and finite pulse width have been omitted.

In summary, the effect of magic angle spinning does not harm the narrowing affects of the MREV-8 sequence. Under the conditions of fast spinning as described above, CRAMPS removes both dipolar broadening and chemical shift anisotropies. It is not necessary to either sample at cycle times of the rotation cycle or synchronize the spinning such that $(\omega_r)^{-1}$ = ntc as suggested previously (18).

Theory of Cross Polarization Experiments

The solid state NMR of dilute spin systems ($\underline{e}.\underline{g}.$, ^{13}C)
suffers from three shortcomings: 1) low sensitivity due to
low natural abundance and small gyromagnetic ratio,
2) dipolar broadening interactions with neighboring abundant
spins ($\underline{e}.\underline{g}.$, ^{1}H), and 3) relatively long T_1's making data
acquisition a formidable task. Fortunately, methods have
been developed to alleviate these problems and have made
high resolution solid state NMR of dilute spin systems
possible (41). The basic ideas of double resonance were
proposed by Hartman and Hahn (31,81).

Since the NMR signal of dilute spins are very weak,
a gain in sensitivity can be obtained by utilizing the
reservoir of abundant spins. This can be accomplished in
two ways: 1) by indirect methods (82) where the dilute
spin is detected via the abundant spin, and 2) by direct
methods (37,38) where the dilute spin magnetization is
enhanced by the abundant spins. It is the second case
which interests us. The double resonance experiment is a
three step process, which may be described by applying
the spin temperature concept (83). The first step requires
a cooling of the abundant I spin system. This may be
accomplished through several schemes (84-87). Since spin
locking (84) has been used exclusively, discussion will be
limited to this mechanism. This is effected by applying a

$\pi/2$ pulse along a chosen axis followed immediately by a locking field of strength $\gamma H_1^I = \omega_I$ phase shifted 90° with respect to the first $\pi/2$ pulse. The inverse spin temperature describing the spin lock condition, β_I is given by

$$\frac{\beta_I}{\beta_L} = \frac{H_o}{H_I} \gg 1 \tag{50a}$$

where β_L is the inverse spin temperature of the lattice. Eqn. (50a) describes the cooling of the I spin system.

Since the I spins are now cold and the S spins are hot, an energy exchange can take place with time constant T_{IS}. This transfer is impossible in the laboratory frame since such a process need occur under total energy conservation, but may occur in the rotating frame as shown in Figure 3, utilizing the ideas adapted by Hartman and Hahn. The dilute spins are irradiated by frequency $\omega_c = \gamma^C H_1^C$ such that the condition

$$\gamma^C H_1^C = \gamma^H H_1^H \tag{50b}$$

is met. Under these conditions mutual I and S spin flips can occur _via_ the I – S dipolar interactions. The result is a cooling of the S spin system by establishing an S spin order (forming a net magnetization along H_1^C) and a heating of the I spin reservior (a loss in magnetization along H_1^H). Pines _et al._ (37) have discussed the theoretical efficiency

^1H spins ^{13}C spins

$\omega_1^H = \gamma^H H_1^H = \gamma^C H_1^C = \omega_1^C$

$\omega_0^H = \gamma^H H_0$

$\omega_0^C = \gamma^C H_0$

ROTATING FRAME

LAB FRAME
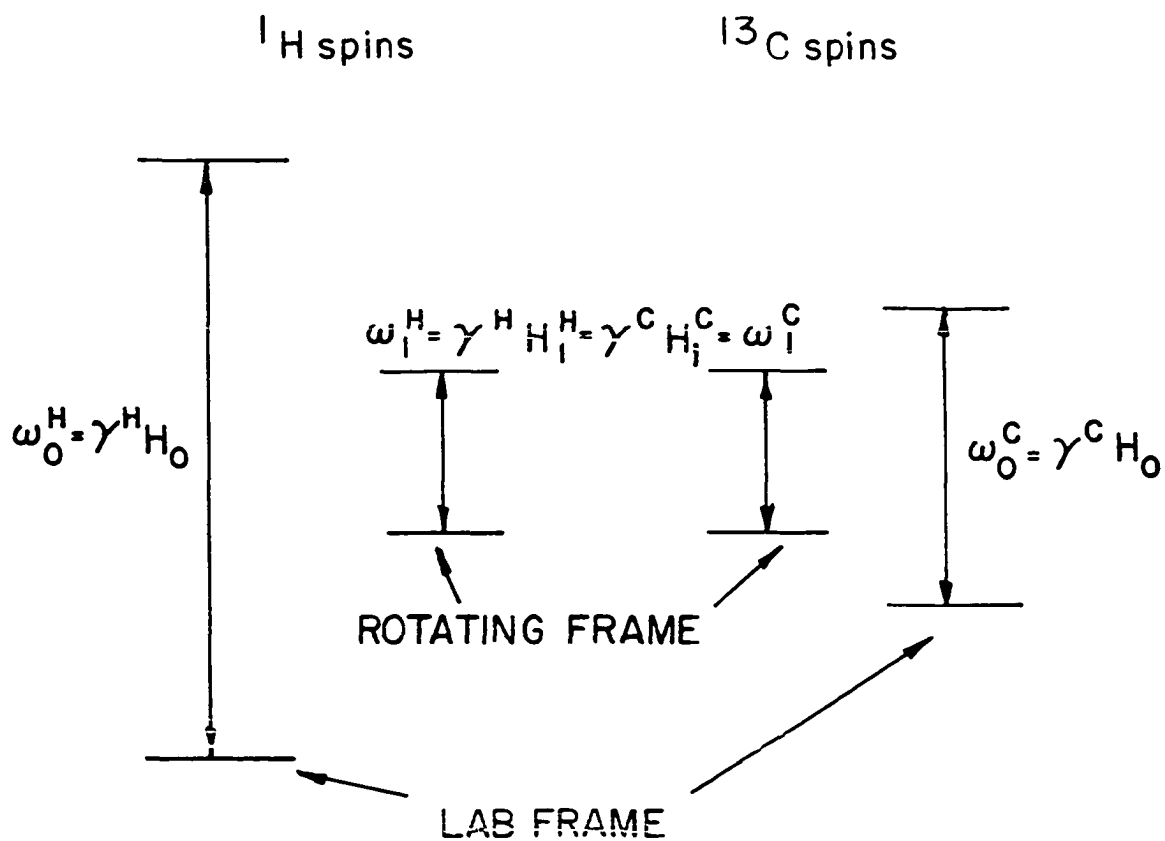
Figure 3. The energy level diagram of the cross polarization experiment. The energy levels of the two systems are equal in the rotating frame when the Hartman-Hahn condition is met.

of cross polarization as well as the concept of "multiple"
contacts.

After a given contact time, the S spin rf pulse is
terminated and the time decay of the S magnetization is
observed while continuing to decouple the abundant spins
to remove the heteronuclear dipolar interaction. The
Fourier Transform of this decay is the S spin NMR spectrum
whose lineshape is determined by the chemical shift
anisotropy.

DESCRIPTION OF SPECTROMETER

The repertiore of multiple pulse NMR experiments developed in the past few years has placed stringent requirements on NMR spectrometer design. These have resulted in two basic types of spectrometers. The first type is a wide banded high power (several kilowatts) spectrometer designed particularly to meet the requirements of "line-narrowing" experiments (88). The second type of spectrometer, which also is capable to performing multiple pulse "line-narrowing" experiments, is a narrow banded spectrometer which in addition to requiring less power provides improved signal-to-noise ratio over the wide banded spectrometer (8,89).

The high Q of the narrow banded spectrometers, can adversely affect the rise and fall of an rf pulse by producing transients. These imperfections can seriously disrupt a multiple pulse NMR experiment as they require the application of several thousand rf pulses, and errors can accumulate over a pulse chain (23). One approach to solving this problem is to avoid when possible the use of tuned circuits, or at least keep the Q's sufficiently low to minimize transients. Another approach (89) has shown it possible to control such transients and effectively cancel their affects. This has allowed the use of high Q

(<100) circuits to improve the signal-to-noise ratio while not adversely affecting the NMR spectrum.

The spectrometer designed and operating in this laboratory basically takes advantage of tuned circuits wherever possible to enhance signal-to-noise ratio, but allows attainment of very short cycle times; less than 30 μsec in multiple pulse experiments using a 400 watt wide band rf transmitter. With few changes, the spectrometer is also capable of double resonance experiments for obtaining high resolution NMR spectra of dilute spins.

Figure 4 is a block diagram of the basic spectrometer. It is a broad band unit operating at 56 MHz for ^{1}H using a Varian 1·4T Magnet. The rf unit has 8 available channels of varying phase and pulse width. The transmitter, an IFI model 404 distributed amplifier system, is capable of producing 400 watts in pulse operation. With proper matching of NMR probe and transmitter, 1.25 μsec 90° pulses are attained with a total dead time from pulse turn off to receiving an NMR signal of 3.5 μsec. This time is dominated by probe ring down since receiver ring down is less than 2 μsec. Pulse phase transients were minimized and symmetrized utilizing a π circuit at the output of the transmitter to match the transmitter to the probe at the field determined by the deuterium lock.

A Biomation 805 transient recorder, with minimum sampling time of 0.2 μsec per channel was used to accumulate
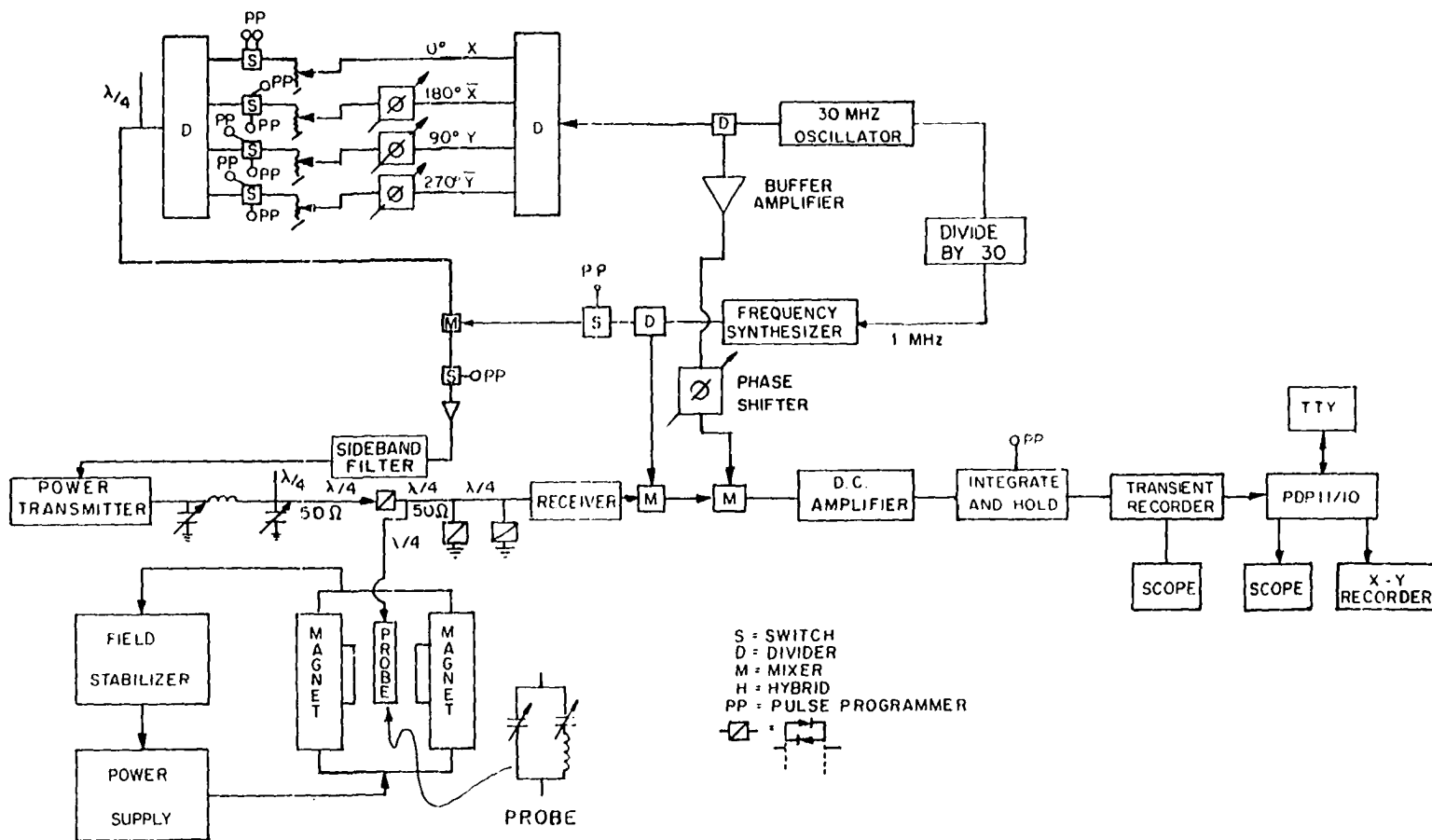
Figure 4. Block diagram of pulse NMR spectrometer used for homonuclear experiments.

all data. The memory of this unit containing 2048 eight bit

words. The Biomation is interfaced to a PDP 11/10 computer

for signal averaging and data manipulation.

The Receiver System

One of the most crucial components of a multiple pulse

spectrometer is the receiving system which consists of an

amplification chain, phase detection-demodulation, and d.c.

amplifier. The nature of most multiple pulse experiments

have placed severe requirements on the amplification chain.

It must be able to withstand over-voltages from radio

frequency pulses and still recover in less than a 2 μsec

in order to detect microvolt NMR signals. The amplification

chain found to perform best both under homonuclear and

heteronuclear decoupling experiments consists of a Avantek

142 wide band amplifier and two SML limiting amplifiers

which provide a total gain of 60 db. The signal-to-noise

ratio of this chain when connected in the receiver system

was determined to be 80 using the NMR signal from

1.6×10^{21} protons. The signal-to-noise ratio is enhanced

by utilizing LC circuits tuned at the operating frequency

of the spectrometer after the first and second stages.

The receiver system is limited only by probe ring down time;

it is capable of recovery in less than 2.0 μsec after a

power pulse.

Prior to amplification the front of the receiver is matched to the NMR probe by having three quarter wavelengths of cable connecting them as shown in Figure 4. The sets of cross diodes to ground prevent amplifier failure due to overloading. The series crossed diodes at the output of the transmitter reduce transmitter noise during signal reception.

NMR Probe for Combined Homonuclear Multiple Pulse Decoupling and Magic Angle Spinning

The present section describes an NMR probe which is designed to be utilized in combined rotation and multiple pulse spectroscopy on randomly oriented solids with strong homonuclear coupling. The discussion dealing with H_1 inhomogeneity and circuit design is applicable to other probes built for use in homonuclear decoupling experiments. The probe has the following features which are either necessary, or convenient, for the combined rotation-homonuclear decoupling experiment:

(1) Rotor design allows the sample to be placed in a sufficiently homogeneous H_1 field for multiple pulse narrowing experiments, using a spectrometer with rf power of less than 500 W.

(2) Identical and rigid shielding is maintained during pulse tuning and data accumulation, such that sample

interchange between tuning and data accumulation does not affect the tuning necessary for a successful multiple pulse experiment.

(3) Facile sample interchange, with the rotor axis set at any desired angle to the magnetic field, is possible.

(4) Rotation of the probe within a 3.81 cm air gap magnet is allowed.

(5) Use of inexpensive, readily available components allowing for operation at 500 W is maintained.

Description of probe

The probe circuitry is a tapped-tuned circuit shown in Figure 5 (90) constructed of inexpensive, readily available components. Fixed ceramic capacitors (American Technical Ceramics) are used in addition to variable trimmer capacitors (Centralab) for fine tuning. Voltage breakdown in C_1 is prevented by the addition of ATC units in series with the tuning capacitor. The sample coil, made of No. 14 copper wire, has nine turns, and is designed such that the length, 18 mm, is greater than the inner diameter to produce the most homogeneous H_1. The center three turns are made of flattened wire, 2 mm in width, in order to increase the volume over which the H_1 field is homogeneous. The homogeneity of the H_1 field is indicated by the decay (21,24,26) in Figure 6. The figure exhibits the response of protons in an undoped, spherical water sample to
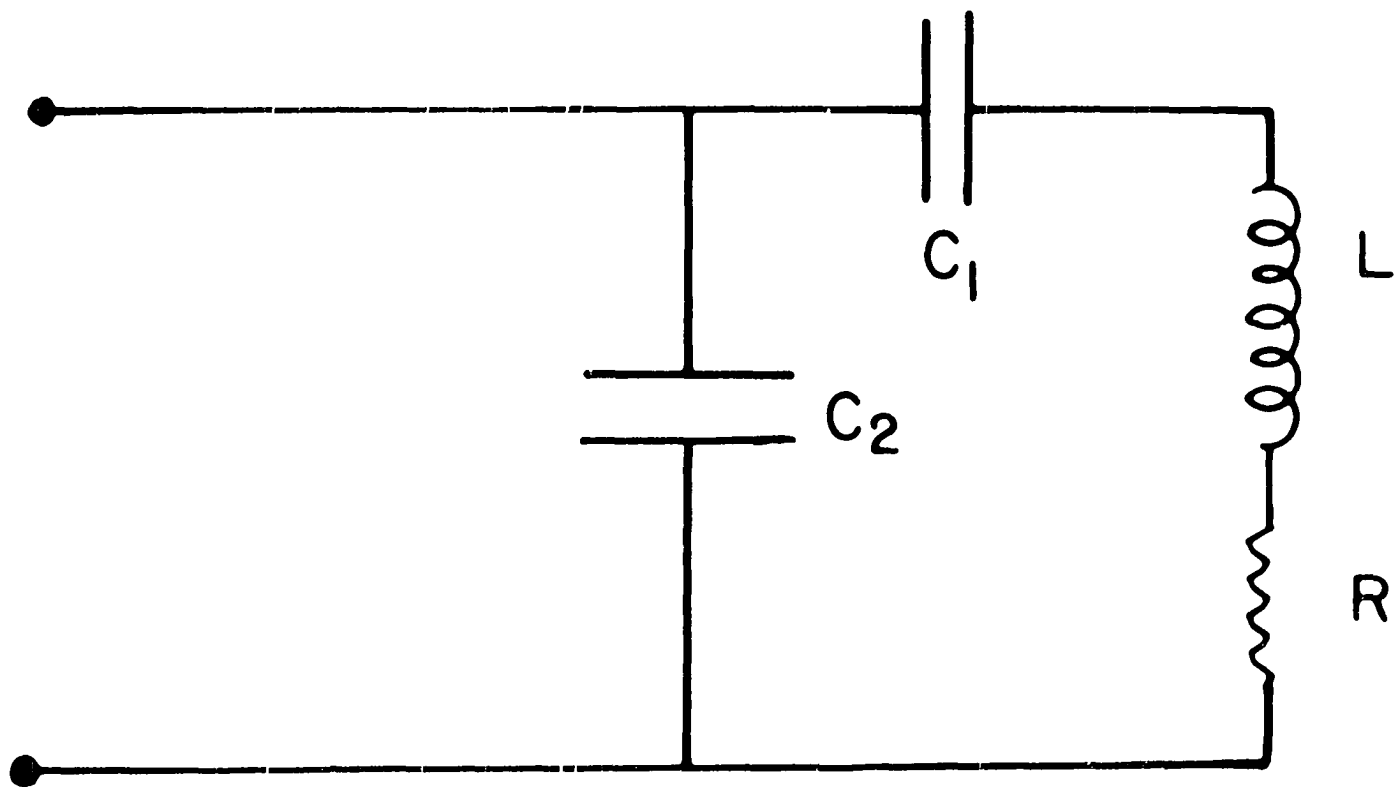
Figure 5.   The tapped-tuned circuit used in the NMR probe.
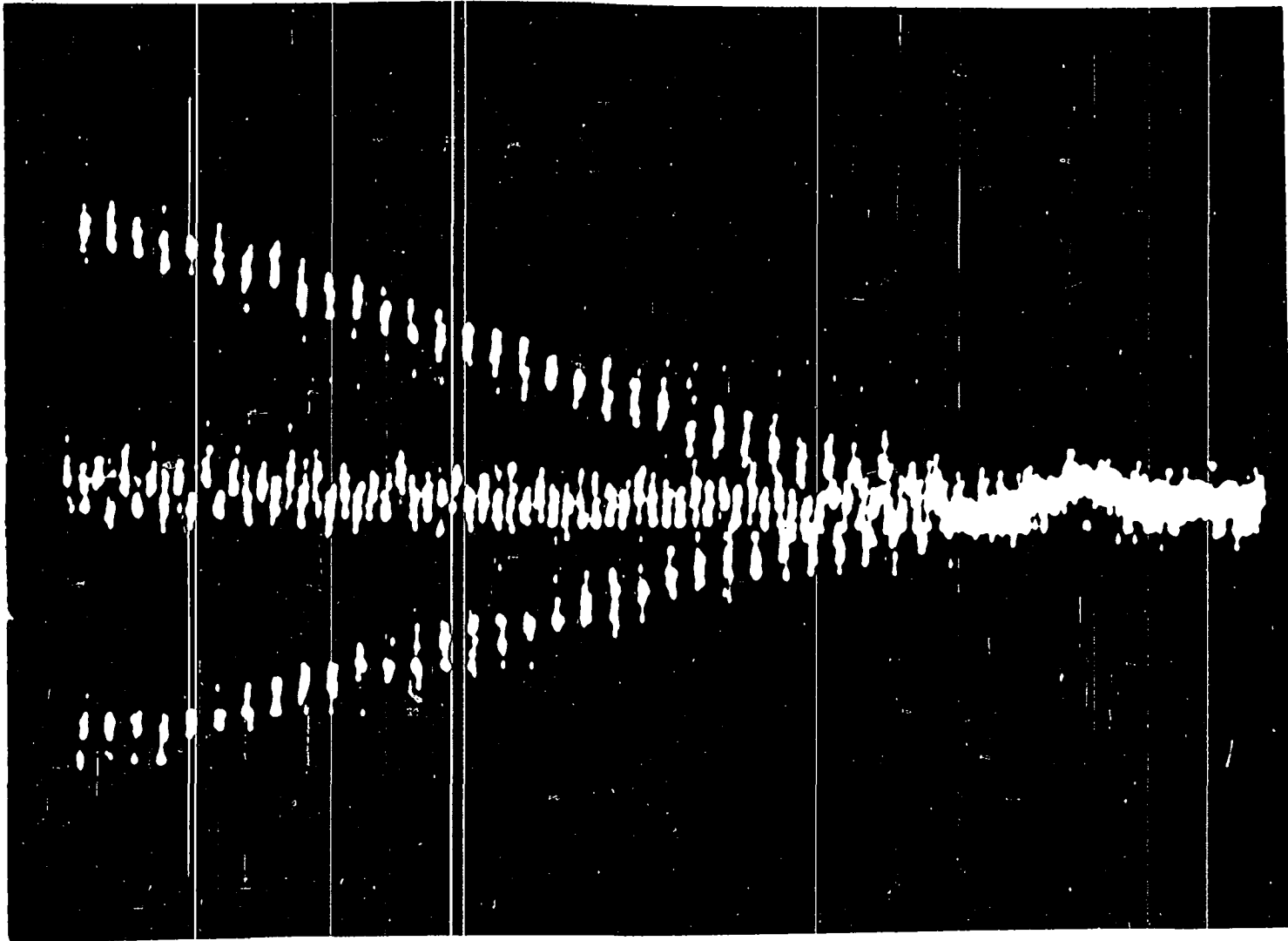
Figure 6.   The response of protons to 128 π/2 pulse.   The total scan is 100 msec.

128 $\pi/2$ pulses on a timescale of 100 ms. With proper impedance matching of the probe to the rf transmitter and a Q of less than 30, $\pi/2$ pulses are attained in 1.5 μs at the magic angle. These pulse widths allow attainment of MREV-8 multiple pulse cycle times, t_c, of 27.6 μs. For the MREV-8 multiple pulse cycle to be effective in removal of homonuclear dipolar broadening, the condition $t_c||H_{int}||<1$ must be met. $||H_{int}||$ is the magnitude of the internal interaction causing the broadening. This cycle time dependence has been shown crucial in samples of polyethylene with crystalline and amorphous portions (91).

Magic angle spinning of the sample is accomplished using a rotor and stator design of the Andrew type (74). The magic angle, 54.7° from the d.c. field, is obtained by rotating the entire probe assembly. The probe, shown in Figure 7 consists of 31.75 mm wall, 3.81 cm o.d., brass tubing machined as shown to allow access to the tapped-tuned circuit. The tube is fitted into a brass mount which has an O-ring bearing to allow for smooth manual rotation of the probe. The mount, in turn, is fixed to an NMR probe stand in the air gap of a 30.5 cm magnet.

The stator design used is shown in Figure 8. Six (rather than eight (92)) air jets were found to give the maximum speed and stability for the rotors. The stator assembly, shown in Figure 7, is machined to allow a matched fit into the probe body below the sample coil. Sample
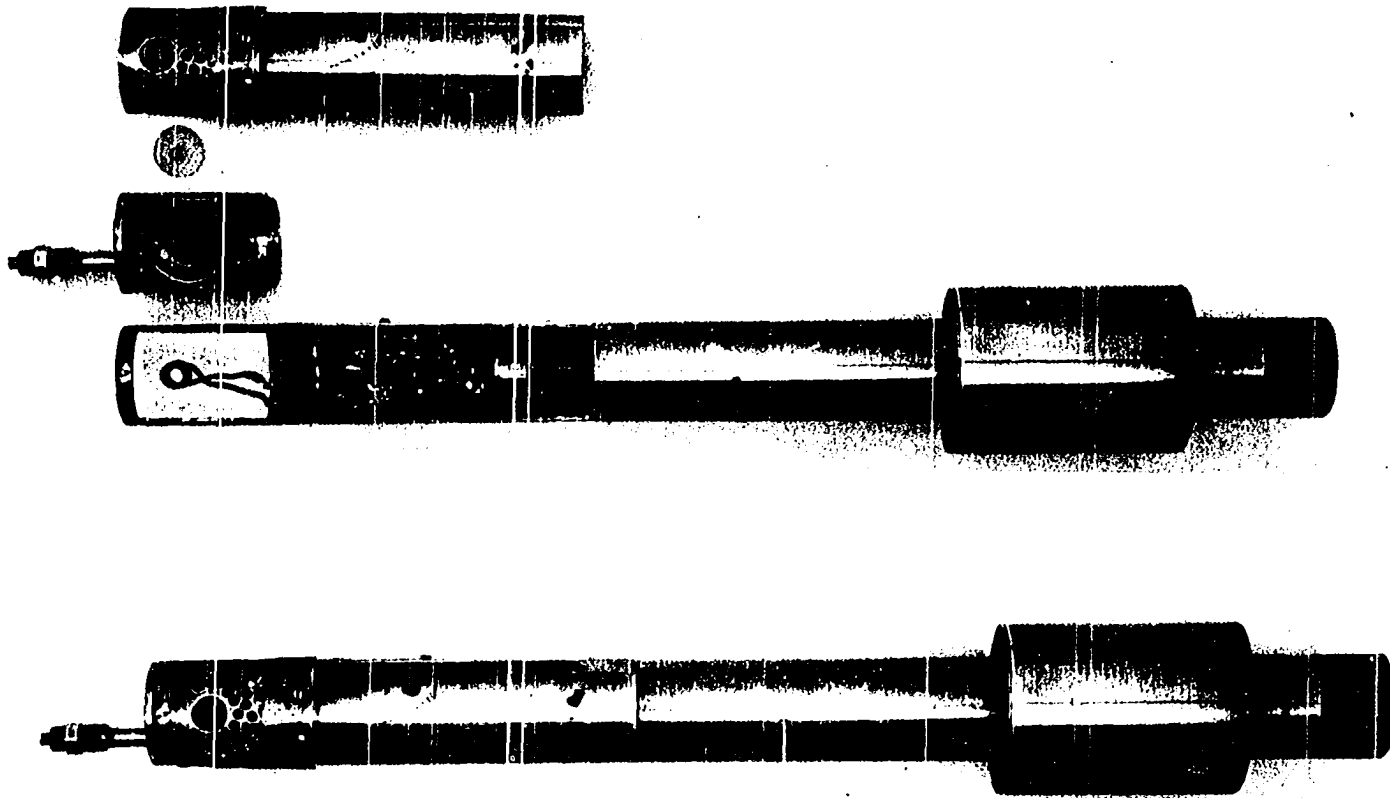
Figure 7. a) From top to bottom, the probe shield, rotor, stator and probe body;
b) The assembled probe.
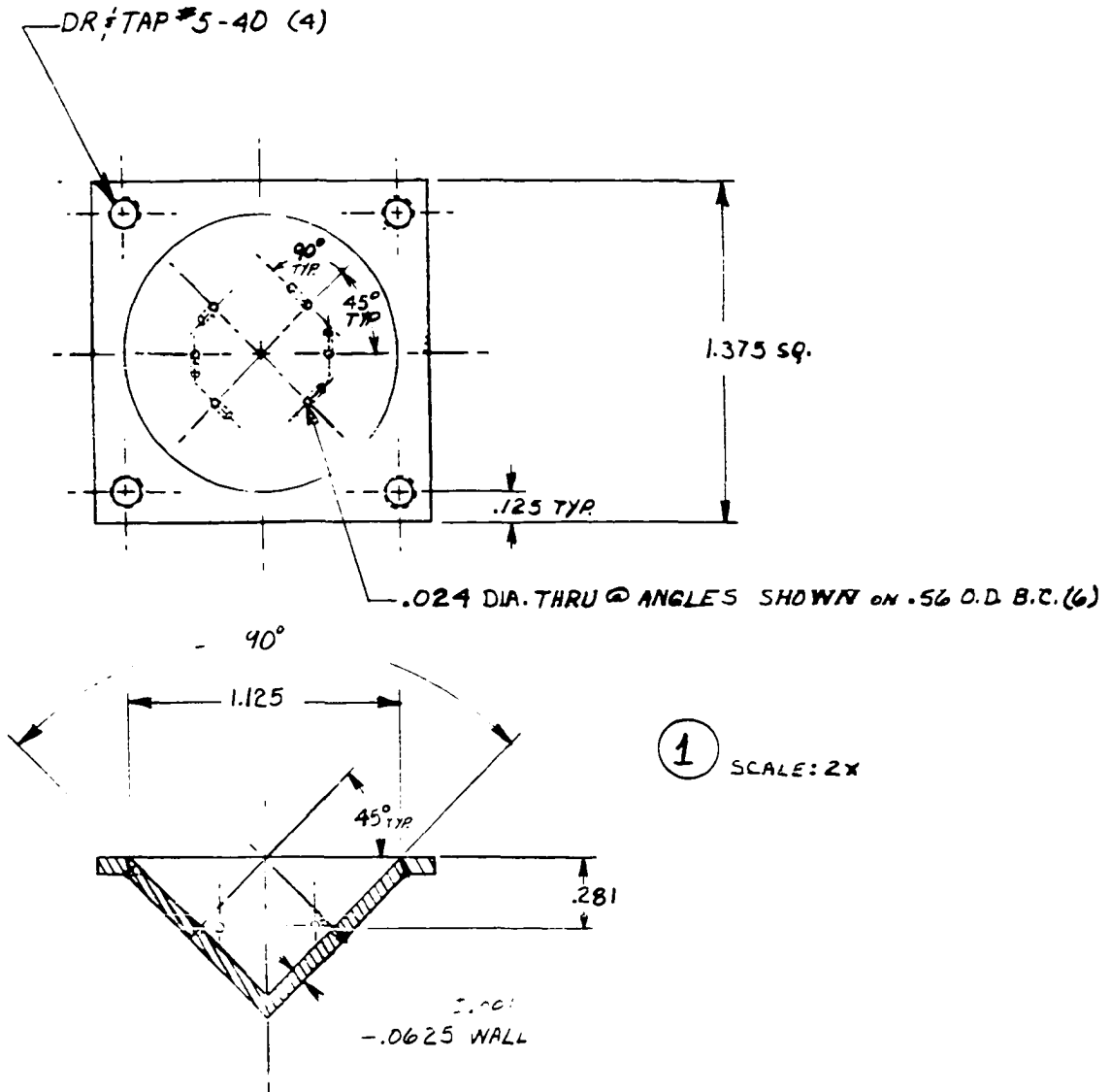
Figure 8. The stator design used to drive rotors at speeds of 3 kHz.

interchange is accomplished by removal of the stator from the probe body. This feature insures that probe tuning and shielding remains fixed between experiments. Compressed air is used to drive the rotors, and, with the present stator design, it is found that the pressure need not exceed 1.75 kg/cm^2 to attain speeds of 3 kHz for rotors of the specified dimensions. A ballast tank of 3-ℓ volume between the compressed air source and probe was found necessary for routine stable operation.

The rotor design presently used is shown in Figure 9. The design was decided on by varying the parameters available until the most stable configuration was found. It was found sufficient to hand cut flutes in the rotors. Rotor stability is greatly enhanced by rounding the bottom of the rotor. Rotors made of polymerized trifluorochloroethylene (KEL-F; trade name, 3-M Co.) were used to detect chemically shifted ^{19}F signals (93) in KEL-F and ^{1}H in coals. For powder samples, a reentrant well is machined into the rotor top, as shown in Figure 9, and the powder is packed below a Teflon cap. Rotational speeds of 2.5 kHz at 1.4 kg/cm^2 air pressure have been achieved with, e.g., 0.065 cm^3 of powdered coal, utilizing such an arrangement.

Once the probe is tuned, a brass shield, shown in Figure 7, is placed on the probe to protect against rf interference. Holes in the shield allow for the tuning C_1
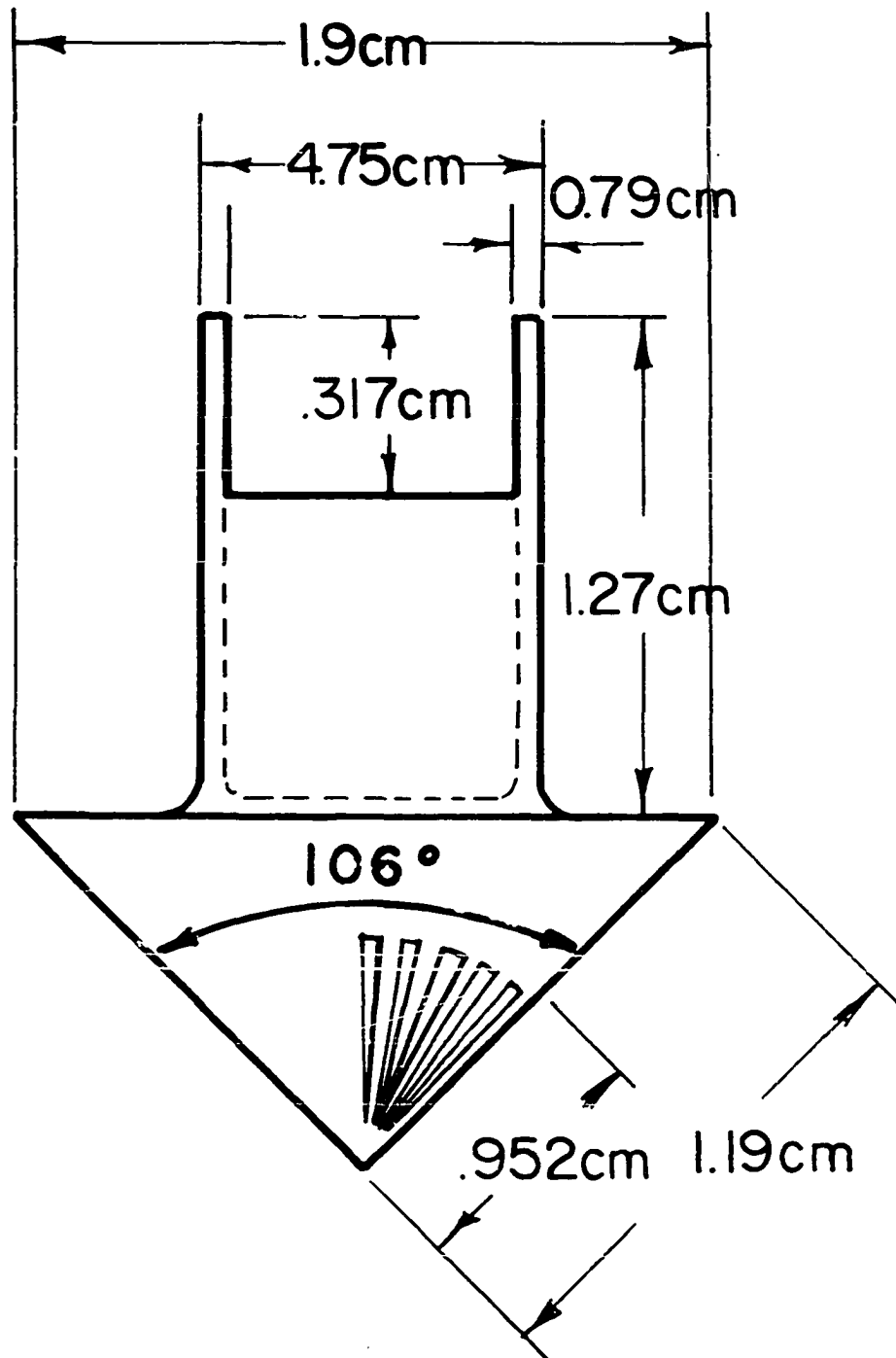
Figure 9. The rotor design. The reentrant port of the neck is used for powder samples.

and C_2 after shielding. This shield, once in place, is rigid and identical for all multiple pulse experiments.

The rotor, stator, and coil design is such that when instabilities in rotation occur the rotors do not self-destruct, and they never leave the confines of the stator.

The Cross Polarization Spectrometer

With a few modifications the basic spectrometer can perform the cross polarization-double resonance experiments (94). A schematic representation of the spectrometer is shown in Figure 10. The double resonance probe is of the single coil variety (95,96). The circuit schematic used in conjunction with the magic angle spinning probe is shown in Figure 11, and is simultaneously tuned at the proton and carbon frequencies, f_H and f_L, to match the desired input impedances. The proton frequency, f_H is tuned using capacitors C_{1H} and C_{2H}. The carbon frequency, f_L is tuned using capacitor C_{1L} and cable length D1. The coil is 12 mm long and 10 mm i.d. The proton decoupling field is isolated from the carbon receiver by the two quarter wavelengths, $\lambda/4)_H$, which provides 33 db of isolation. The experimental Q's of the circuits are 25 at the proton frequency and 36 at the carbon frequency. Figure 12 shows the circuit incorporated in the magic angle spinning probe. Cross polarization fields of 10^{-3} T for
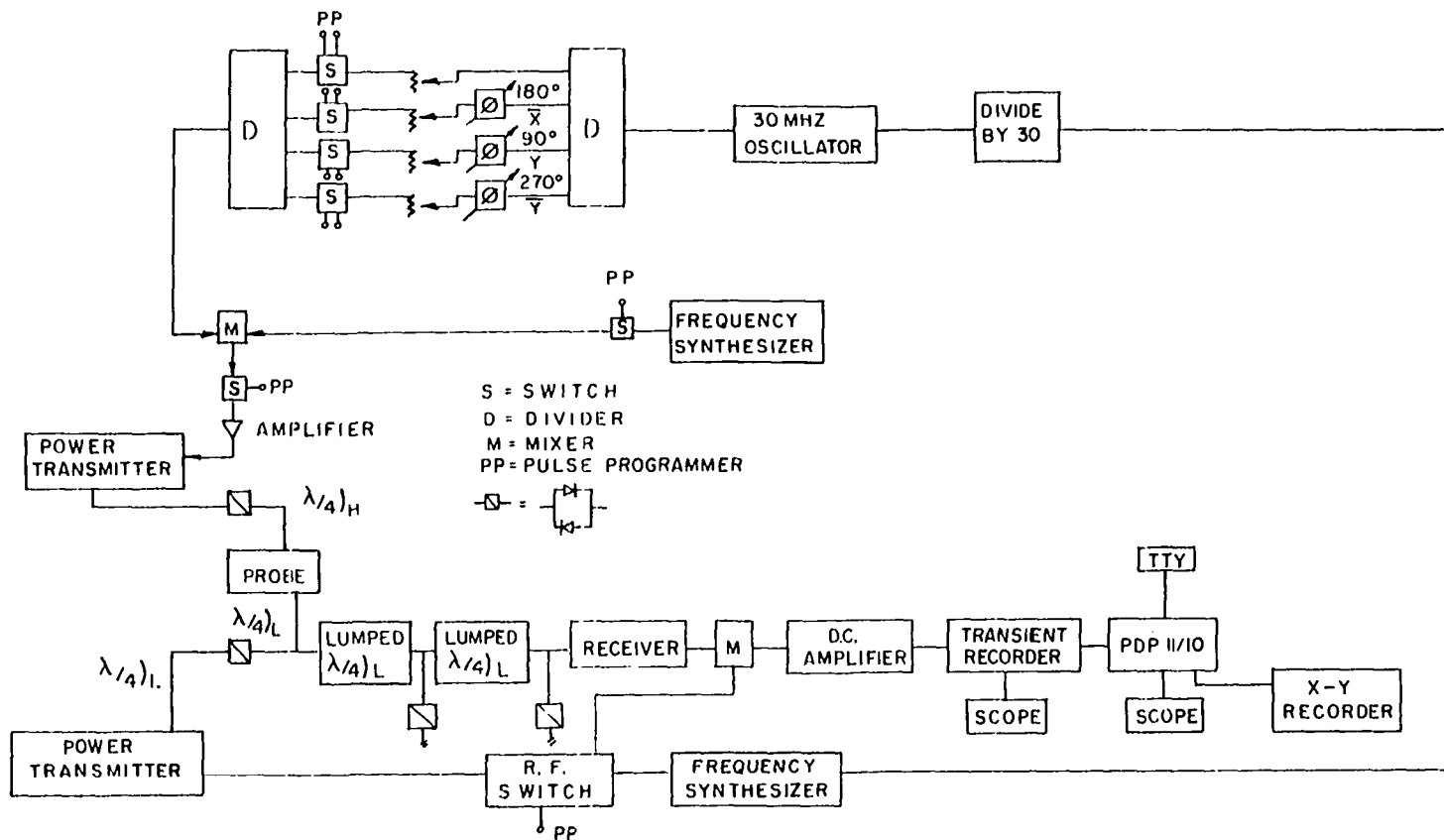
Figure 10. Block diagram of the NMR spectrometer used for double resonance experiments.
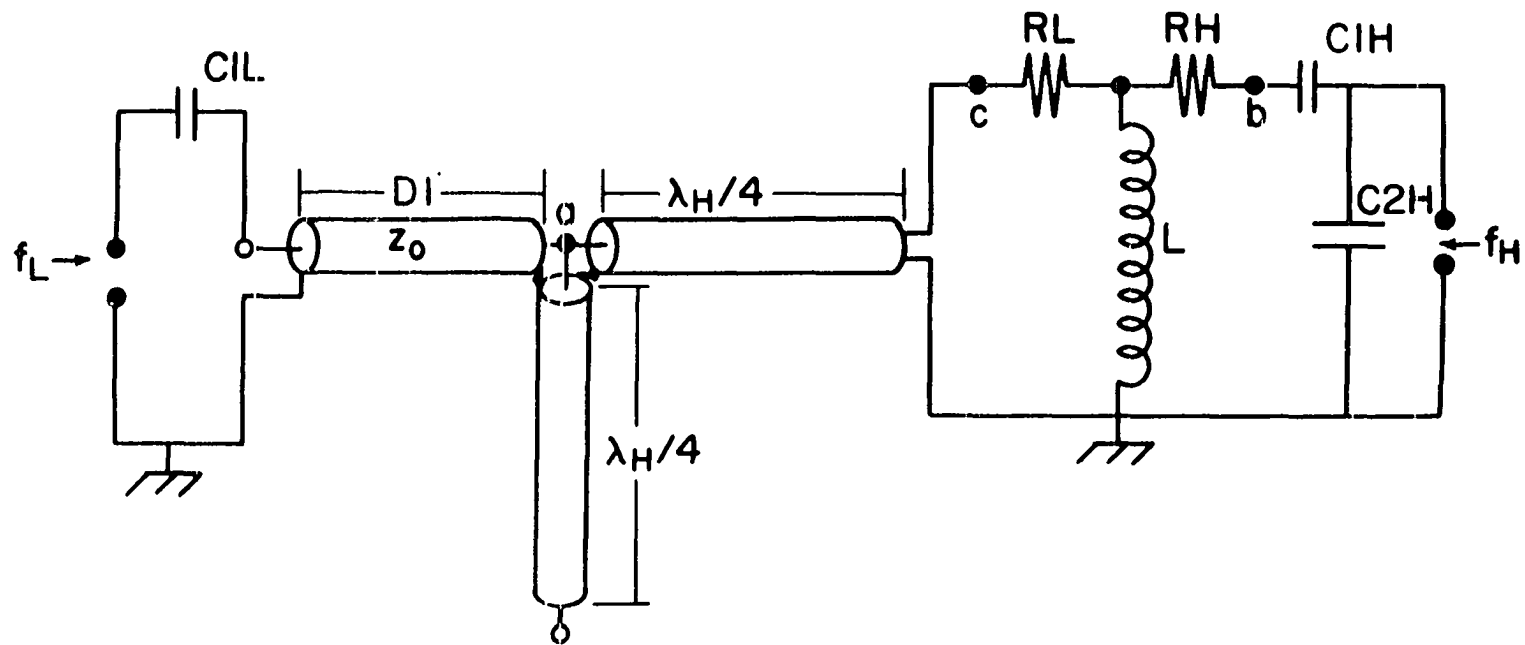
Figure 11. Circuit schematic for single coil double resonance NMR probe.
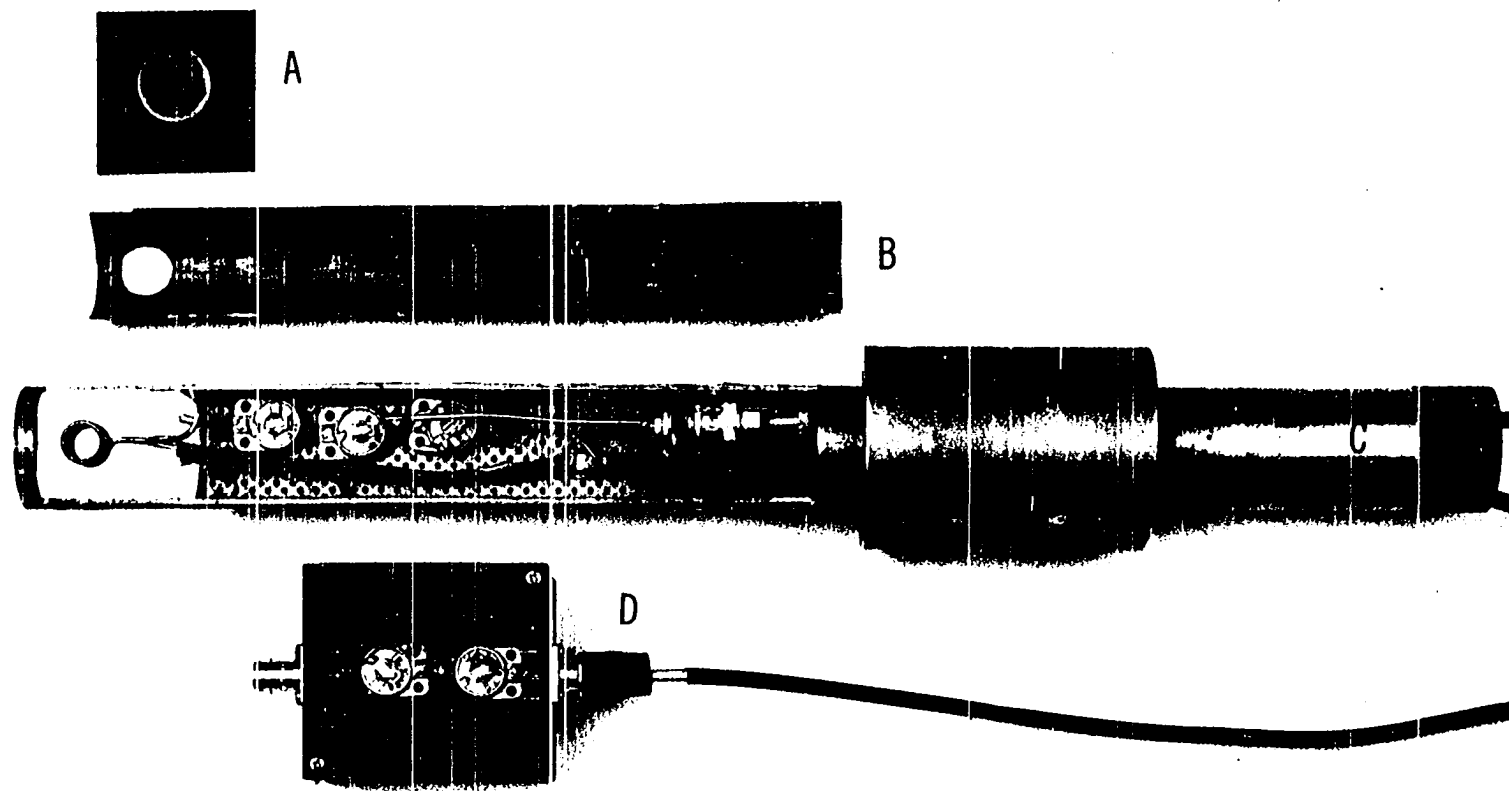
Figure 12. The "magic angle" spinning probe with incorporated electronics

a) rotor
b) shield
c) probe body
d) 14 mHz tuning capacitor

the protons and 4×10^{-3} T for the ^{13}C were obtained with 81 watts from a transmitter, constructed in this laboratory, tuned at 56 MHz, and 250 watts from a Arhenberg transmitter tuned at 14.1 MHz. Proton decoupling fields were phase altered to avoid artifacts (97).

RESULTS AND DISCUSSION

Utility of Multiple Pulse NMR to Determine the
Amorphous Fraction of Polyethylene

Polyethylene is considered to consist of at least two
major macroscopic phases. One is a relatively rigid crystal-
line phase and the other an amorphous phase in which the
loose packing of the polymer chain allows for considerable
molecular motion. The present section describes a multiple
pulse NMR technique which provides a unique separation of
the response of the protons in the amorphous phase from the
response of the total proton spin system to a resonant radio
frequency excitation. The advantage of the present technique
for determining crystallinity relative to others (65-69) is
that the measured variable in other methods contains contri-
butions from both phases of the polymer, making an
unambiguous separation of the contributions of the amorphous
and crystalline regions difficult to obtain. In the present
method, the response of the spin system to a nuclear magnetic
resonant perturbation may be arranged to reflect the magneti-
zation due to 1) all protons in the sample, or 2) only
those protons associated with the amorphous phase by proper
adjustment of experimental conditions.

The strong convergence condition of the Magnus formula,
Eqn. (24), is the basis for the separation of the response

of the amorphous phase of polyethylene from the response
of the total system, since the magnitude of internal inter-
actions responsible for broadening in polyethylene in the
crystalline and amorphous phase differ by a factor of 4
(vide infra).

A single pulse excitation experiment on polyethylene
yields a free induction decay (FID) response which exhibits
two distinct damping constants, as shown in Figure 13. The
shorter decay is Gaussian near t = 0 and corresponds to an
effective damping constant, T_2^*, of 12 μsec. The longer
decay appears to be Lorentzian for t>>12 μsec with T_2^* of
48 μsec. These values of T_2^* roughly characterize the spin-
spin relaxation for the crystalline and amorphous phase of
the polymer, respectively. The full width of the NMR
spectrum at half-height, $2\Delta f$, is a measure of the internal
interaction and for a Lorentzian line is related to T_2^* by
$2\Delta f = 1/\pi T_2^*$. For a Gaussian T_2^* is related to the internal
interactions by $2\Delta f = (2\ln 2)^{1/2}/\pi T_2^*$. The corresponding
linewidths in polyethylene are 6.6 and 31 kHz.

One possibility for inferring ratios of crystalline to
amorphous polymer is to associate each fraction with the
initial amplitude of the free induction decay response
associated with that fraction. This technique tends to be
unreliable because the beat pattern, which appears in the
FID between the short and the long decays (cf. Figure 13)
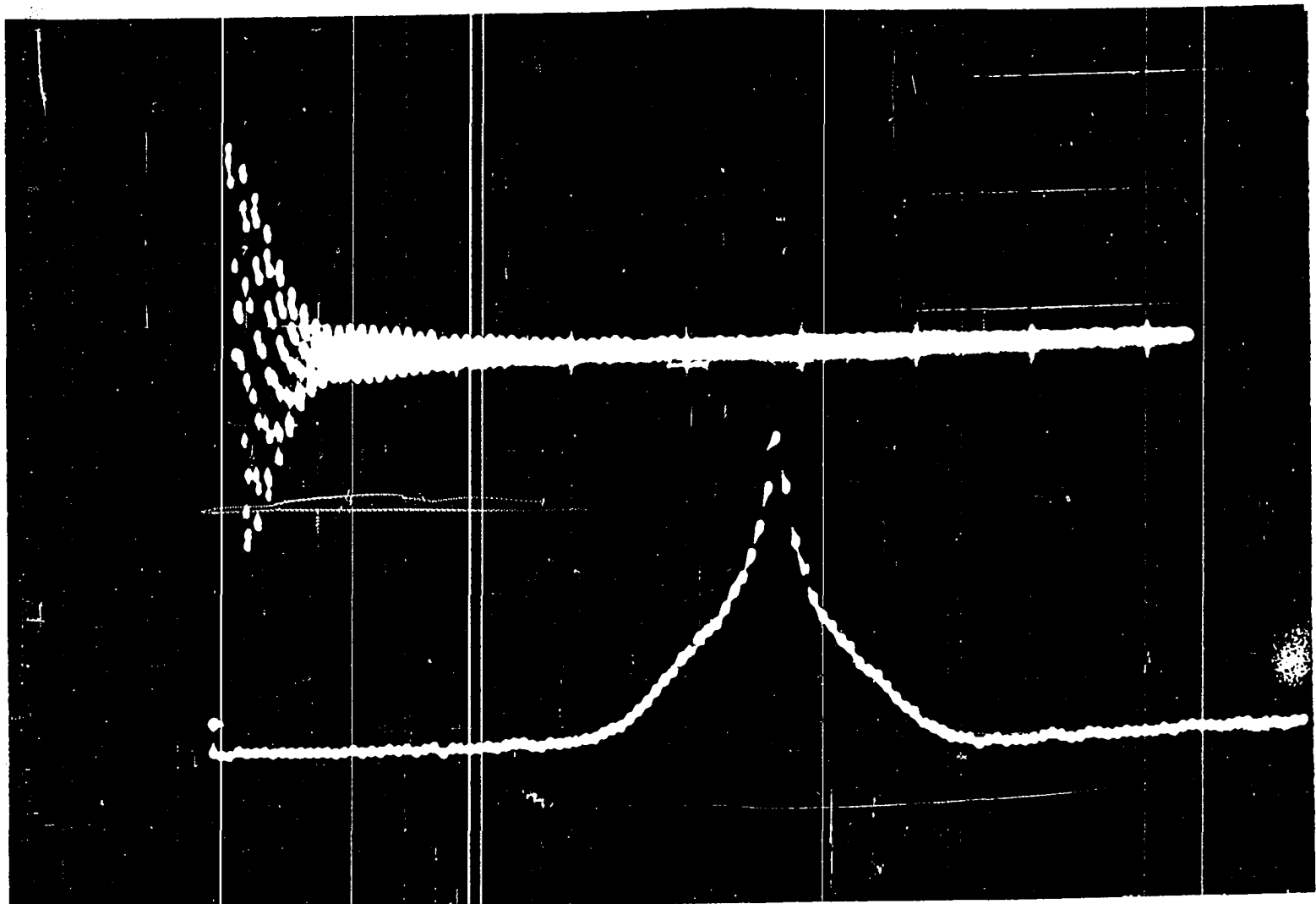
Figure 13. A typical FID and spectrum of polyethylene. The total scan of the decay is 200 µsec with 400 kHz offset. The linewidth of the sharp component of the spectrum is 6.6 kHz.

prevents an accurate evaluation of the initial amplitude of the decay associated with the amorphous portion. This problem may be avoided by sampling the magnetization in such a manner that only the response associated with the amorphous portion is seen. A sufficient condition to allow for this sampling procedure is that the averaging condition be violated for the rigid but not for the amorphous portion of the polymer, and that spin-lattice interactions are small relative to those associated with the broadening.

A multiple pulse sequence designed for removal of homonuclear dipolar broadening, which is the dominant internal interaction in polyethylene, is the MREV-8 sequence, shown in Figure 14 (23,26). The cycle time is 12τ, and the sequence satisfies the cyclic and periodic conditions described above. The initial pulse sequence is preceded by a unique preparation pulse, P_u, as shown in Figure 14. The time from the center of the unique pulse to the beginning of the averaging sequence, which is taken to be t_0, is called τ'. The response of a sample of polyethylene to the MREV-8 sequence is shown in Figure 15. The cycle time of the experiment was 22.8 μsec, which satisfies the averaging condition for both the crystalline and amorphous phases. The initial portion of the decay is found to be Lorentzian, and the envelope of the decay may be extrapolated to $t = t_0$ utilizing a least squares fit of $\ln A(t)$ vs t, yielding the value of the amplitude at t_0, $A(t_0)$.
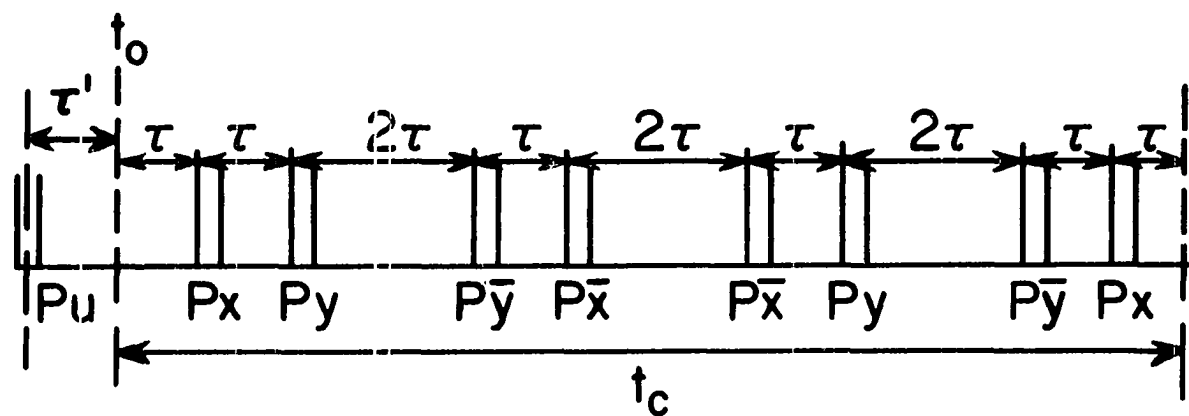
Figure 14. The rf pulse sequence for homonuclear decoupling is shown. All pulses are $\pi/2$ with the phase indicated. Pu is a preparation pulse applied prior to the first eight pulse sequences.
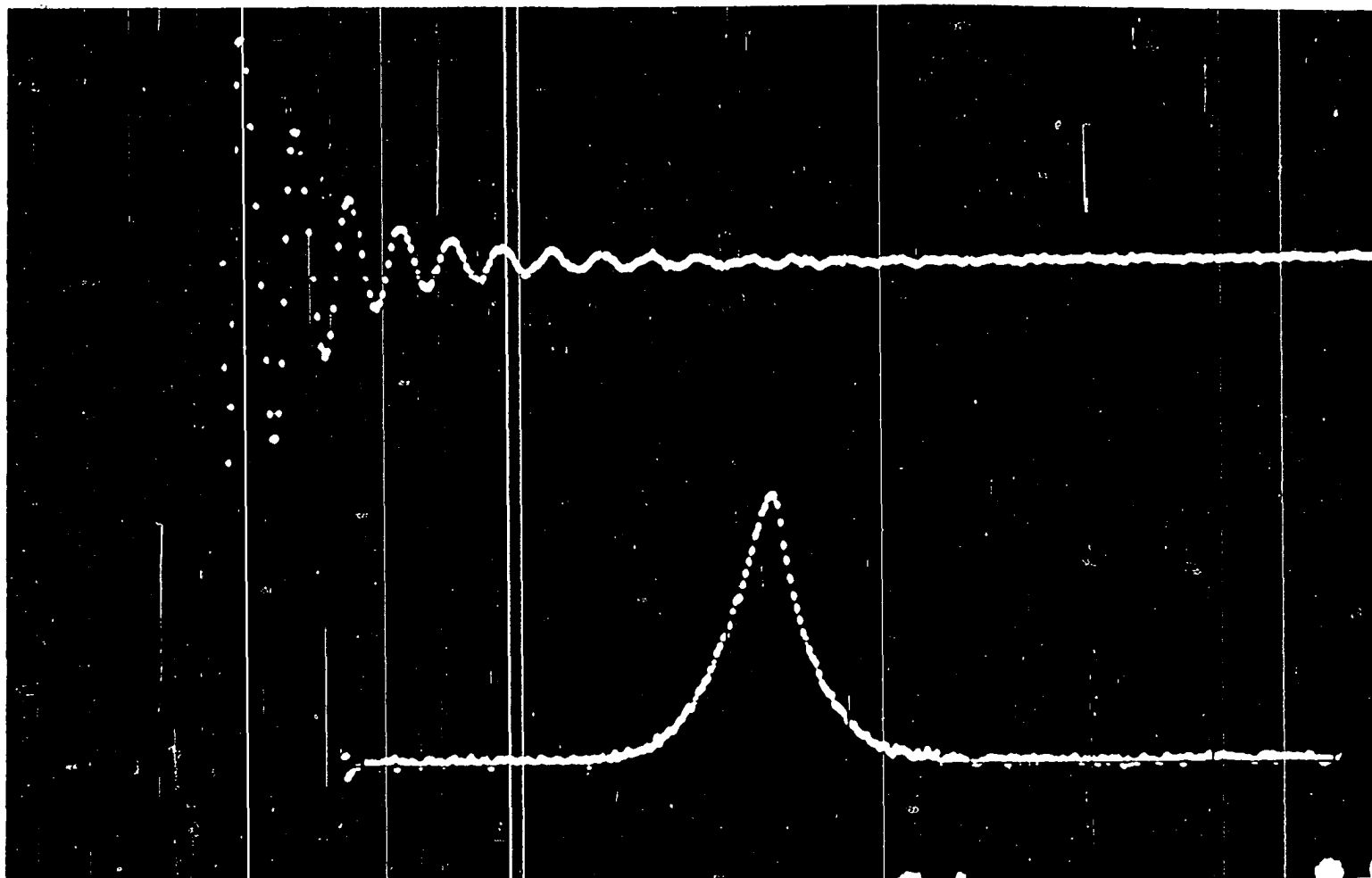
Figure 15.   Response of polyethylene to the MREV-8 multiple pulse sequence.
Top: Total scan of 16 msec shown of decay
Bottom: Fourier transform spectrum with 150 Hz linewidth

For the purpose of spin counting under the MREV-8 sequence, the initial amplitude at the center of the preparation pulse must be determined (72) in order to account for transverse relaxation during τ'. This is accomplished by determining the initial amplitude of the magnetization under the MREV-8 sequence, $A(t_0)$, as a function of τ', and extrapolating to $\tau' = 0$ (vide infra).

To infer the total number of protons in the sample from this method, a cycle time of 22.8 μsec was used. Since the decay of the magnetization after the unique pulse was found to be roughly Gaussian for times short compared to 12 μsec, the assumption was made that $\ln A(t_0)$ would be linear in $(\tau')^2$. The validity of this assumption is shown in Figure 16. The value of $A(t_0)$ evaluated at $\tau' = 0$ was found by extrapolating this plot to zero. The number of protons associated with the value of $A(t_0)$ thus referred was determined by comparison with the initial decay of a weighed, spherical water sample measured under exactly the same conditions as was the polyethylene. Care was taken to insure that both water and polyethylene were both in the homogeneous H_1 field. The decay of the initial amplitude of the water sample during the times τ' was, of course, negligible, since T_2^* of the water was always greater than 30 msec. The number of protons thus inferred for the polyethylene agreed with the stoichiometry $(CH_2)_n$ to within
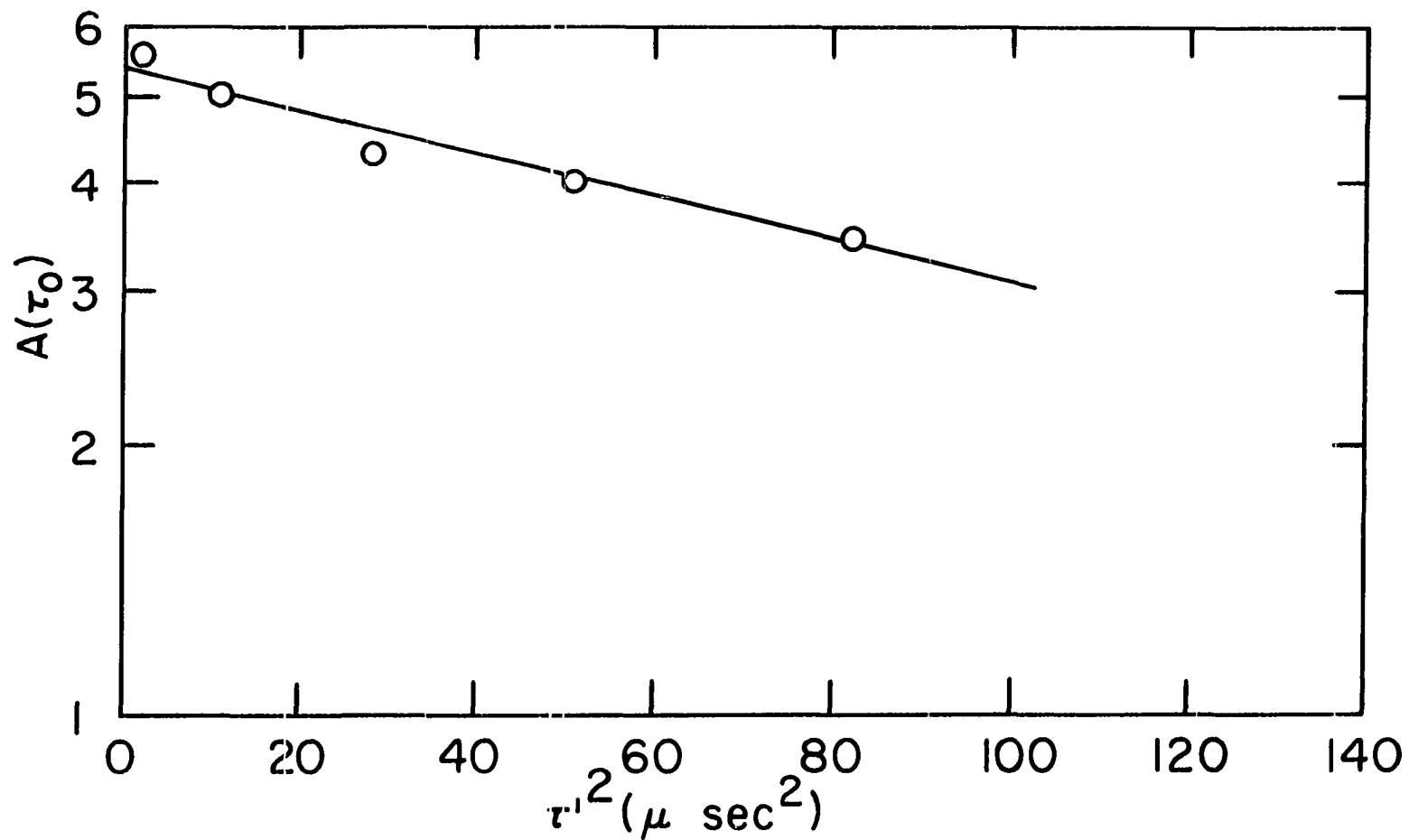
Figure 16. The value of the magnetization at t_0 (see Figure 2) is plotted as a function of time after the unique pulse squared $(\tau')^2$ for $t_c = 22.8$ μsec. The value of $A(t_0)$ at time zero may be used to infer the total number of protons in the sample.

1.2%, and agreed with the value inferred from spin counting utilizing the initial amplitude of a FID (98) to within 0.4%.

To uniquely observe the response of the amorphous fraction of the polymer, the cycle time of the pulse sequence was increased to a value for which Eqn. (24) was satisfied for the amorphous, but not for the crystalline fraction. In order to determine the cycle time which satisfied these conditions, an approximate value for the number of protons counted, as inferred from $A(t_0)$, was determined as a function of cycle time. The expectation was that for a cycle time which satisfied Eqn. (24) for both amorphous and crystalline regions, the number of protons counted would not vary with t_c. As the value of t_c became long compared to that needed for the averaging condition for the rigid phase, the protons counted would decrease with increasing t_c. At the value of t_c for which no averaging was accomplished for the rigid phase, but dipolar interactions in the amorphous phase were averaged to zero, the number of protons counted would again be relatively independent of t_c. The results of protons counted as a function of t_c is shown in Figure 17. The number of protons counted as shown in Figure 17 should not be taken to accurately represent the number of protons in the amorphous phase in particular, since the accounting for the decay after the unique pulse was not accomplished as described above. Rather, a rough accounting of the decay
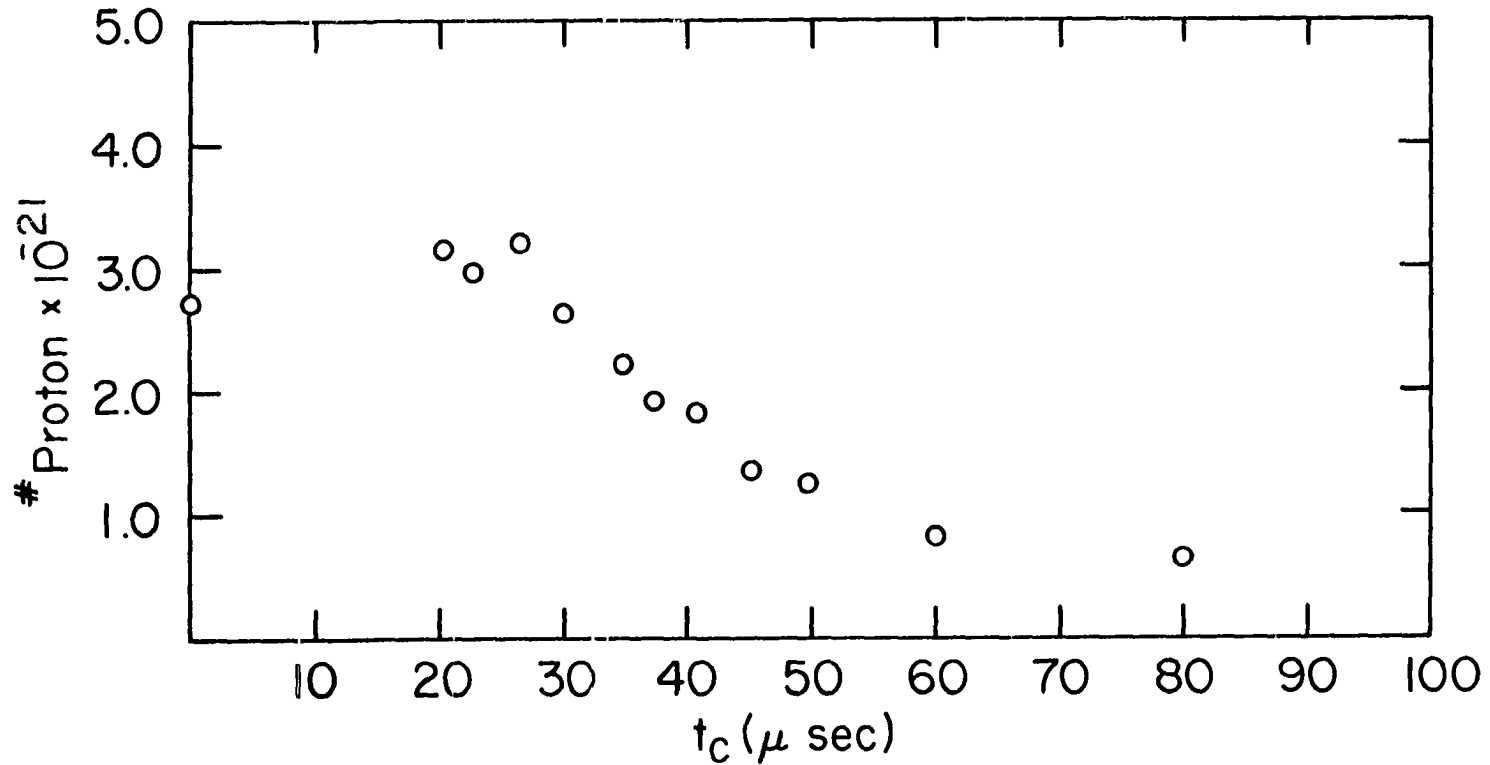
Figure 17. The "estimated" number of protons is shown as a function of cycle time. This shows the effect of the averaging condition (Eqn. (12)). The value plotted at t_c equal zero represents the correct value for the total number of protons in the sample.

after the unique pulse was made by simply assuming it to be
Gaussian, with time constant 12 μsec, and correcting the
value obtained at t_0 back to the center of P_u. The important
point that Figure 17 illustrates is that as the cycle time
increases, the protons counted decrease, and above a cycle
time of 60 μsec, the number of protons counted remains
constant. Sixty μsec was therefore taken to be the value at
which Eqn. (24) is satisfied for the amorphous but not the
crystalline phase in the polyethylene sample used in these
experiments. In the measurements used to obtain the plot
in Figure 17, the interval τ', over which the decay was
roughly corrected, was $t_c/12$, which is the minimum time
interval between pulses in an MREV-8 pulse experiment, as
can be seen from Figure 14. Clearly, as t_c becomes shorter,
the correction for decay during τ' becomes less important.
In fact, as the agreement between points at t_c = 22.6 μsec
and the point at t_c = 0, obtained by total spin counting
utilizing the initial amplitude of a FID response to a
single pulse experiment, demonstrates, all of the spins are
being accurately counted at the shortest cycle times, with
no correction to the measured $A(t_0)$ as a function of τ'
needed.

To count spins associated with the amorphous phase, a
cycle time of 60 μsec was used, the value of $A(t_0)$ determined
as a function of τ', and the results extrapolated to τ' = 0

assuming Lorentzian behavior, as shown in Figure 18. The initial value of the magnetization so determined was compared to that of a spherical water sample, measured under exactly the same conditions of MREV-8 cycle time and offset, with care taken to insure that all of the water was in a uniform H_1 field.

From the number of protons counted t_c = 22.6 μsec compared to that counted at t_c = 60 μsec, a fraction of crystallinity f_{xtl} = 0.73 ± 0.02 was determined. This value compares to f_{xtl} inferred from density and heat of fusion of 0.73 and 0.63, respectively.

Five polyethylene samples of various crystallinities were examined using this technique. From the number of protons counted at t_c = 22.6 μsec compared to that counted at 60 μsec, a fraction of crystallinity was determined. The fraction crystallinity determined from this method is compared with crystallinities determined using FID, heat of fusion and density measurements (99) in Figure 19.

High Resolution NMR in Randomly Oriented Solids
with Homonuclear Dipolar Broadening: CRAMPS

The theoretical basis for combined multiple pulse sample spinning experiments has been developed in a previous section of this dissertation. It is the purpose here to give two examples which will illustrate the power of the
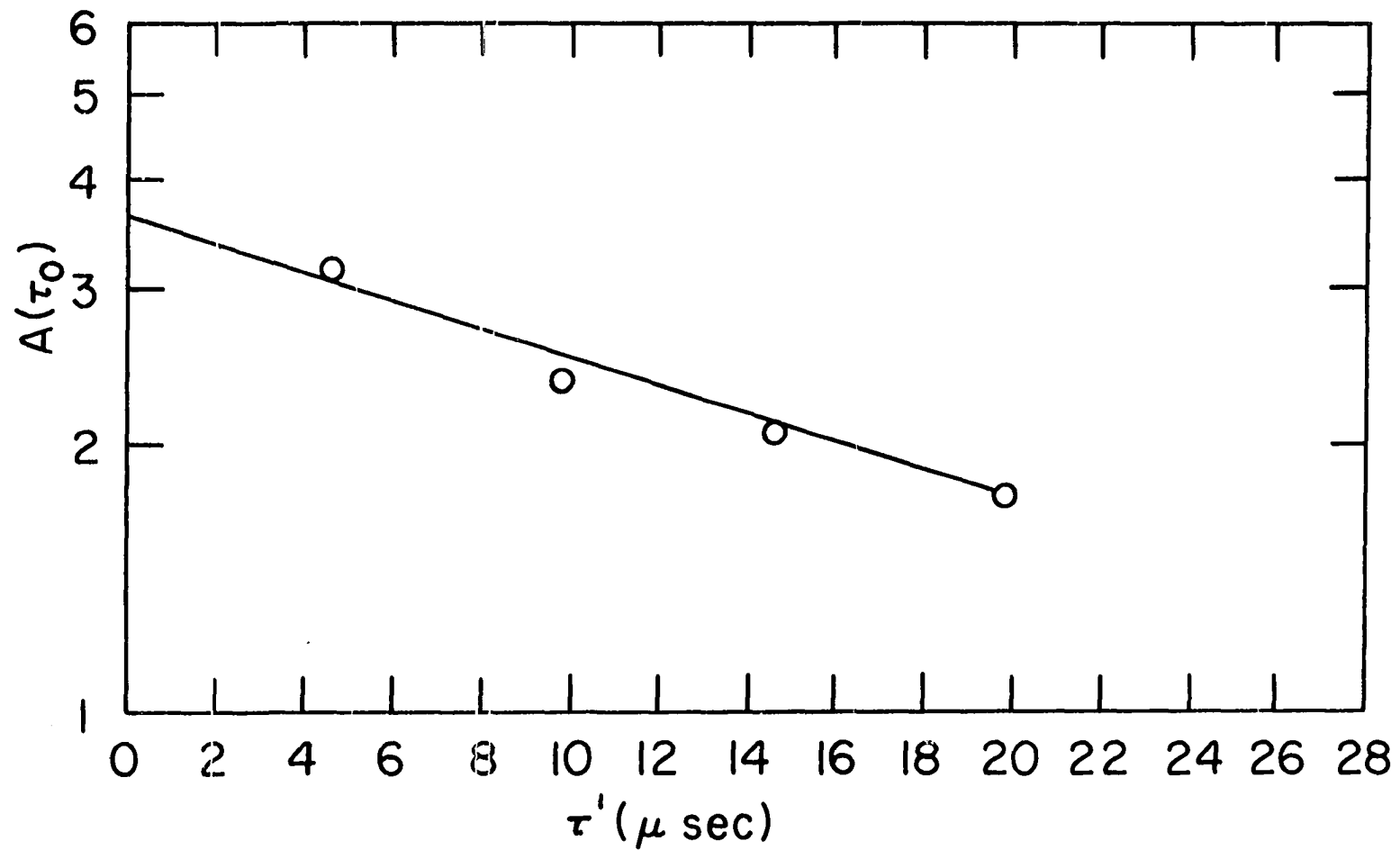
Figure 18. At a cycle time of 60 μsec, the value of the magnetization at t_0 is plotted as a function of τ'. The value at time zero may be used to imply the number of protons in the amorphous phase of the polyethylene.

f_{XTL}

1.00

0.90

0.80

0.70

0.60

0.50

DENSITY · FID · MREV-8

DENSITY · FID · MREV-8 · ΔHfus

DENSITY · FID · MREV-8 · ΔHfus

DENSITY · FID · MREV-8 · ΔHfus

DENSITY · FID · MREV-8 · ΔHfus

AMES LAB   DOW #3   DOW #2   DOW #1   DOW #4
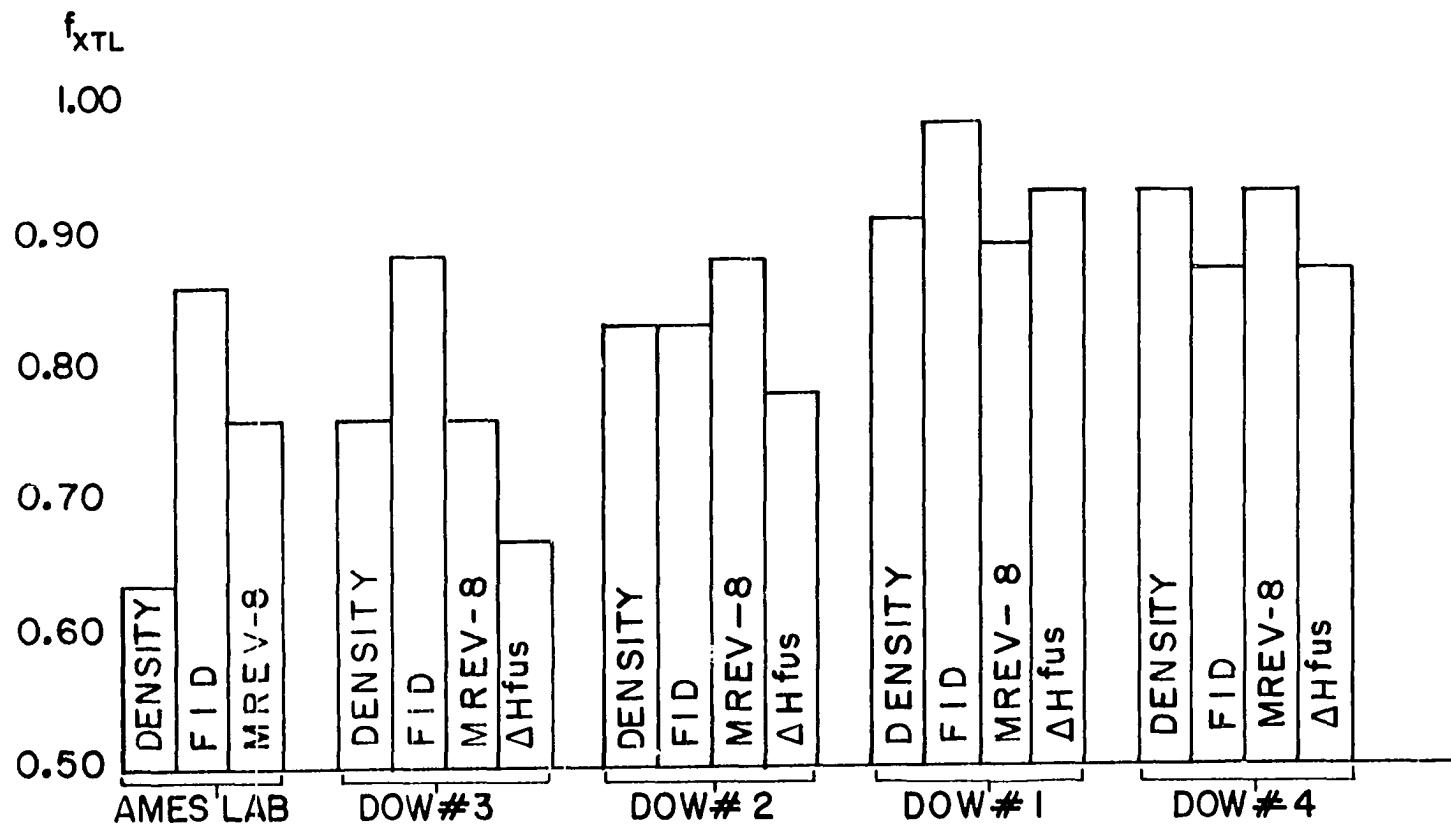
Figure 19.   The crystallinity of five polyethylene samples have been determined
using FID spin counting, heat of fusion, density, and multiple
pulse spin counting.

technique for obtaining high resolution NMR spectra of solids. In addition, some prospects for further experiments will be discussed.

The total average Hamiltonian under CRAMPS, including resonance offset $\Delta\omega$, finite pulse width, $t\omega$ and rf in-homogenieties, ε_i experienced by the ith spin is given by

$$\bar{H} = + \frac{\delta\omega}{3}\{[1 + \frac{6t\omega}{t_c} (\frac{4}{\pi} - 1)](I_z + I_x) - \sum_i \varepsilon_i I_{zi}\}$$

$$+ \frac{1}{3}\sum_i \frac{1}{3} T_r \underline{\underline{\sigma}}_i\{1 + \frac{6t\omega}{t_c} (\frac{4}{\pi} - 1)(I_{zi} + I_{xi})$$

$$- \sum_i \varepsilon_i I_{zi}\}\omega_o \qquad (51)$$

The chemical shift scaling factor is roughly $\sqrt{2}/3$. This factor is experimentally determined from the spectrum of a water sample taken with successive scans of 1, 2, 3 and 4 kHz off resonance under the MREV-8 sequence and found to be 0.55. The average Hamiltonian in Eqn. (51) assumes that we have met the condition for motional averaging. The dipolar interaction vanishes to first order. Figure 20 shows the natural linewidth of the ^{19}F resonance of KEL-F (trademark, 3M Co., polymerized $FClC=CF_2$) under a single pulse free induction decay is 30 kHz. Figure 21 shows the increase in resolution obtained by application of the REV-8 pulse sequence. The total range of chemical shifts in this sample is roughly 3 kHz. Figure 22 shows the spectrum
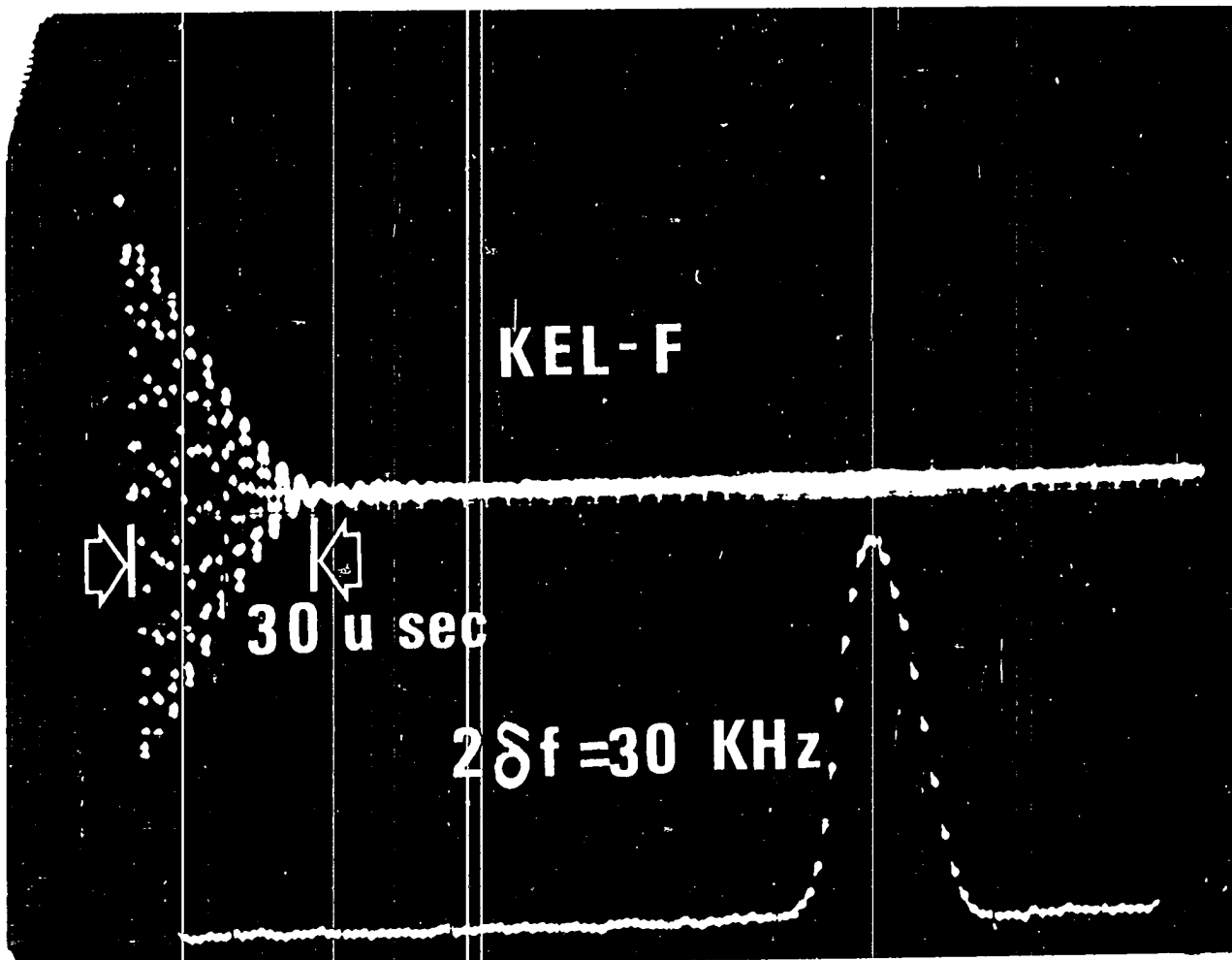
Figure 20. The response of KEL-F to a single pulse experiment 200 µsec of the decay is shown. The linewidth is 30 kHz.
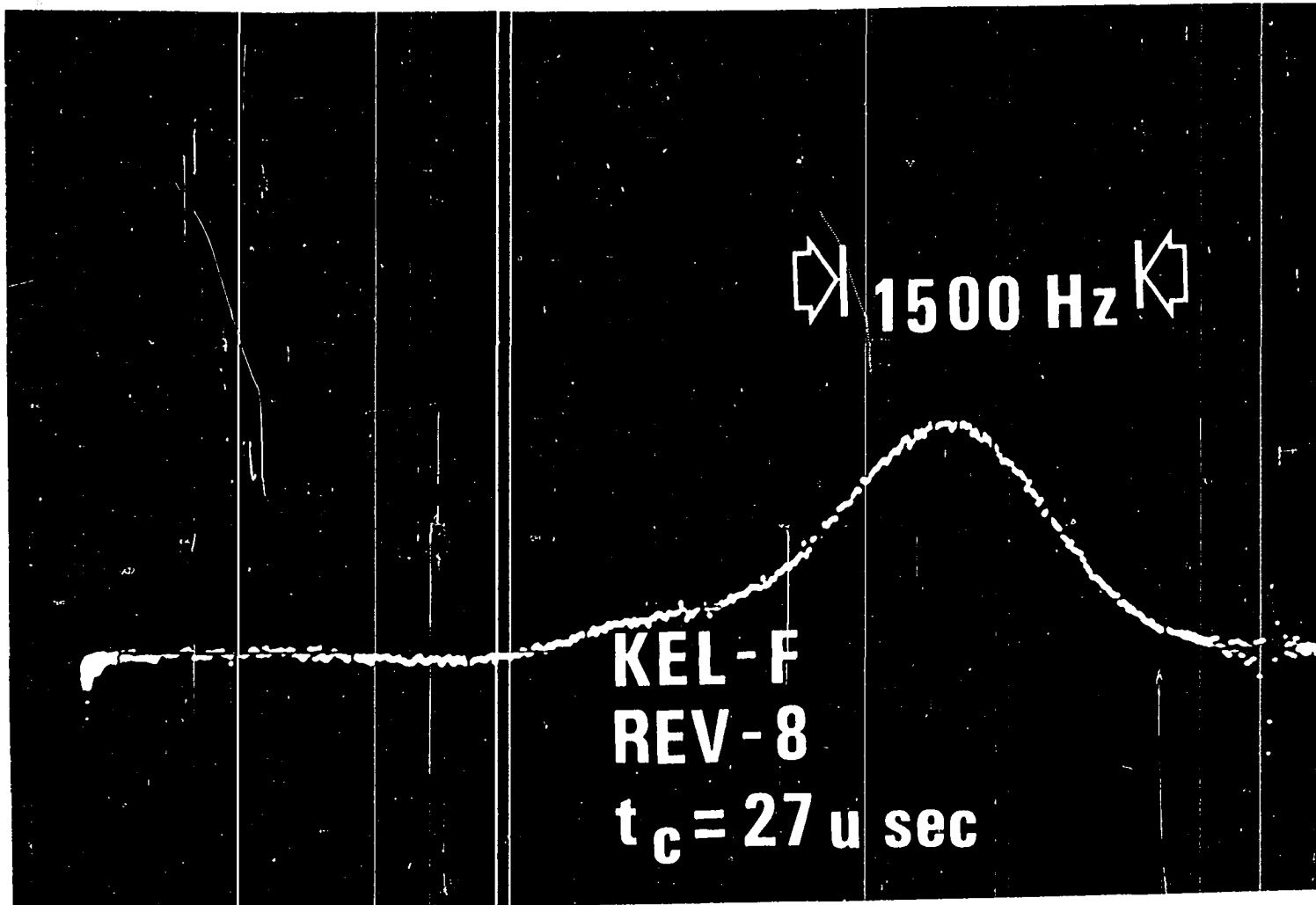
Figure 21. ^{19}F spectrum of KEL-F under MREV-8, cycle time is 27 μsec.
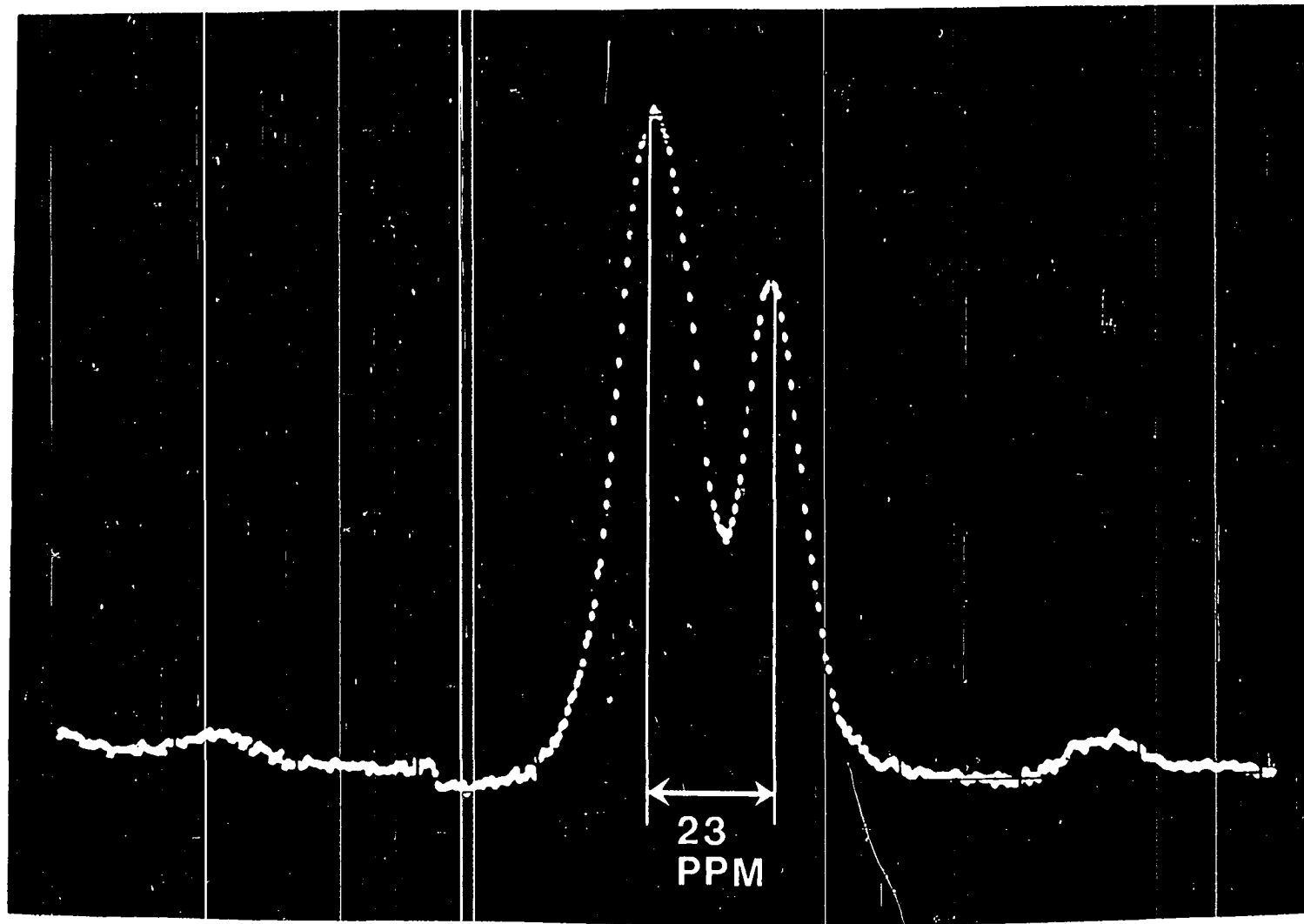
Figure 22. ^{19}F of KEL-F under combined MREV-8, t_c = 27 μsec, and magic angle spinning at 2.5 kHz.

obtained utilizing both the MREV-8 sequence for removal of homonuclear dipolar interactions, and magic angle rotation at 2.5 kHz for removal of both homonuclear dipolar broadening and chemical shift anisotropies. Residual linewidths could be associated with chemical shift dispersion due to differing stereochemical environments of the fluorine nuclei (100). The two peaks at a separation of 23 ppm with component ratios of 2:1 are identified as fluorines bound to the same carbon, and a carbon bound to a chlorine, respectively. The peak corresponding to the CFCl fluorine is at high field relative to that of the CF_2 fluorines. The splitting and relative shifts are the same as those found for KEL-F in 3,3'-bisfluoromethylphenyl by Tiers and Bovey (101).

The natural linewidth of the ^{1}H resonance in 4,4'-dimethylbenzophenone under a single pulse free induction decay is 25 kHz. Figure 23 shows the increase in resolution obtained by the application of the MREV-8 sequence. The cycle time of the multiple pulse sequence was 33.6 μsec. Figure 24 shows the spectrum obtained under CRAMPS with a spinning frequency of 2.0 kHz. While not as dramatic as the ^{19}F resonance in KEL-F, Figure 24 shows the ability of the technique, and suggests that higher magnetic field (e.g., 6T) would make CRAMPS a powerful tool in the study of proton resonances in solids such as coals. As a comparison, Figure 25 is a high resolution NMR spectrum of 4,4'-dimethylbenzophenone in solution.
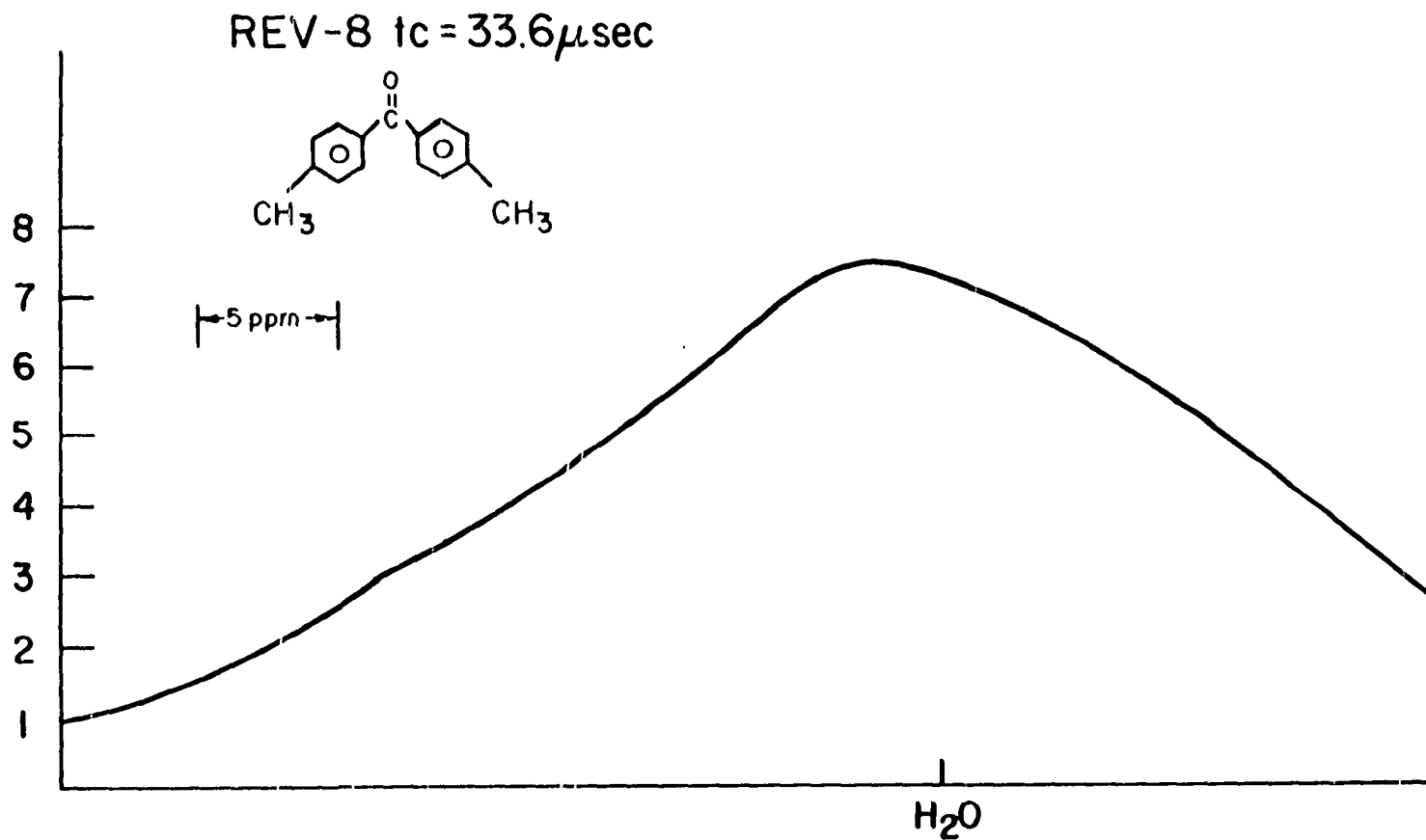
Figure 23. ^1H spectrum of 4,4'-dimethylbenzophenone. MREV-8 cycle time is 33.6 µsec.
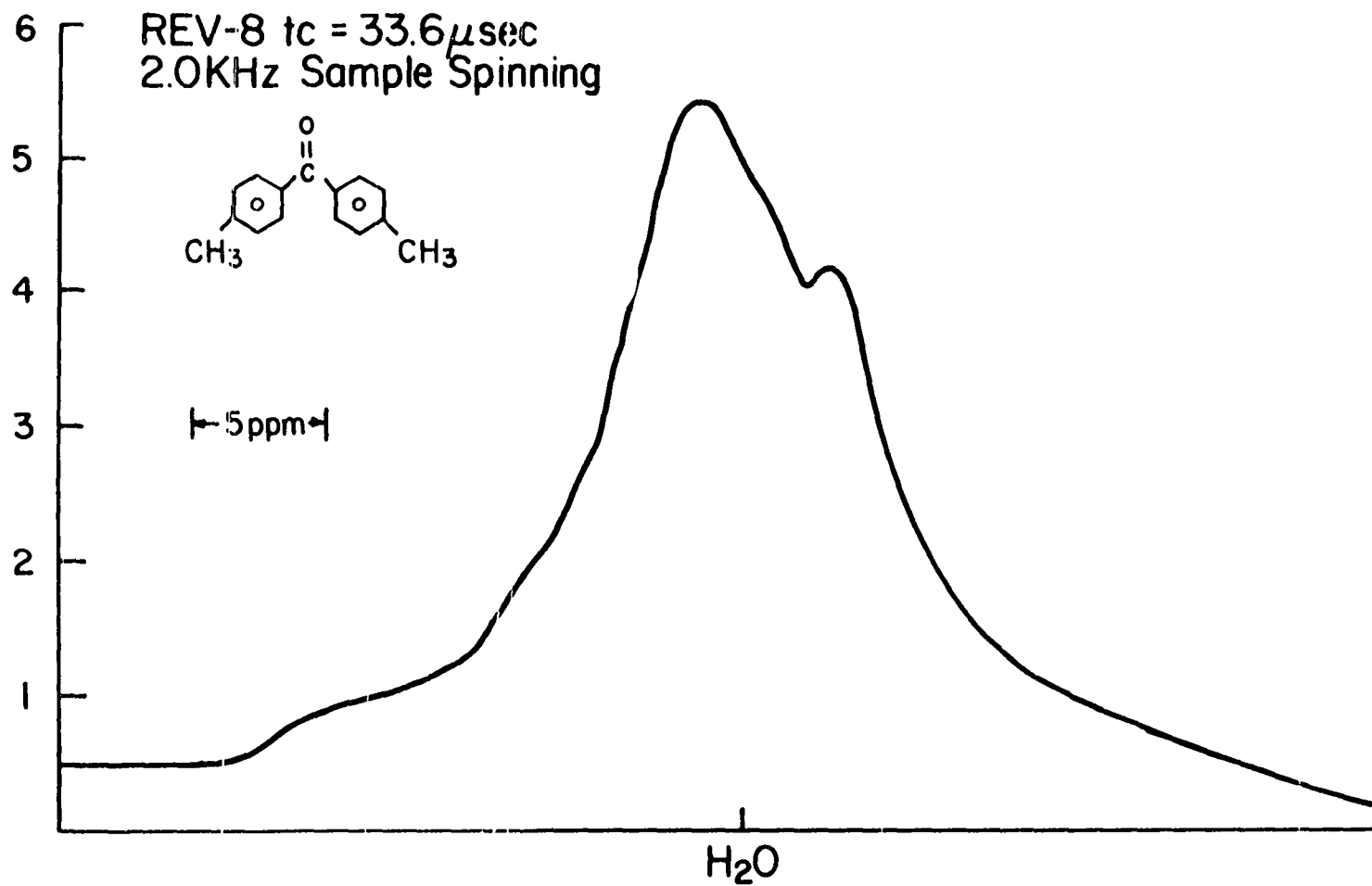
Figure 24. ^{1}H spectrum of 4,4'-dimethylbenzophenone under combined 2.0 kHz "magic angle" spinning and MREV-8 sequence, t_c is 33.6 μsec.
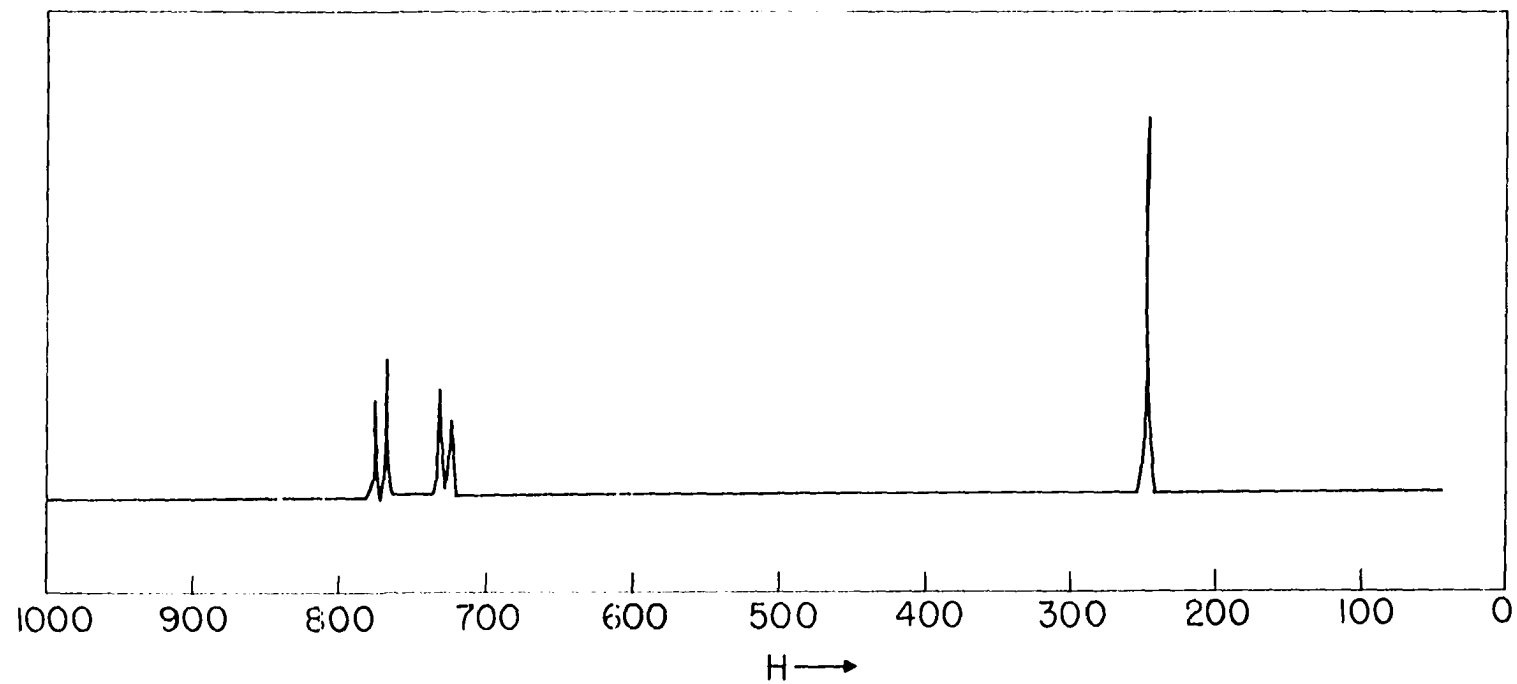
Figure 25. ^{1}H spectrum of 4,4'-dimethylbenzophenone in solution.

In an attempt to calculate proton aromaticities in coals CRAMPS spectra were obtained from five vitrain coals. As will be discussed in a later section, multiple pulse techniques reduce the NMR linewidth to 700 Hz. This residual broadening makes it impossible to obtain the necessary chemical information. Unfortunately, the CRAMPS spectra shown in Figures 26-30 have not provided sufficient narrowing to determine the aromatic and nonaromatic components of the spectra. This broadening, which spans the entire range of proton chemical shifts, is due to the variety of chemical environments present in the coal sample. It is probable that higher magnetic fields would make possible the separation of the aromatic and nonaromatic components.

Another interesting prospect of the combined sample spinning multiple pulse techniques is experiments that would allow for the determination of the components of chemical shift tensors in systems containing a number of chemically different nuclei. In general, these components would be unavailable under a multiple pulse experiment alone due to overlapping chemical shift anisotropies. These experiments, while lacking complete theoretical development, utilize both fast and slow sample spinning techniques and to date have only dealt with systems experiencing heteronuclear dipolar broadening (102-104). Eqn. (39) describes the general chemical shift Hamiltonian of a system being rotated at a
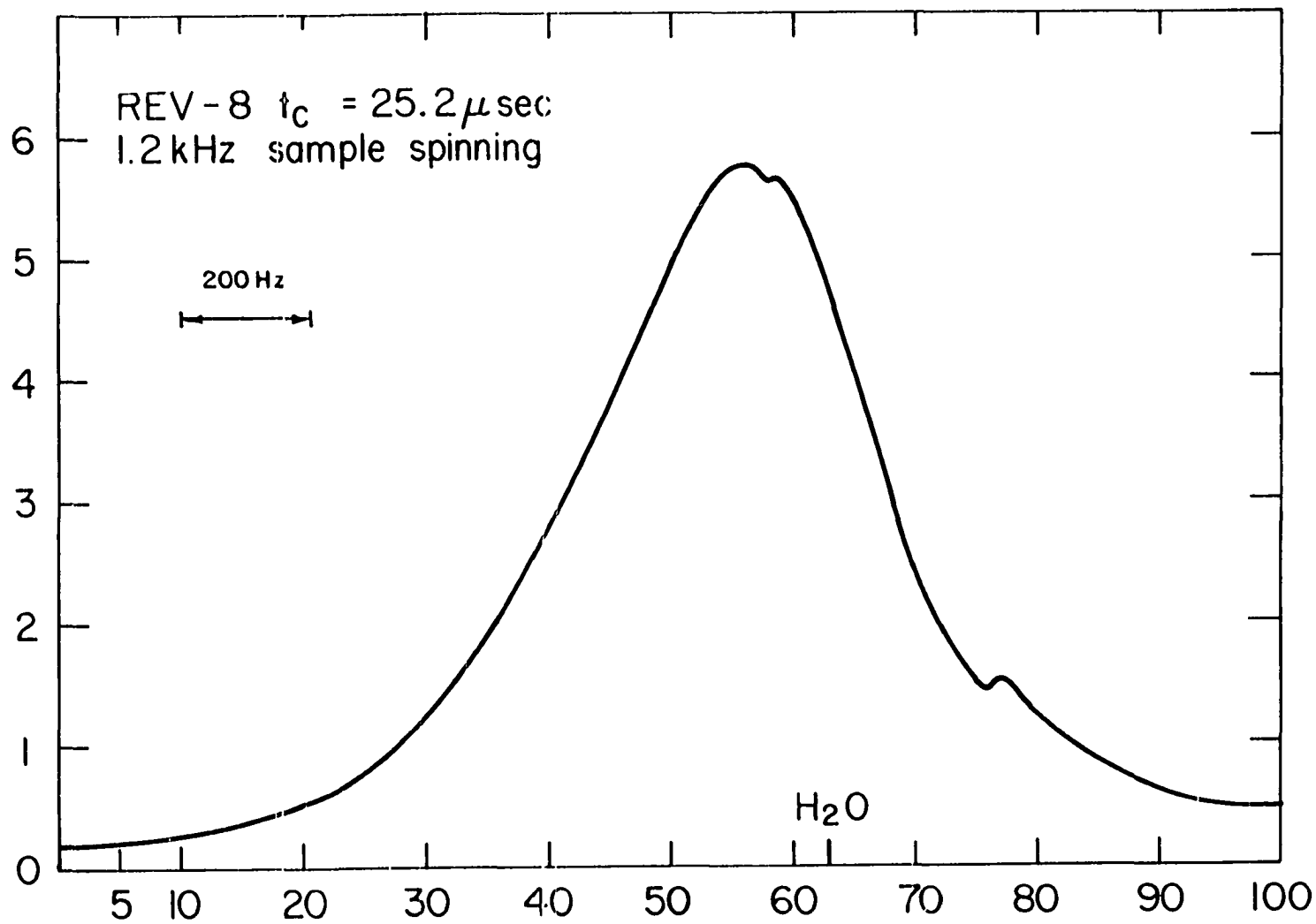
Figure 26. ^1H spectrum of Star vitrain under CRAMPS. t_c is 25.2 μsec.
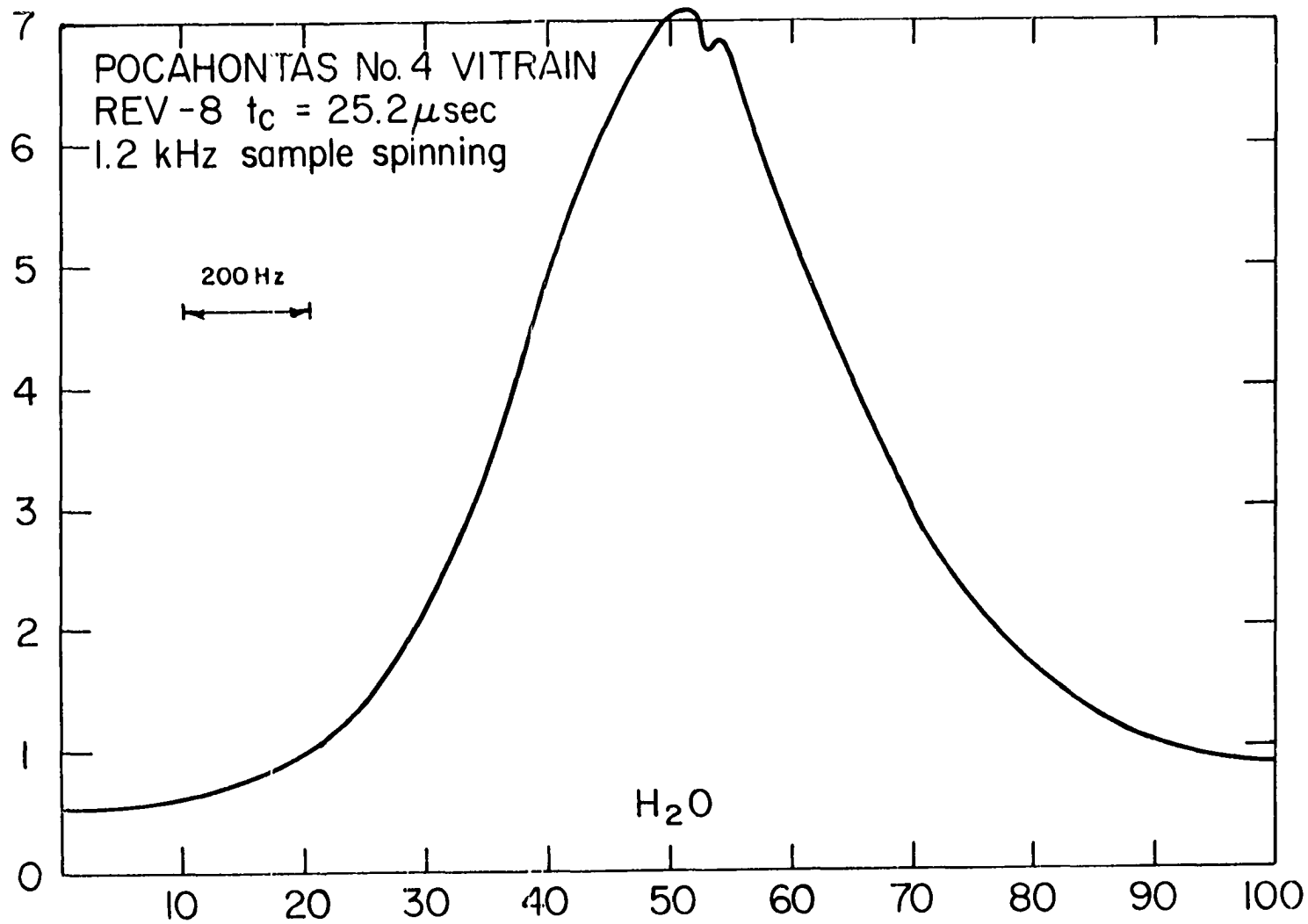
Figure 27. ^1H spectrum of Pocahontas No. 4 vitrain under CRAMPS. t_c is 25.2 μsec.

REV-8 t_C = 25.2 μsec
1.2 kHz sample spinning

200 Hz

H_2O
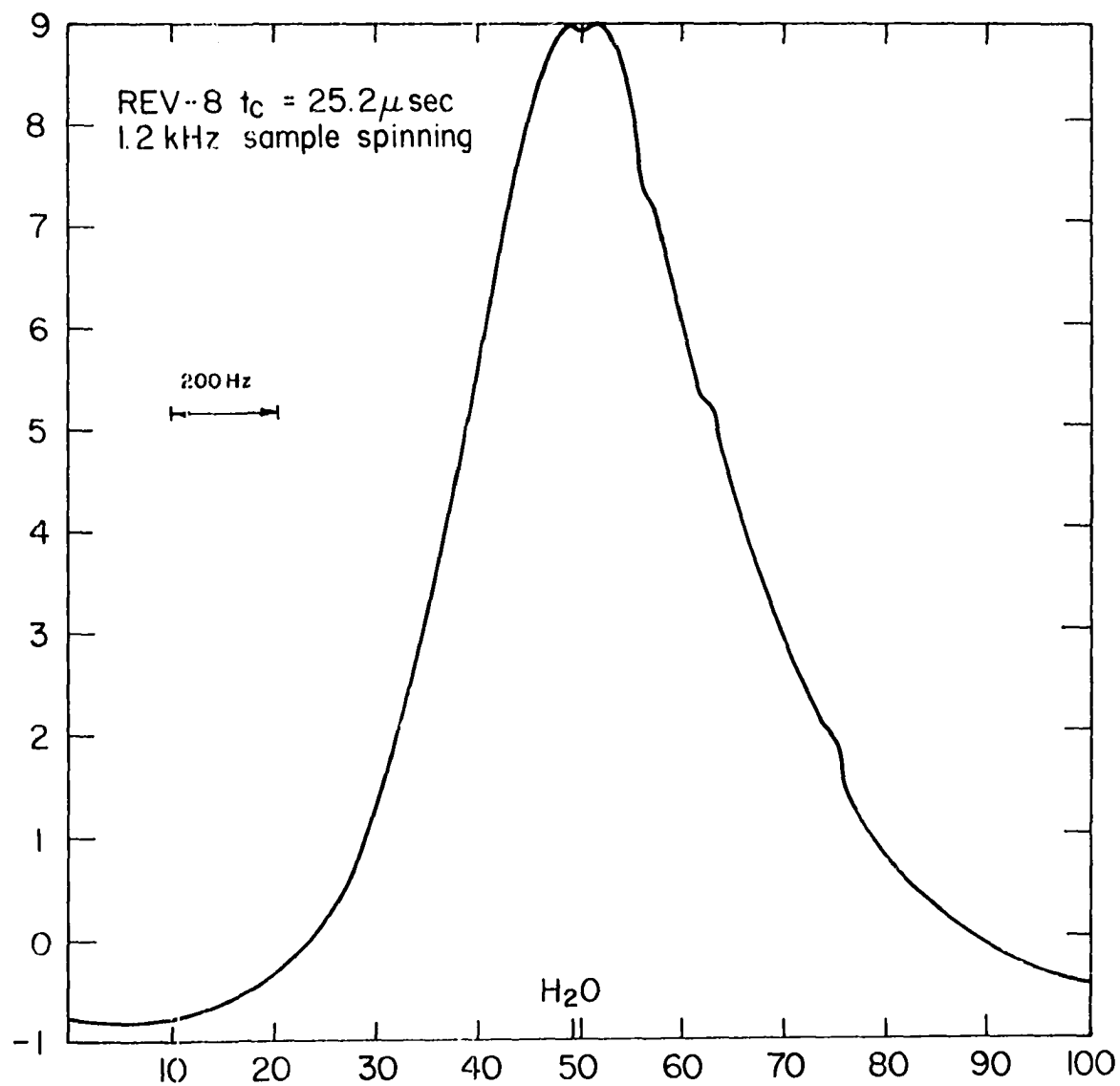
Figure 28. ^{1}H spectrum of Powellton vitrain under CRAMPS. t_c is 25.2 μsec.

REV-8 t_c = 25.2 μsec
1.2 kHz sample spinning

200 Hz

H_2O
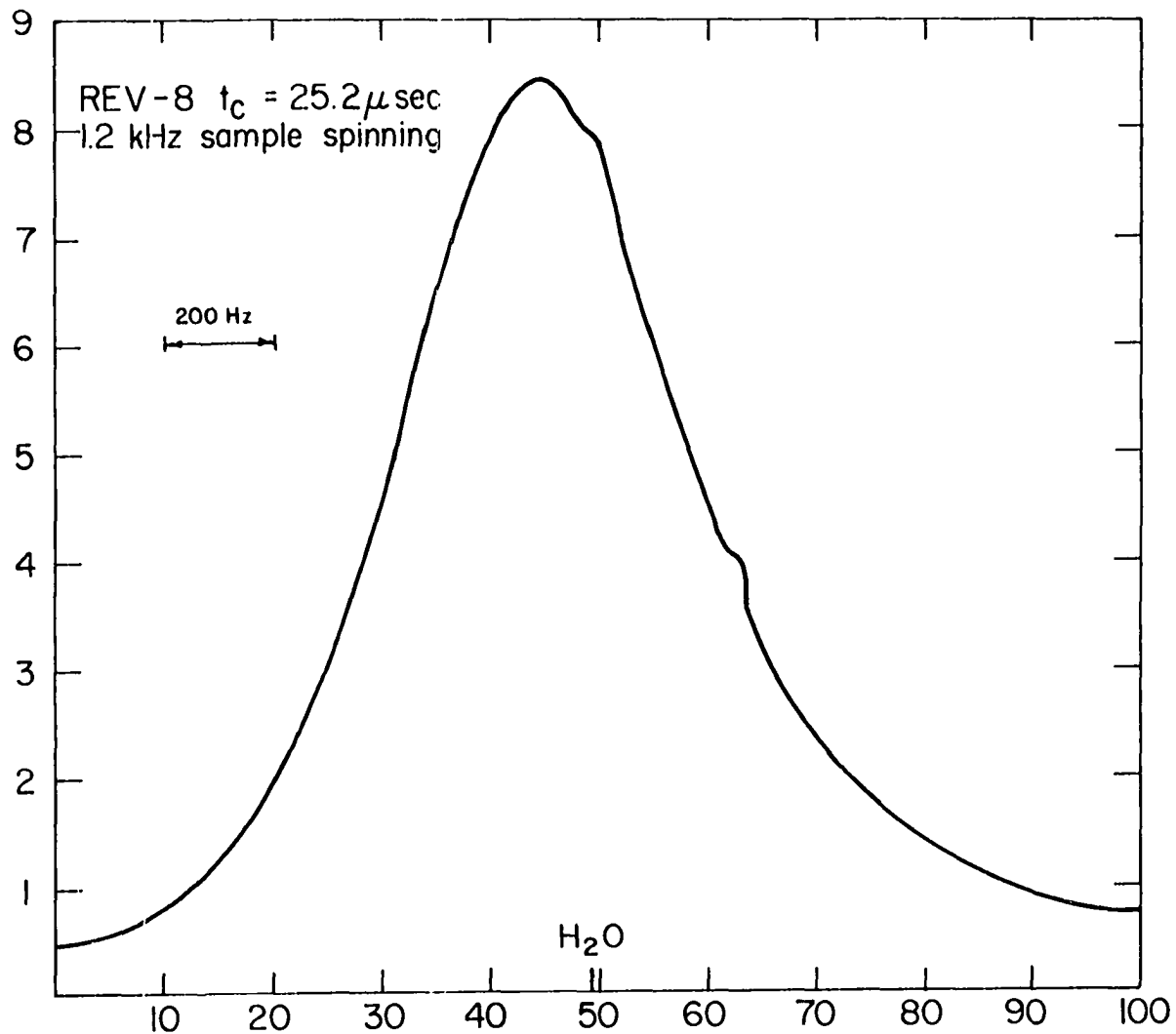
Figure 29. ^1H spectrum of Upper Mich vitrain under CRAMPS. t_c is 25.2 μsec.
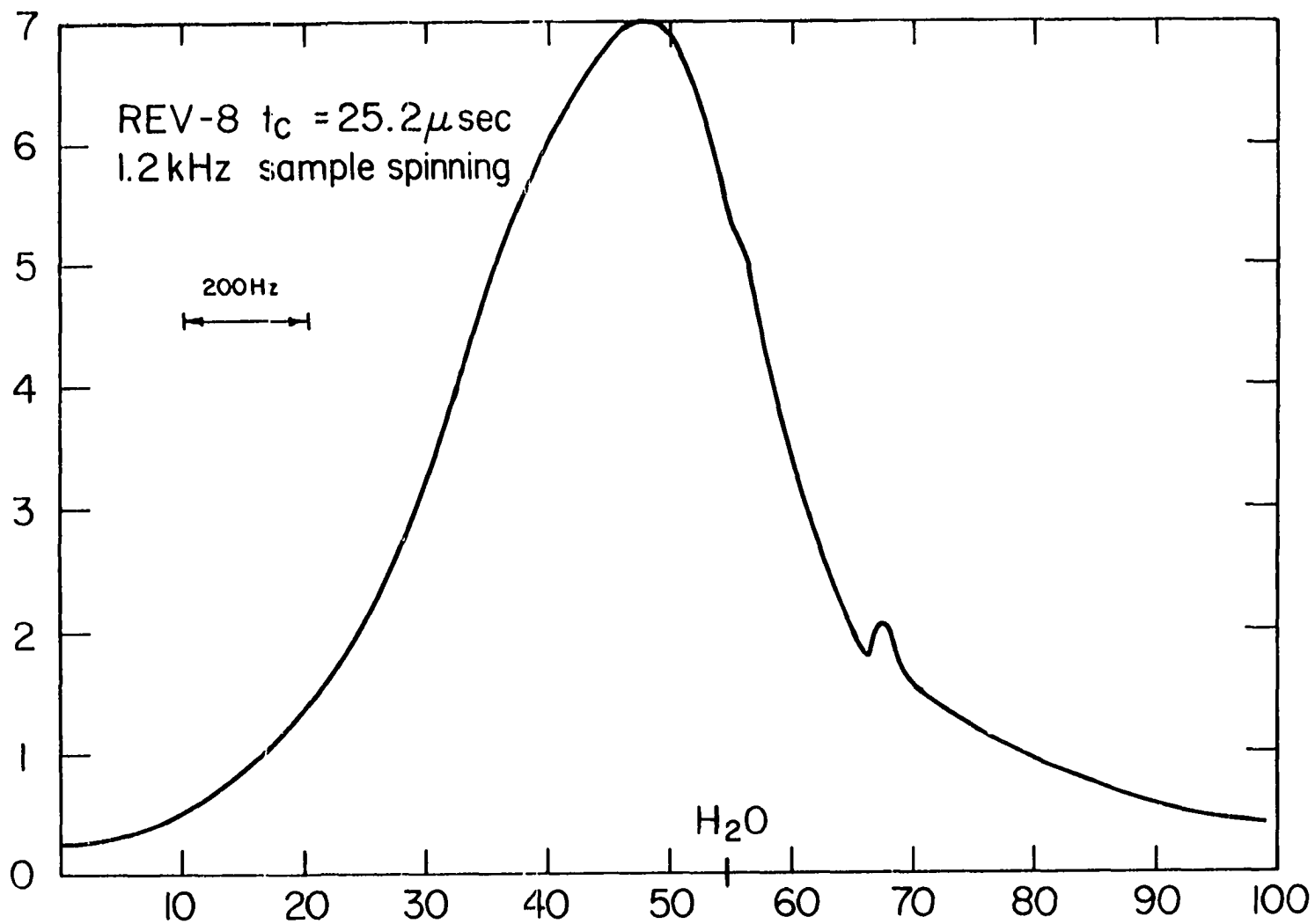
Figure 30. ^1H spectrum of Lovilia vitrain under CRAMPS. t_c is 25.2 μsec.

frequency ω_r about an axis inclined at an angle θ from the magnetic field. Under the conditions of motional averaging and θ equal to 54.7°, the anisotropic chemical shift power spectrum reduces to a symmetric lineshape value as shown by Eqn. (48). If, however, θ is something other than the magic angle, the lineshape retains characteristics of the chemical shift anisotropy but is scaled in a manner governed by the A term in Eqn. (39). To illustrate this point, Figure 31 shows a typical proton powder spectrum with an anisotropy of 200 ppm. A Lorentzian broadening function of 175 Hz has been built into the spectrum to account for spin-lattice relaxation and instrumental effects. Under magic angle spinning (in the "fast" limit) the tensor collapses onto its isotropic center as illustrated in Figure 32. Figures 33 and 34 show spectra generated with θ equals 90° and 45°, respectively. These two spectra show that while the linewidth is reduced it is still dependent upon the anisotropy. These types of measurement would have application to systems with several types of nuclei whose resonance lines could be separated under combined spinning and multiple pulse allowing for the determination of the individual tensor components.
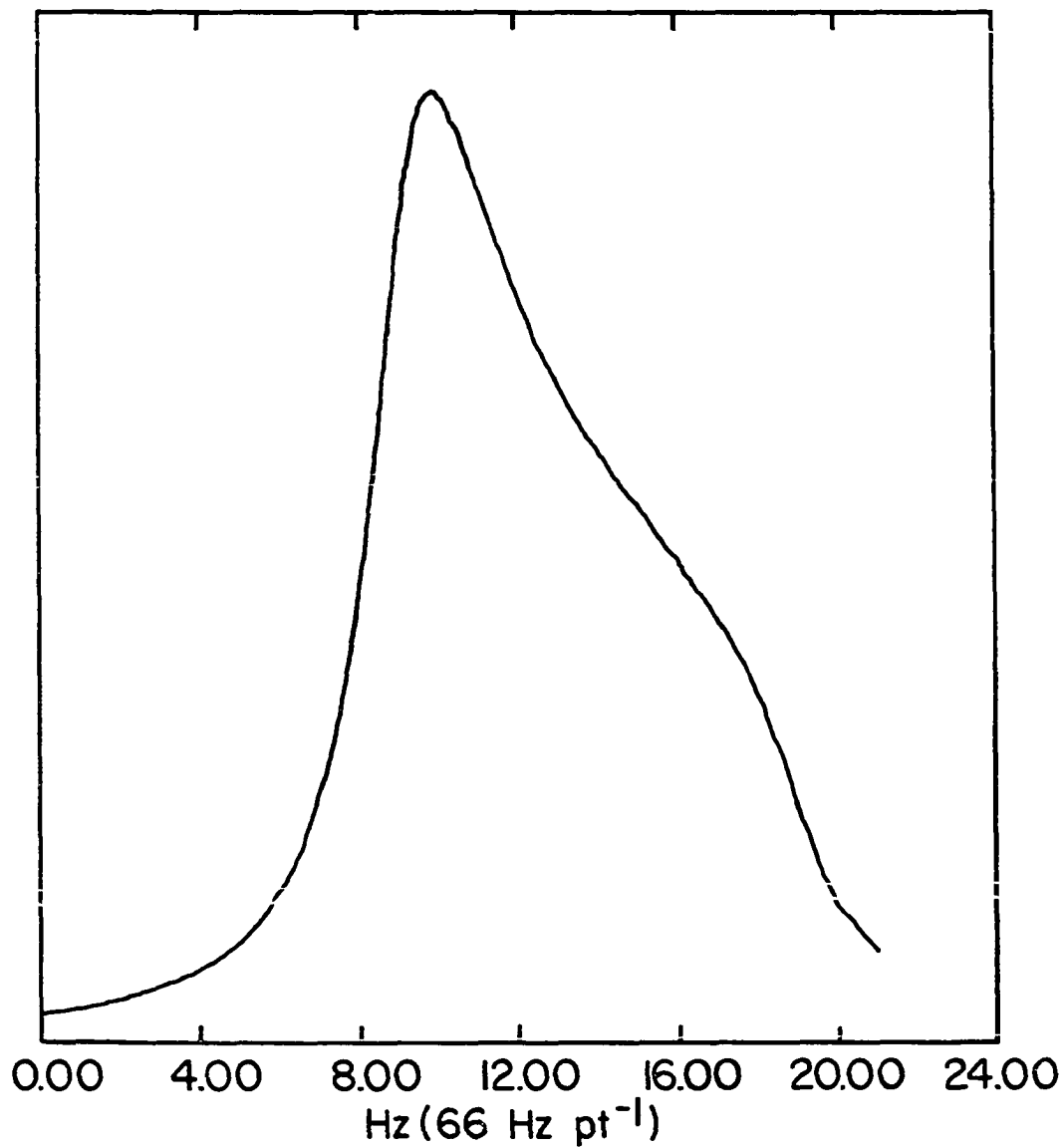
Figure 31. A typical ^{1}H powder pattern spectrum with axial symmetry. The chemical shift anisotropy is 20 ppm.
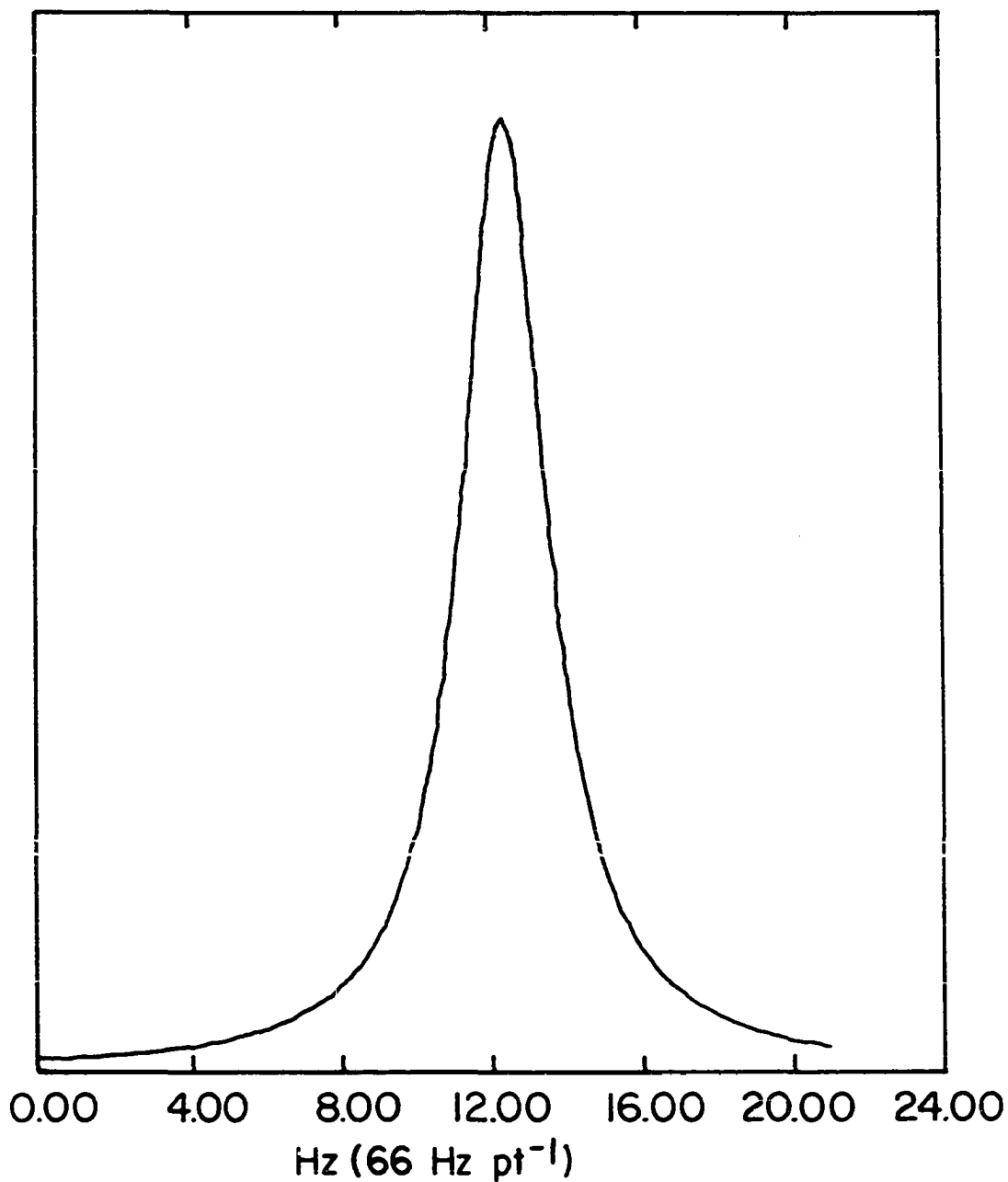
Figure 32.   The NMR spectrum under magic angle spinning.
The Lorentzian lineshape is centered about the
isotropic value $\bar{\sigma}$ of the tensor.
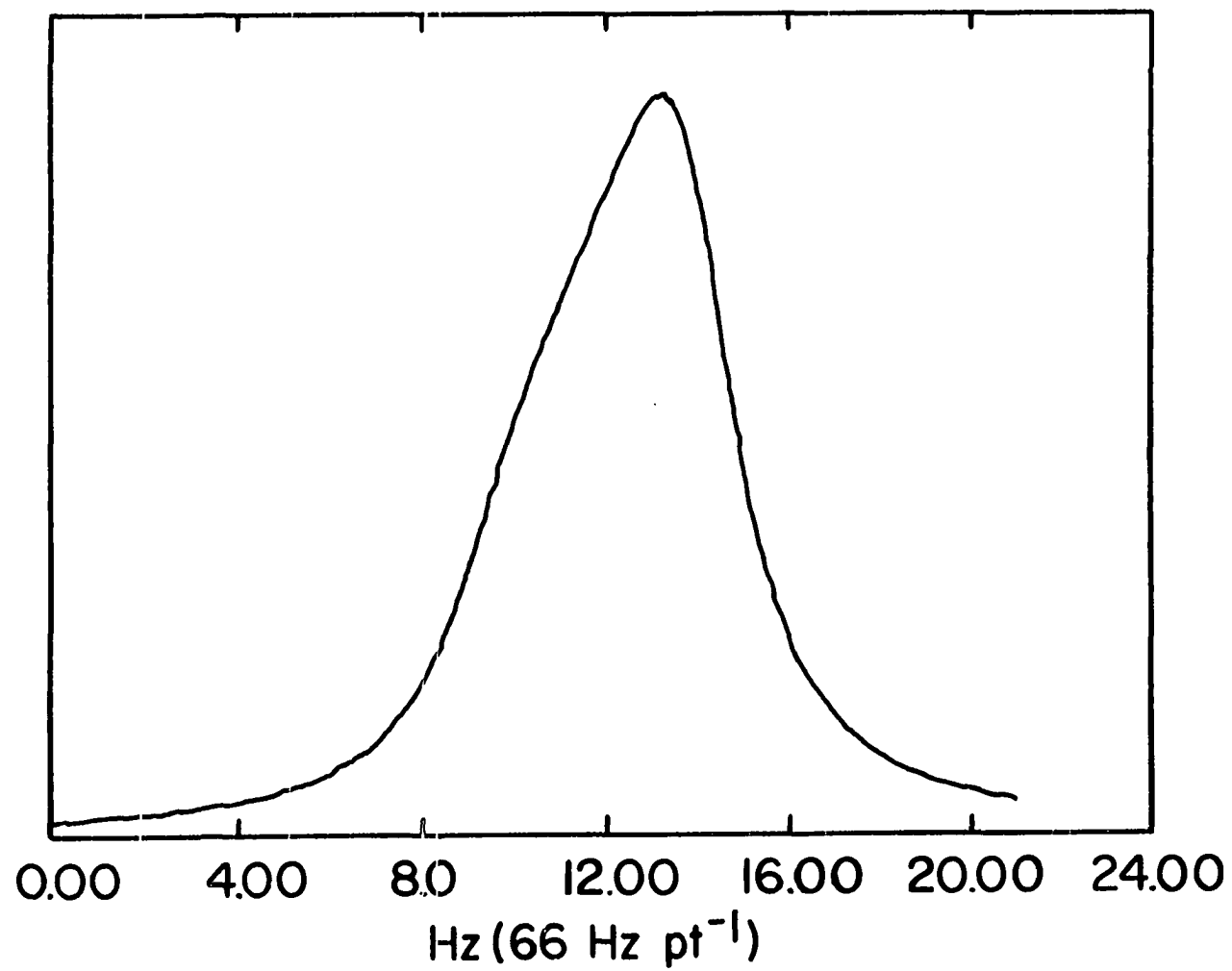
Figure 33. The "scaled" powder pattern resulting from spinning at 90° to the
d.c. field.
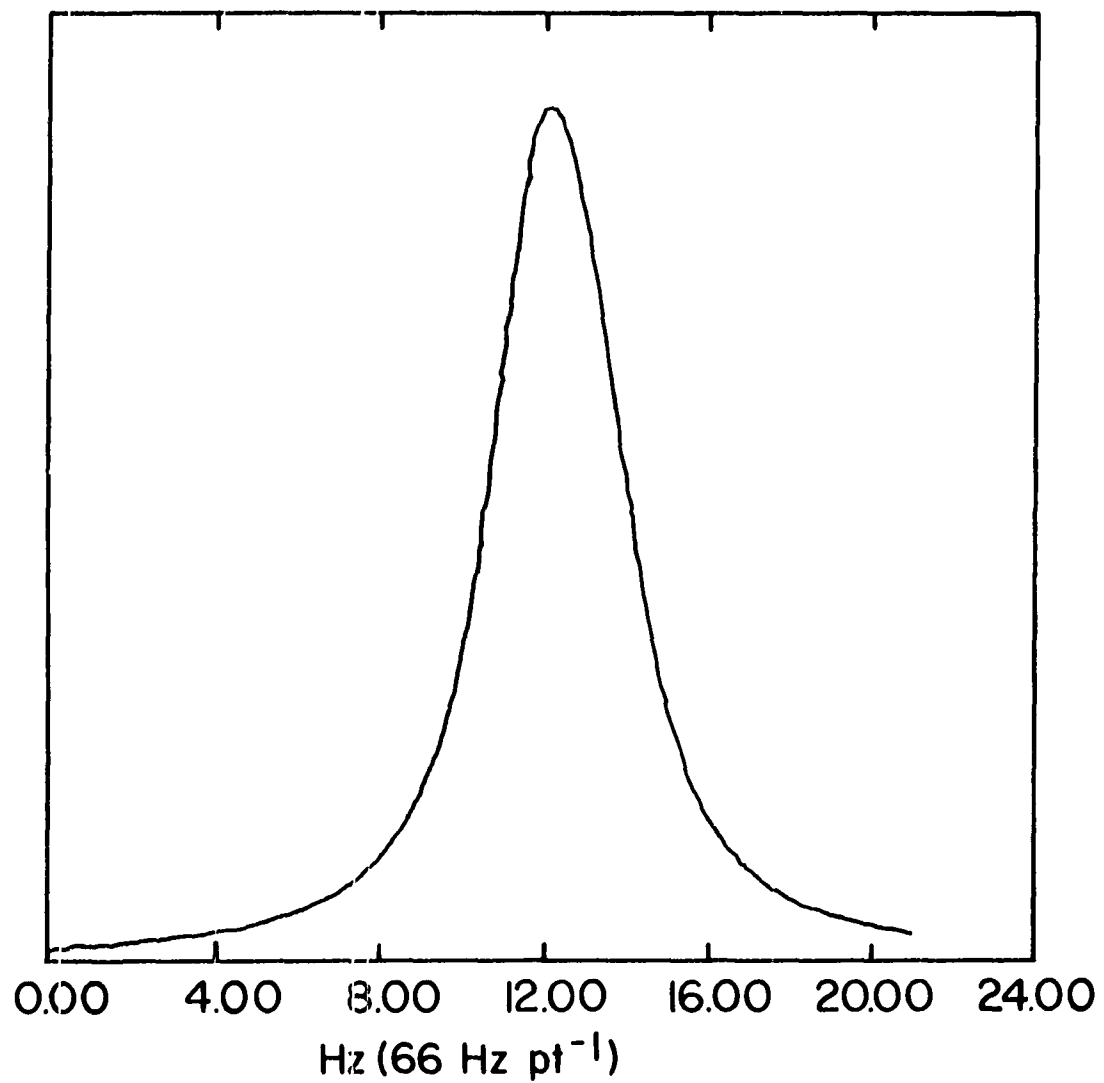
Figure 34. The "scaled" powder pattern resulting from spinning at 45° to the d.c. field.

Utility of Pulse NMR in Studying
Protons in Coals

With the advent of recent advances in pulsed and multiple pulse NMR, it is possible to further separate damping constants associated with differing relaxation mechanisms, since one may selectively design pulse sequences which remove specific interactions leading to spectral broadening. For example, under appropriate conditions, the CPMG sequence (105), used to determine transverse relaxation times, selectively eliminates internal interactions associated with d.c. field inhomogeneities, and with spin-other spin coupling. The multiple pulse phase altering experiments recently introduced by Dybowski and Vaughan (106) are capable of removing chemical shifts (and shift anisotropies). The multiple pulse sequence described by Waugh and co-workers (20), by Mansfield (26), and by Rhim, Elleman, and Vaughan (23) are capable of selectively removing homonuclear dipolar relaxation while scaling chemical shifts, providing the cycle time is short compared to the magnitude of the dipolar interaction. This section is devoted to investigating the utility of a combination of these techniques to determine chemical environments of protons in coals.

In the past, the utility of NMR to the study of protons in coals has been limited to broad line work, utilizing second moments to infer chemical information (50), and to

high resolution work on solvent extracts of coals (45,47,48, 51,52). There are two difficulties with these approaches. First, the interpretation of broadline NMR failed to take into account the effect of variable concentrations of free radicals upon line broadening. Second is the problem of justification in assuming that soluble extracts, representing less than 30% of the total in most cases, bear a close relation to the parent structures. With respect to the latter, there is also the possibility of a change in structure in the solution process.

In this section we determine free radical content by electron spin resonance, and investigate the feasibility of utilizing recently developed NMR pulse techniques to distinguish chemical environments of protons in samples of two Virginia vitrains, three Iowa vitrains, and selected model compounds. Free induction decays are used to measure the effective transverse relaxation damping constant, T_2^*. The MREV-8 multiple pulse sequence is used to remove the effect of homonuclear dipolar coupling, in the region where the magnitude of such coupling is not large compared to a 21-μs eight-pulse cycle time. The phase of the preparation pulse is phase altered to remove instrumental artifacts. Finally, a standard [π, τ, $\pi/2$] sequence is used to measure damping constants associated with spin-lattice relaxation (8).

Coal samples

Measurements were made on two Virginia vitrains; Powellton and Pocahontas No. 4, supplied by H. L. Retcofsky of the Pittsburgh Energy Research Center, ERDA, and on vitrain samples obtained from the Mich, Star, and Lovilia mines in southeastern Iowa. All samples were measured before and after drying for 8 hrs at 100°C and a pressure of 10^{-7} Torr. Analysis for major constituents of all samples are given in Table I. Carbon and hydrogen were determined by combustion analyses ASTM D3178. Nitrogen was determined by ASTM D-3179. Sulfur was determined by ASTM D-3177. The mineral matter content was determined by the method of Bishop and Ward (107). Oxygen was determined by neutron activation analysis.

Model compounds

Naphthalene, (α-methylnaphthalene, m=tolylacetic acid, 4,4'-bismethylbenzophenone, polystyrene), isopolybutadiene, and polyethylene were used as models of prototype aromatic, (mixed aromatic-aliphatic), and aliphatic compounds, respectively. The first four samples in the above list were checked for purity _via_ standard IR and high-resolution NMR, and found to be at least 98% pure. Polyethylene, of density 0.945, was obtained in rod form from Cadillac Chemical Co., Davenport, Iowa. The measured density corresponded to a crystalline fraction of 0.64.

Table I. Major constituent analyses of coals, wt $\%^a$

Sample	C	H	N	S	O^b
Pocahontas No. 4	$90.3(2)^c$	4.43(4)	1.28^d	0.85^d	4.96(20)
Powellton	85.1(3)	5.36(5)	1.54^d	0.79(3)	9.11(38)
Upper Mich	81.0(3)	6.14(6)	0.98(11)	5.53^d	15.7(63)
Lower Mich	81.55(18)	6.58(16)	1.37	4.16^d	---
Star	77.0(1)	6.04(4)	1.17(14)	5.02^d	7.11(29)
Lovilia	75.0(1)	5.80(4)	1.36(9)	2.64	13.6(54)

[a] Moisture, ash free.

[b] Oxygen analyses performed utilizing neutron activation so oxygen in mineral portion is included. The Upper Mich contained the largest fraction of mineral matter (13.45%) of all coals studied.

[c] Numbers in parentheses are root mean square deviations.

[d] Only one determination made.

ESR measurements (108)

ESR spectra were recorded at room temperature with both a Varian V-4500 spectrometer and a Strand Labs 602 spectrometer operating at a nominal frequency of 9.5 GHz. g factors were determined by sample interchange with a standard DPPH sample. Linewidths were calibrated utilizing the hyperfine splitting of DPPH in benzene and a proton gaussmeter. Spin concentrations were estimated by comparing the area of the absorption curve, or the second moment of the derivative spectrum, with a standard DPPH sample freshly prepared, and calibrated against a standard Mn^{2+} sample. Sample sizes were adjusted to keep the absolute number of spins similar in all samples, with the result that a minimum adjustment of the spectrometer was necessary when changing samples. No noticeable changes in cavity attenuation were observed as a function of sample. The major uncertainty in the estimation of spin concentration lay in the calculation of the absolute spin concentration present in the standard DPPH. The precision of the measurements was found to be 15%.

The g values, linewidths and free radical concentrations of all coal samples are listed in Table II. All samples exhibited Lorentzian line shapes with the exception of Star and Pocahontas. The heated Pocahontas sample exhibited a narrow line superimposed upon the same line observed in the other coals. One explanation for this effect is the presence

Table II. Results of ESR measurements on coals

Sample		g value[a]	Line width, G	Free radical concn, spins, $g^{-1} \times 10^{-19}$
Pocahontas No. 4	u			4.0
	h	2.0025	6.8(2)	9.5
Powellton	u			3.0
	h	2.0025	6.8(2)	3.4
Upper Mich	u			1.8
	h	2.0025(2)	8.5(2)	1.8
Star	u			1.6
	h	2.0025(2)	8.9(2)	2.4
Lovilia	u			1.0
	h	2.0025(2)	8.4(2)	1.3

[a]U = unheated, h = heated at 100°C and pumped at 10^{-7} Torr for 8 hrs.

of a small amount of fusain contained within the predominantly vitrain sample. Heating and pumping would remove the broadening effect of the oxygen in the sample, and allow for observation of the characteristically sharper line in the fusain. The g values of the Virginia vitrains agree to within experimental error with those found by Retcofsky et al. (109). The free radical concentrations are higher by a factor of 3 for the heated Powellton, and a factor of 2 for the heated Pocahontas No. 4.

Relaxation measurements

The results of proton NMR relaxation measurements on the coal samples are given in Table III, as are the second moments of the absorption spectra obtained from the Fourier transformed free induction decays. Where more than one damping constant characteristic of a particular pulse sequence was observed, the fraction of the species characterized by that damping constant is given. These values were obtained from an appropriate extrapolation of the decays to zero time, taken to be the center of the preparation pulse (72). Values in parentheses are root mean square deviations obtained from a least squares fit of the log of the amplitude of the envelope of the signal vs time.

Spin-lattice damping constants

The spin-lattice relaxation times surprisingly decreased with decreasing free radical concentration. One Virginia

Table III. Results of proton NMR relaxation measurements on vitrain coals[a]

Coal		T_1, ms	T_2 under FID, μs	$10^{-9} M_2$, H^2	%C[b]	$2\delta f$, REV-8	$2\delta f$, φ Pull
Pocahontas No. 4	u	116(5), 100%	9.5(1), 100%			900(5)	
	h	425(10), 100%	10.6(3), 100%		90.3		
				4.34		1058	540
Powellton	u	214(20), 91(2)%	10(1), 100%				
		237(20), 8.7(3)%			85.1	730(20)	
	h	412(13), 100%	17(1), 100%				
				3.33		753(30)	480
Upper Mich	u	42(4), 23(1)%	9.2(8), 92(15)%				
		119(4), 77(1)%	120(1o), 7.8(1)%		81.0	500(100)	
	h	139(3), 100%	10(1), 96(11)%				
			61(4), 4.0(2)%			542	310
Star	u	19.2(4), 100%	92(21), 5(2)%			675(50)	
			8(1), 95(33)%		78		
	h	99(3), 100%	6.0(5), 100%				
				2.92		700(50)	360
Lovilia	u	32(1), 100%	102(1), 710(5)%			650(30)	
			6.6(4), 93(17)%		75		
	h	115(7), 100%	7.7(1), 100%				
				2.63		753(30)	500

[a]U = unheated, h = heated.

[b]Moisture, ash free.

91

vitrain, Powellton, and one Iowa vitrain, Upper Mich,

exhibited two spin-lattice damping constants when unheated.

When heated at 100°C and pumped at 10^{-7} Torr for 8 hrs, all

spin-lattice damping constants increased, and the multiple

damping constants disappeared for the Powellton and the

Upper Mich samples. Increase of spin-lattice damping times

upon pumping and heating is an expected effect of the removal

of paramagnetic oxygen from the samples. It could also be

associated with removal of volatile free radical containing

molecules. Free radical content as inferred from ESR

indicates that the heated samples contain more free radicals

than do the unheated, however. The damping constants of

42 ms for the Upper Mich, 32 ms for the Lovilia, and 19 ms

for the Star samples are particularly interesting. If an

important mechanism for spin-lattice relaxation is inter-

action with the magnetism of the antiferromagnetic pyrites

in the samples, then spin-lattice damping constants of the

Iowa coals compared to the Virginia coals is in accord with

the higher sulfur content of the Iowa coals. However, for

the Iowa coals, the shorter T_1's are associated with lower

sulfur contents. Since there is no satisfactory means of

distinguishing between pyrite sulfur and organic sulfur in

coals, and since, in fact, standard methods of analysis may

well be missing portions of the pyrite sulfur in the form of

10 μm diameter polyhedra (110), the sulfur contents reported

in Table I may not accurately reflect pyritic magnetic centers available for spin-lattice relaxation. The results may indicate the possibility of utilizing spin-lattice relaxation to fingerprint inorganic sulfur in coals.

Transverse damping constants. Free precession following a single pulse excitation

Under the FID response to a single pulse experiment, all of the coals exhibit an effective transverse damping constant of the order of 10 μs with the species exhibiting this value of T_2^* being the major contributor in all samples. In addition, all unheated Iowa vitrains exhibit a second T_2^* of roughly 100 μs, the fraction contributing to relaxation being roughly 5%. Upon heating, only the Upper Mich sample maintains two damping constants, again of order 10 and 100 μs. As noted in the Introduction, the rigid lattice value for a transverse damping constant for an aromatic molecule such as naphthalene is roughly 10 μs. The rigid lattice value for a long chain hydrocarbon might be expected to be shorter by roughly a factor of 2. On the other hand, in an amorphous material such as coal, one might expect appreciable motional narrowing, and the existence of two damping constants as observed above gives rise to the possibility that these values might be a fingerprint of aromatic and aliphatic protons in coals. Results of T_2^* measurements on selected model aromatic, aliphatic, and mixed compounds

(vide infra) indicate that this is not the case, that the
shorter damping constant characterizes both aliphatic and
aromatic protons in rather rigidly held structures, and that
the longer damping constants may be associated with relatively
small, mobile molecules which are removed, at least for the
Lovilia and Star samples, upon pumping at 100°C. The second
moments obtained from the FID response to a single pulse
excitation would be expected to decrease with increasing
carbon content if the only contribution to broadening is
interproton dipolar interaction. This is just a reflection
of the idea that the average interproton distance increases
with increasing carbon content. The observed second moments,
however, increase with carbon content, as shown in Table III,
and in Figure 35. One possible explanation for the increase
in second moment with decreasing proton content is the fact
that the free radical concentration increases with decreasing
proton content, and that the increase in second moment is
associated with the free radical-proton dipolar broadening.
Normalization of second moment to unit free radical content
leads to the "expected" trend, shown as the lower curve in
Figure 2. Results of multiple pulse decoupling experiments
on both coals and model compounds (vide infra), however,
prove that the maximum line width contributed to the proton
NMR spectra by the free radicals is about 700 Hz. Second
moments associated with this broadening are only of order
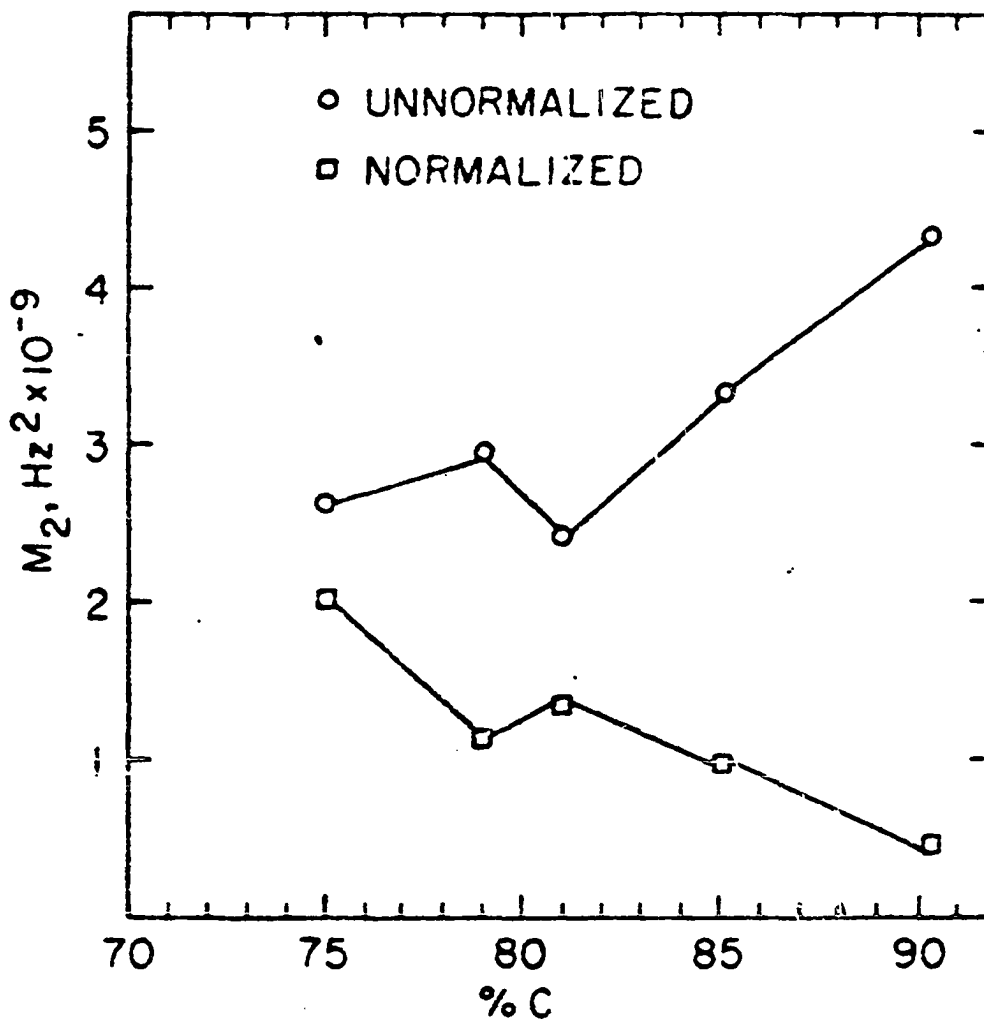
Figure 35. Second moments obtained from FID response to
single pulse experiment. Results normalized to
unit free radical concentration show "expected"
decrease with increasing carbon content, but the
"expected" result is incorrect (see text).

of 10^7 Hz^2, compared to the observed total value of 10^9 Hz^2.
Free radical-proton interactions therefore cannot account
for the observed trend in proton NMR second moments under a
single pulse excitation experiment. The observed increase in
second moments with decreasing proton content appears to be
real, and not an artifact associated with impurities. One
possible explanation for this observed trend is that upon
aging, i.e., increase in carbon content, protons move from
relatively mobile aliphatic structures to more rigid
aromatic structures, with linewidths characteristic of the
proton linewidth in naphthalene, and that this enhanced
rigidity more than compensates for increase in average
interproton distance.

Multiple pulse NMR measurements

Two sequences were used in this study. The first was
the MREV-8, which removes homonuclear dipolar broadening to
second order (23). The second was the phase altered version
of this sequence (106), in which a preparation pulse is
lacking, offset is due only to the zeroth order Hamiltonian,
$\bar{H}_p^{(0)} = (2/t_c)(\phi_{\bar{x}} - \phi_x)I_y$ associated with phase errors $\phi_{\bar{x}}$
and ϕ_x in the x and $\bar{x}$ pulses and both chemical shift
anisotropy and homonuclear dipolar broadening are removed to
first order. In addition, the operator I_z is scaled by a
factor of $\sqrt{2}/3$, i.e., chemical shifts and spin – other
spin interactions are scaled by roughly a factor of 1/2.

The results of these two sequences on the coals are given in the last two columns of Table III, and a typical spectrum of a coal under MREV-8 is shown in Figure 36. The two Virginia vitrains, with higher carbon and free radical content, are narrowed from 30 kHz to about 1 kHz under the MREV-8. The lower carbon content, lower free radical content Iowa vitrains are narrowed from 30 kHz to about 700 Hz. All heated vitrains are further narrowed by 300 to 500 Hz upon application of the phase altered sequence. From these results, and the results on the model compounds (vide infra), we infer that an upper limit to the free radical-proton broadening is about 400 Hz for the samples studied and that residual line widths under the phase altered sequence are associated with quadrupole broadening of protons by, e.g., ^{33}S, and by ^{14}N, and with instrumental broadening associated with failure to remove second-order dipolar terms. The line shape under MREV-8 is Lorentzian with no structure indicative of separation between aliphatic and aromatic protons.

Model compounds

To aid in an interpretation of the results of pulse and multiple pulse experiments on the coals, similar measurements were made on model aliphatic, aromatic, and mixed aromatic-aliphatic compounds. These results are presented in Table IV. We note that typical aromatics
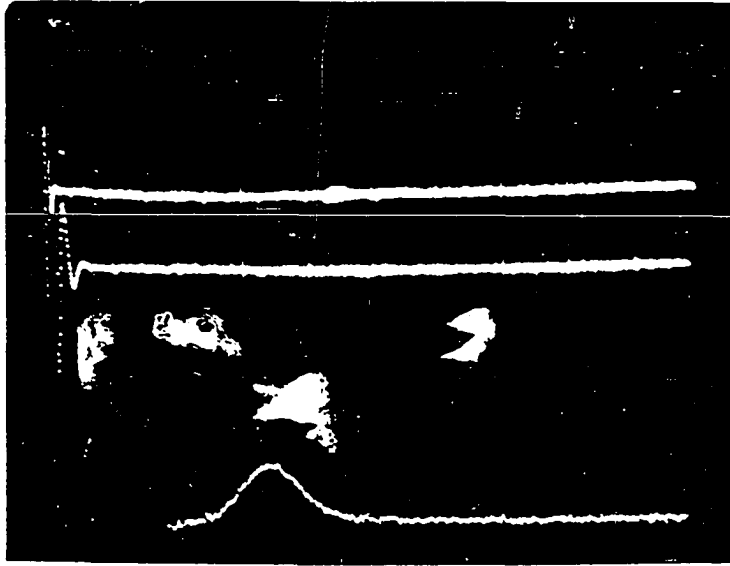
Top decay – total 49 msec
Middle decay – total 24.5 msec
Bottom spectrum – 750 Hz linewidth

Figure 36. Response of coal under MREV-8 sequence.

Table IV. Results of NMR measurements on model compounds
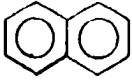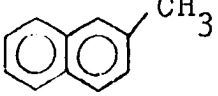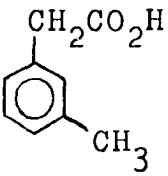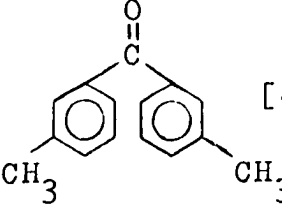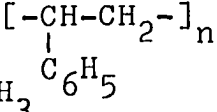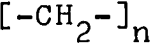
Model Compound	(naphthalene)	(methylnaphthalene) CH_3	CH_2CO_2H / CH_3	(ketone) CH_3 / CH_3	$[-CH-CH_2-]_n$ C_6H_5	$[-CH_2-]_n$	Isopoly-butadiene
T_2^* FID, μs	13	~13	17 241	19	19	12 48	300
$(2\Delta f \cong 1/\pi T_2)$	(24 kHz)						(1400 Hz)
T_2^* CPMG, μs	94		360 2593			44.1 433	
T_2^*, μs rigid lattice limit	13.9					3 (106 Hz)	3
$2\Delta f$, Hz REV-8 $t_c = 25$ μs	262		338		276	129	30
$2\Delta f$, Hz phase pull	271		250		261	~100	5

exhibit one transverse damping constant, of order 10 μs under a single pulse excitation. This is as expected for these compounds in the rigid lattice limit. In addition, mixed aliphatic-aromatics such as 4,4'-bismethylbenzophenone, α-methylnaphthalene, and polystyrene also exhibit only one transverse damping constant, of about the same value. Rotation of the methyl groups and rocking of methylene bridges are not sufficient for narrowing beyond 30 kHz. Polyethylene exhibits two distinct damping constants of 12 and 48 μs associated with the rigid, crystalline fraction of the sample, and the relatively loose, amorphous portion, respectively, indicating that aliphatics alone in polymeric type form can give rise to at least two spin-spin damping constants. m-Tolylacetic acid does exhibit two damping constants, of magnitude 17 and 241 μs, with relative fractions contributing to each in the ratio of 6/4. It is tempting to associate the longer damping constant with the aliphatic protons, but the results on the other mixed compounds do not support this association. Linewidths of all model compounds with the exception of polyethylene, under MREV-8, are roughly 300 Hz. Polyethylene narrows to 129 Hz under MREV-8, indicative of a smaller chemical shift anisotropy for the protons in this compound. The limit of narrowing under MREV-8 is determined by application of the phase altered sequence, and is typically 200 Hz. Residual

linewidth is due to pulse imperfections and to second-order dipolar effects. The results of multiple pulse measurements on the model compounds indicate a chemical shift anisotropy of 250 Hz, or 8 ppm including the chemical shift scaling factor, for the aromatic and mixed aliphatic-aromatic compounds. This value supports the contention that the free radical-proton broadening is about 400 Hz for the coals.

Pulsed NMR Spectrometry for Nondestructive
Determination of Hydrogen in Vitrain Coals

The use of nuclear magnetic resonance spectrometry (NMR) for quantitative analysis of elements in solids is not common for a number of reasons. For elements with sufficiently high gyromagnetic ratios and abundances to give good signal-to-noise ratios, e.g., ^1H, ^{19}F, and ^{31}P, dipolar broadening makes most lines unobservable to continuous wave techniques. Commercial pulse instruments in general do not have sufficiently rapid receiver recovery times to provide facile data recovery in the tens of microsecond range. In a great many solids, spin lattice relaxation times, T_1, are sufficiently long to make rapid accumulation of data unfeasible. The work of Schreiber and Vaughan (111) is one example of the power of pulse techniques for quantitative determination of nuclei in solids.

With relatively inexpensive and straightforward modification, commercial pulse NMR spectrometers may be arranged to

have sufficiently rapid receiver recovery times such that decays of tens of microseconds may be recovered for measurements in the 60-MHz or higher range. Coals generally have a sufficient concentration of free radicals such that electron-nuclear spin coupling leads to T_1's of the order of tenths of seconds, thus allowing for rapid accumulation of data. The present work describes the application of a rapid recovery receiver-d.c. amplifier system to the quantitative determination of protons in coals, and the conditions to be met for such determinations to be quantitatively valid. Instrumental artifacts were minimized during data accumulation by phase inverting the rf pulse on alternate samplings. Seven coal samples were used in the present determinations. Two were Virginia vitrains (Pocahontas No. 4 and Powellton) obtained from H. L. Retcofsky at the Pittsburgh Energy Research Center of the U. S. Department of Energy. Five were obtained from three mines in Iowa. All samples were crushed to 200 mesh and analyzed "as received". No attempt was made to dry the samples, or to remove volatile matter by heating at reduced pressure.

A sample transfer method was used to determine relative concentrations of protons in coals to that of a standard water sample. The number of protons in the water sample was determined to be $3.94(2) \times 10^{21}$ by weighing the NMR tube

containing the water standard before and after sealing in the
water. The lengths of the coal samples in the NMR coil were
kept the same size or smaller than that of the water sample
in order to ensure that the coals were exposed to the same
homogeneous H_1 field as was the water. Under this condition
of H_1 homogeneity, it was not necessary to have a coal sample
of accurately known packing density. An alternative would
have been to have both the coal and water samples long
compared to the NMR coil. While this would have resulted in
better signal-to-noise because of the higher filling factor,
a determination of the packing density would have been
necessary for a quantitative comparison of numbers of protons
in the standard and the coals.

The basis of utilizing sample transfer to determine
relative numbers of protons in coals compared to a standard
is that the polarization of the protons in the sample is
proportional to the total number of protons in the sample.
If the pulse width of the rf field is small compared to the
effective transverse relaxation time of the system, T_2^*,
or, if appropriate corrections are made when this condition
is not fulfilled, the initial value of the free induction
decay (FID) is proportional to this polarization, and
therefore to the number of protons in the sample. Proton-
proton dipolar coupling in solid coals has been found to be
the order of 30 kHz (112), which is to say that transverse

relaxation times as short as 10 µs are observed. With pulse widths of 1.3 µs, it is clear that the pulse width is a non-negligible fraction of the decay, and that two problems must be confronted. The first is the choice of the zero of time from which to calculate the initial amplitude of the FID, A(0). It has been shown that the appropriate zero of time to choose for the case where nonnegligible dephasing is occurring during the pulse is the center of the pulse (72). The second problem is an appropriate function of A(t) to use in order to extrapolate A(t) to zero time. Abragam (5) has suggested that for the case of solids, the FID should decay exponentially as t^2. This choice has been used success-fully by Lowe in studies on single crystal CaF_2 (72). For quantitative determination of hydrogen in solid coals, the zero of time was chosen to be the center of the pulse, and the initial amplitude of the FID was chosen as the zero intercept in a ℓn A(t) <u>vs</u> t^2 plot.

Hydrogen contents of seven coals were obtained using the initial value of the FID as described. A typical plot of ℓn A(t) <u>vs</u> t^2 is given for 500 data accumulations in Figure 37. A(t) are the extrema in the oscillations of the FID.

Comparison of hydrogen contents determined chemically, and <u>via</u> the initial value of the FID is given in Table V. The values of "%H by NMR" are those obtained from three

Table V. Comparison of quantitative analysis of hydrogen in coals by pulse NMR and combustion analysis[a]

Coal sample	rf pulse length, μs	%H	
		NMR	Combustion analysis
Pocahontas No. 4 Vitrain	1.25	4.72(03)	4.12(07)
Powellton Vitrain	1.25	4.87(03)	4.80(05)
Star Vitrain	1.25	5.63(05)	5.53(04)
Star Vitrain	3.0	6.31(50)	5.53(04)
Star Vitrain	5.0	5.60(40)	5.53(04)
Lovilia Vitrain	1.25	5.88(03)	5.54(03)
Upper Mich Vitrain	1.25	5.05(03)	5.32(04)
Lovilia Channel	1.25	5.29(07)	5.40(11)
Mich Run of Mine	1.25	6.20(02)	5.63(11)

[a]Uncertainties are mean square deviations from least square fits.

separate least squares fits of ℓn A(t) <u>vs</u> t^2 for all samples except the Star vitrain at 3.0 and 5.0 μs pulse widths. With the exception of the latter, values in parentheses represent mean square deviations of the three values of the initial amplitudes. Values in parentheses for the Star vitrain at 3.0 and 5.0 μs pulse width are mean square

deviations of one set of extrema to a linear least squares fit of $\ln A(t)$ <u>vs</u> t^2. Chemical determinations of hydrogen in the coals were made by combustion gravimetry, according to ASTM standard D271.

In order to determine the effect of pulse width upon the results, hydrogen content of one coal sample, Star vitrain, was determined as a function of pulse width. Pulse widths of 1.25, 3, and 5 µs were used. The results are not a function of pulse width to within the precision of the measurements, as can be seen from Table V. Because the initial amplitude of the FID is a sinusoidal function of the pulse width, with decreasing amplitude as the pulse width Hamiltonian becomes comparable in size to the offset Hamiltonian (113), it was impossible to obtain a reasonable signal-to-noise ratio for pulse widths more than 5 µs with offsets of 400 kHz. This result may be shown utilizing a straightforward calculation of the time evolution of the density matrix under the influence of the Hamiltonian $H = \Delta\omega I_z + \omega_1 I_x$. For this reason, it appears that the technique is limited to those cases in which the pulse width is less than a quarter of the decay time.

We note that the only factors preventing commercially available Fourier Transform NMR spectrometers from utilizing this technique for the quantitative analysis of hydrogen in solids in which spin-lattice relaxation times are sufficiently

short to allow for rapid data accumulation are: 1) lack of a sufficiently rapid receiver recovery time, and 2) lack of a sufficiently rapid analog to digital conversion for recovery of signals disappearing in less than 40 μs. The former may be avoided by the use of the receiver described herein, which is easily constructed from commercially available units at a cost less than $700. The latter problem may be circumvented by the use of an appropriate transient recorder, a number of which are commercially available with sampling rates useful in the microsecond range of data accumulation.

In summary, initial values of free induction decays are shown to yield a rapid, nondestructive quantitative measure of protons in coals provided: 1) an appropriate t^2 vs time plot is made, 2) the zero of time is chosen to be the center of the pulse, 3) the pulse width for a 90° rf pulse is not longer than $T_2/4$, 4) recovery time of the receiver-d.c. amplifier system is of the order of the pulse width, 5) both coal sample and calibration sample are exposed to a uniform rf field, and 6) the calibration sample is measured under the same experimental conditions as is the coal sample.
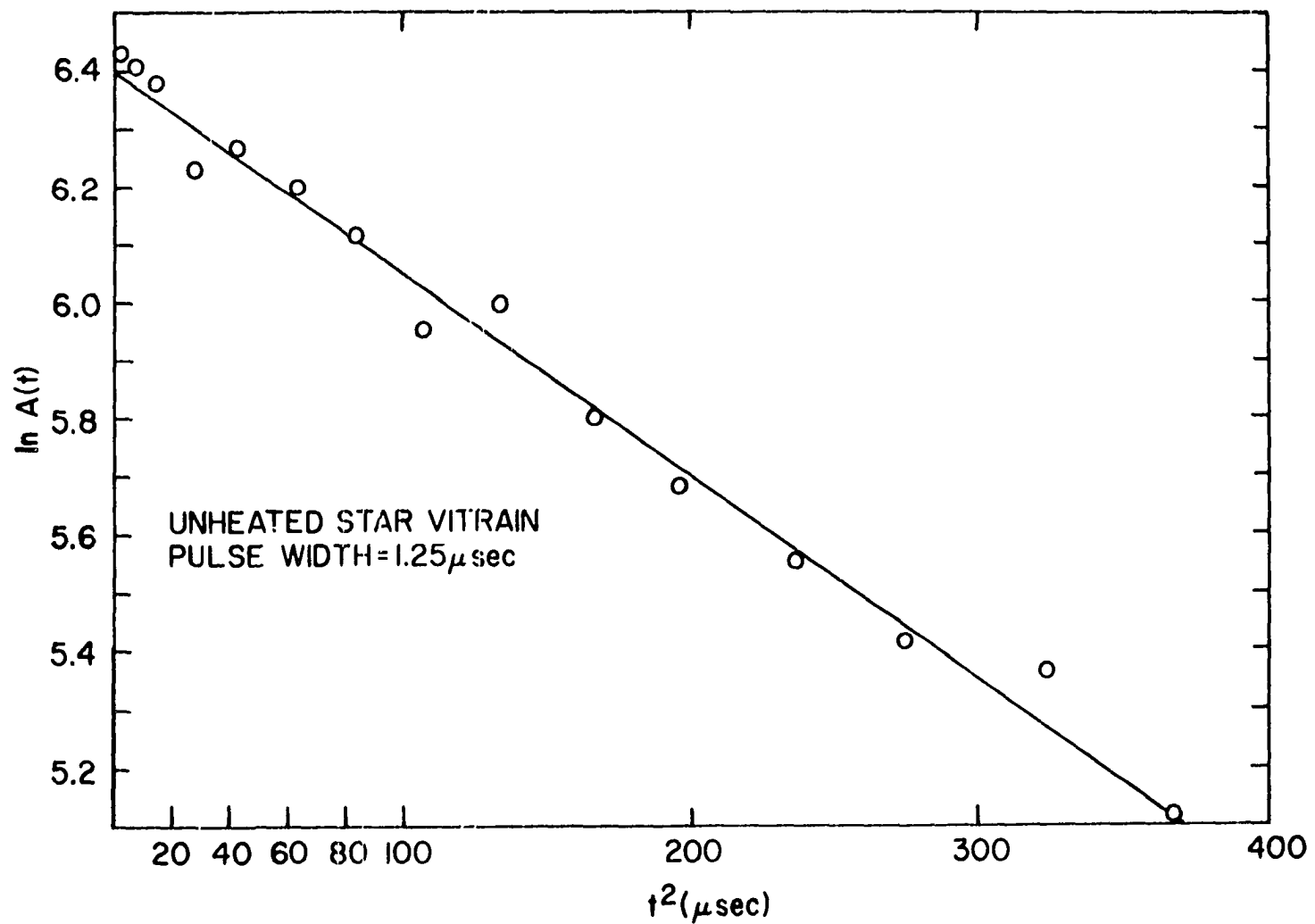
Figure 37. A typical ℓn A(t) vs t² plot for 500 scans.

Analyses of ^{13}C Aromaticities of Vitrain Coals

Cross polarization and strong heteronuclear dipolar decoupling combined with magic angle spinning has been shown to be capable of yielding high resolution NMR spectra of ^{13}C in solids (44), despite reasonable fears that the combined techniques would be mutually exclusive (37,42). The combination of the two techniques is necessary to remove the two major interactions which mask chemical shift information, i.e., heteronuclear dipolar interactions between ^{13}C and ^{1}H and ^{13}C chemical shift anisotropies. An additional problem is long ^{13}C spin lattice relaxation times (T_1) which govern how rapidly a pulse NMR experiment can be repeated for purposes of signal averaging. In liquids, most of these problems are eliminated by rapid molecular tumbling. This motion causes an averaging of the dipolar interaction to zero, an averaging of chemical shift anisotropies to the isotropic value, and a reduction of T_1's.

Pulse dipolar decoupling (37) and magic angle spinning (74) have both been shown to narrow the resonance lines in NMR spectra, but by two different mechanisms. The former requires strong radio frequency irradiation of the ^{1}H spin system at the proton Larmour frequency. This is effectively a decoupling through a manipulation of the spin part of the heteronuclear dipolar interaction, and is the predominant

mechanism in suppressing dipolar broadening in these experiments. Prior to the recently developed multiple pulse techniques for obtaining high resolution NMR in solids, magic angle spinning was the sole method of circumventing dipolar broadening in rigid solids containing a high fraction of nuclei such as ^{1}H or ^{19}F. Spinning modulates the spatial part of the dipolar interaction, given by $r_{ij}^{-3}(1-3 \cos^2\theta_{ij}(t))$, where $\theta_{ij}(t)$ is the angle between the internuclear spin vector and the external magnetic field. By rapidly spinning the sample about an axis tilted at an angle of 54.7°, the so-called "magic angle", with respect to the external magnetic field, the average θ_{ij} will lie along the axis of rotation. It is under these conditions that the dipolar interaction is eliminated if the spinning frequency is comparable to the dipolar linewidth. Dipolar interactions between ^{13}C and protons in solids can be as large as tens of kHz. The use of magic angle spinning for removal of this interaction under such circumstances is a formidable, if not impossible, task. However, dipolar decoupling can easily be accomplished utilizing an rf decoupling field of 10 gauss produced by a transmitter with power less than 200 watts.

The additional use of magic angle spinning eliminates the chemical shift anisotropy. This interaction is governed by a spacial term identical to the spacial term in the

dipolar interaction. Chemical shift anisotropies rarely exceed 200 ppm for ^{13}C nuclei (41) and the requirement of spinning at speeds larger than the linewidth is not nearly as severe nor necessary, if the addition of side bands to the spectrum of interest is not an undesirable complication (104).

The problem of circumventing the long ^{13}C spin lattice relaxation times has been solved by cross polarization techniques (37). Cross polarization is accomplished in a two step process: the protons are placed in the x-y plane of their rotating frame by a $\pi/2$ pulse at a given phase angle followed by spin locking in an rf field shifted by 90° from the first pulse, and a magnitude $H_1^H = \omega^H/\gamma^H$, where γ^H is the gyromagnetic ratio of the proton spins. The carbons are then placed in their rotating frame by irradiating the ^{13}C spins with an rf field of frequency $\omega^C = \gamma^C H_1^C$. Under the Hartman-Hahn conditions (31) $\gamma^C H_1^C = \gamma^H H_1^H$, there can exist an effective cross relaxation of proton magnetization into the carbon spin system, with time constant T_{CH}, enhancing the carbon magnetization by γ^H/γ^C, or 4 in the most favorable case. This cross polarization is a spin-spin process depending on the magnitude of the dipolar interaction with time constant roughly hundreds of microseconds (42,44). The time between experiments is now determined by the proton spin-lattice constant,

rather than the much longer carbon T_1. The pulse sequence used for combined cross polarization and heteronuclear decoupling is shown in Figure 38.

Recently, Bartuska et al. (57) discussed the prospects of utilizing the above described technique of combined dipolar decoupling and magic angle spinning to obtain high resolution ^{13}C NMR spectra of solid fossil fuels. As an analytical tool, this technique has advantages over previous NMR studies of coal both in the solid state (58,59) and of liquid extracts (45). In dealing with extracts it cannot be certain that the resulting NMR spectrum is representative of the parent coal. Previous solid state NMR studies of vitrain coals (59) have not taken advantage of magic angle spinning techniques for removing chemical shift anisotropies. Heteronuclear decoupling without spinning results in spectra with severe overlap of the aromatic and nonaromatic line shapes. This paper describes utilization of the combined techniques to determine the relative amounts of aromatic and nonaromatic carbons as a function of carbon content in vitrain portions of five coals.

Results

^{13}C NMR spectra have been obtained for the five vitrain coals using cross polarization and dipolar decoupling alone, and in combination with magic angle spinning. Figures 39-43 show the spectra obtained without magic angle spinning. The
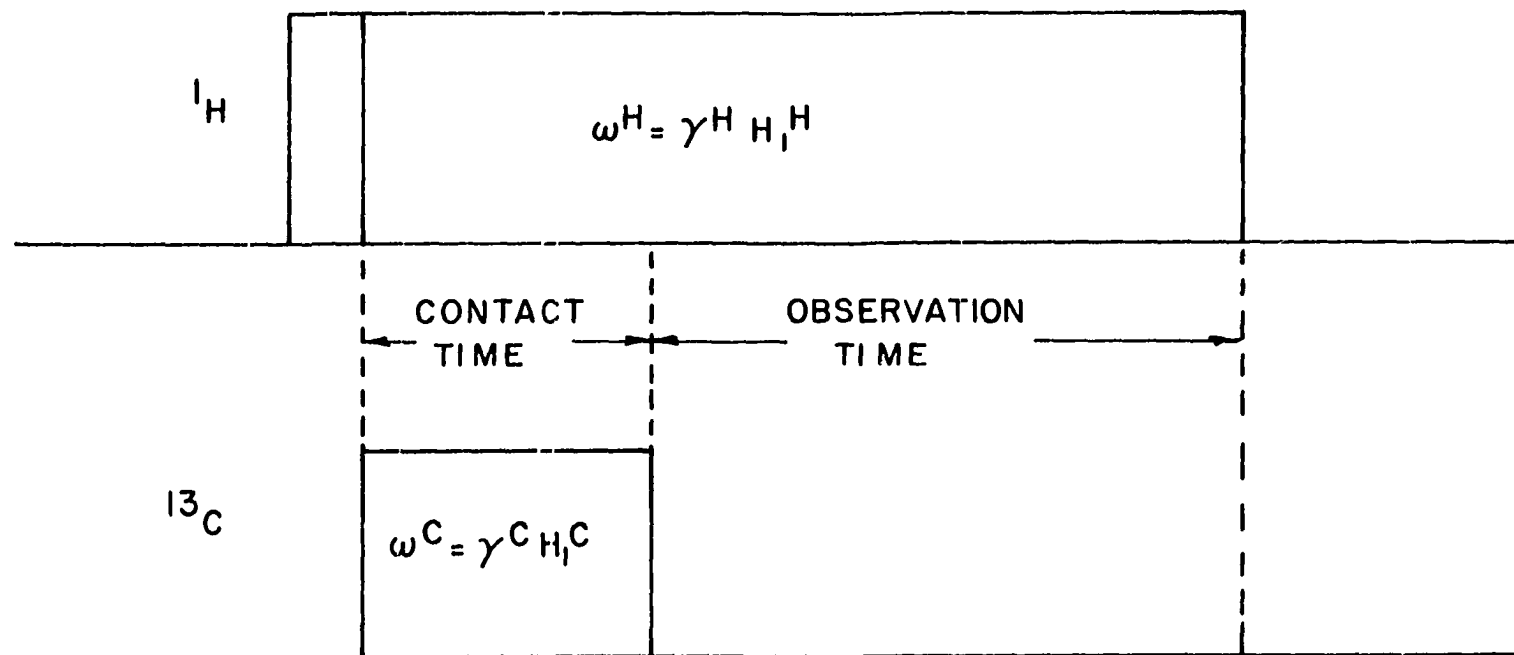
Figure 38. The pulse sequence used for combined cross polarization and heteronuclear decoupling ^{13}C NMR experiments.

Figure 39.   Dipolar decoupled ^{13}C NMR spectrum of Pocahontas No. 4 vitrain.

AROMATIC   ALIPHATIC

SHIFT (PPM, CS_2) x 10^{-1}
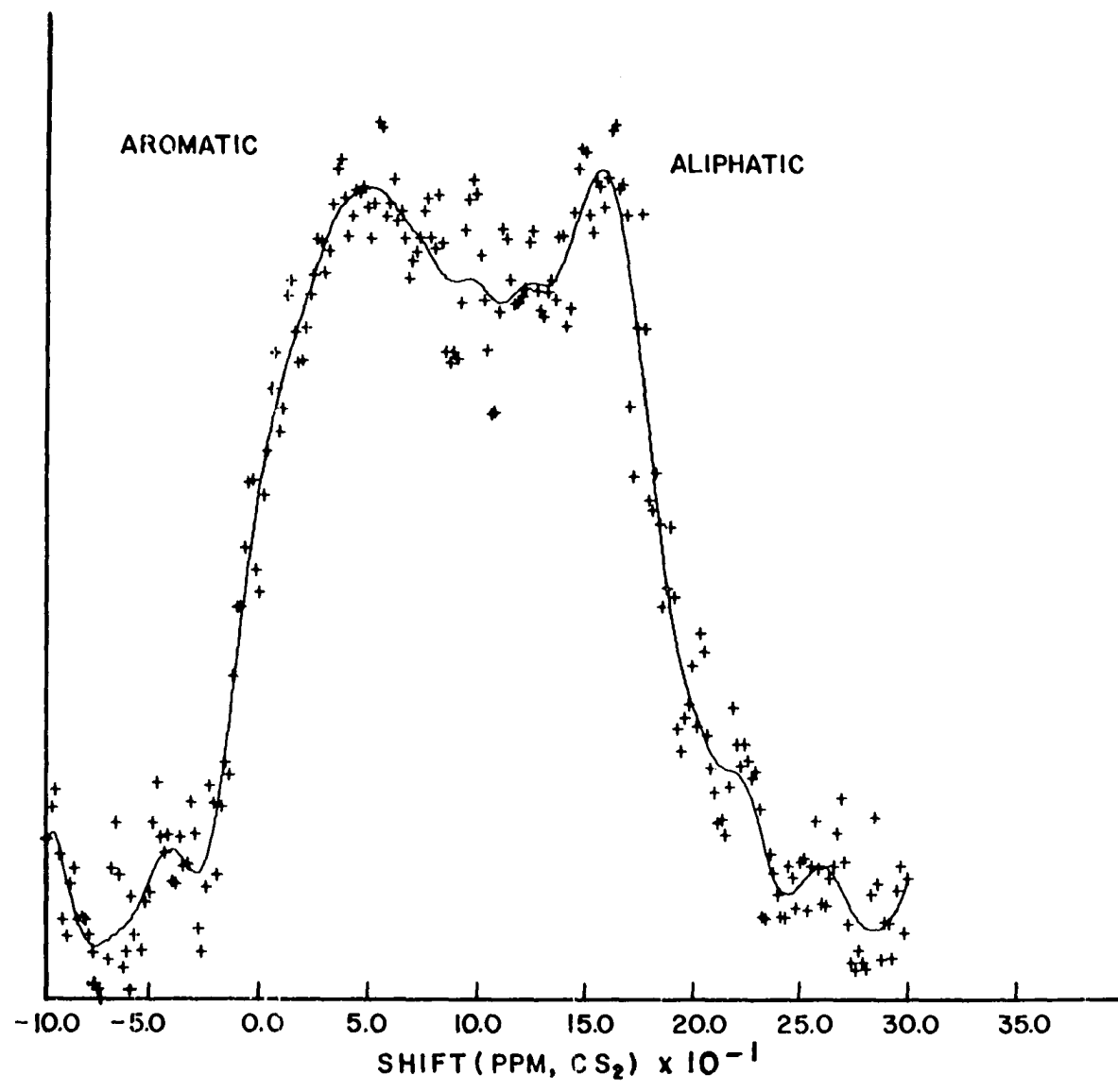
Figure 40.   Dipolar decoupled ^{13}C NMR spectrum of
Powellton vitrain.

AROMATIC   ALIPHATIC

SHIFT (PPM, CS$_2$) x 10^{-1}
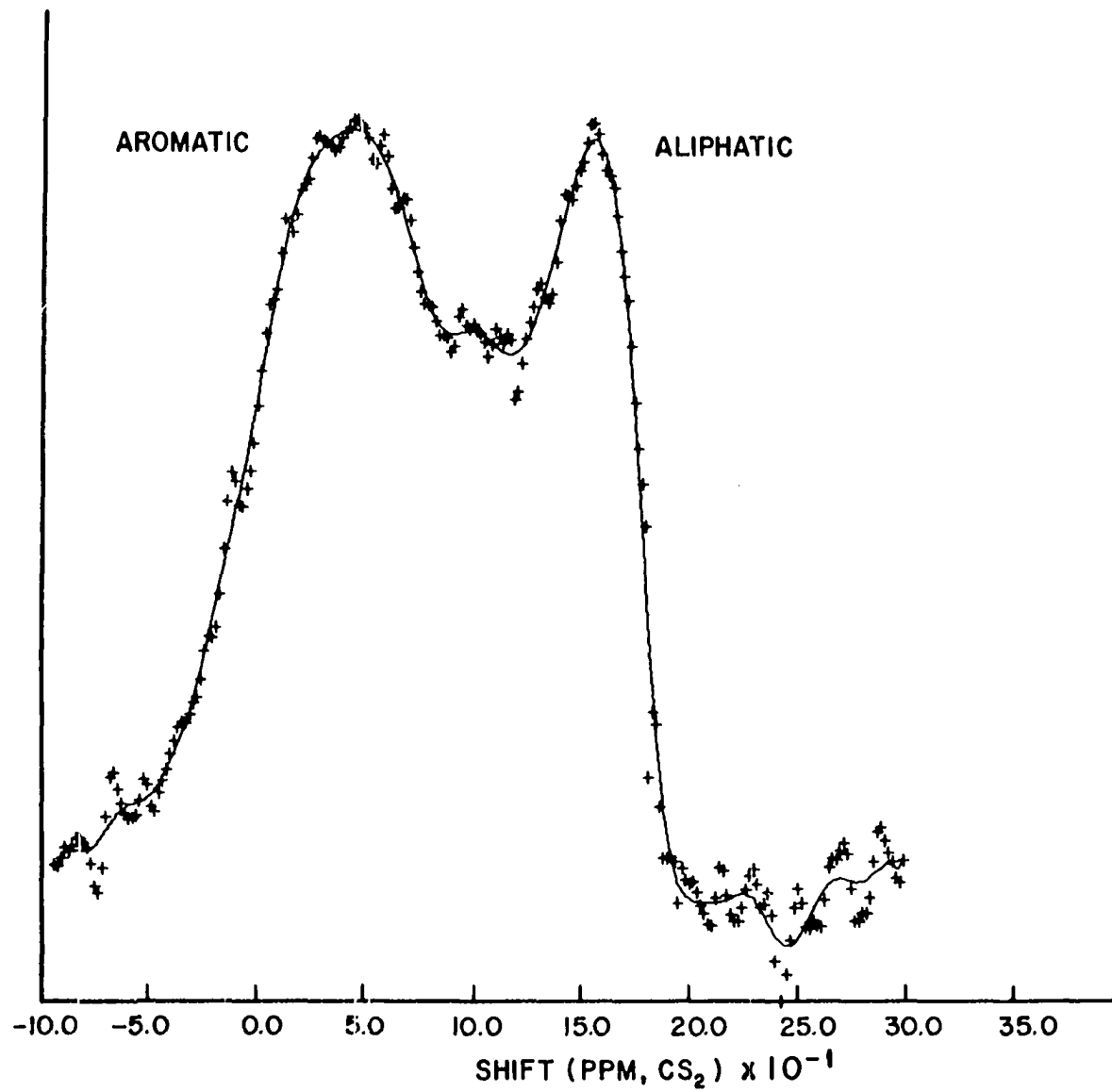
Figure 41. Dipolar decoupled ^{13}C NMR spectrum of Upper Mich vitrain.
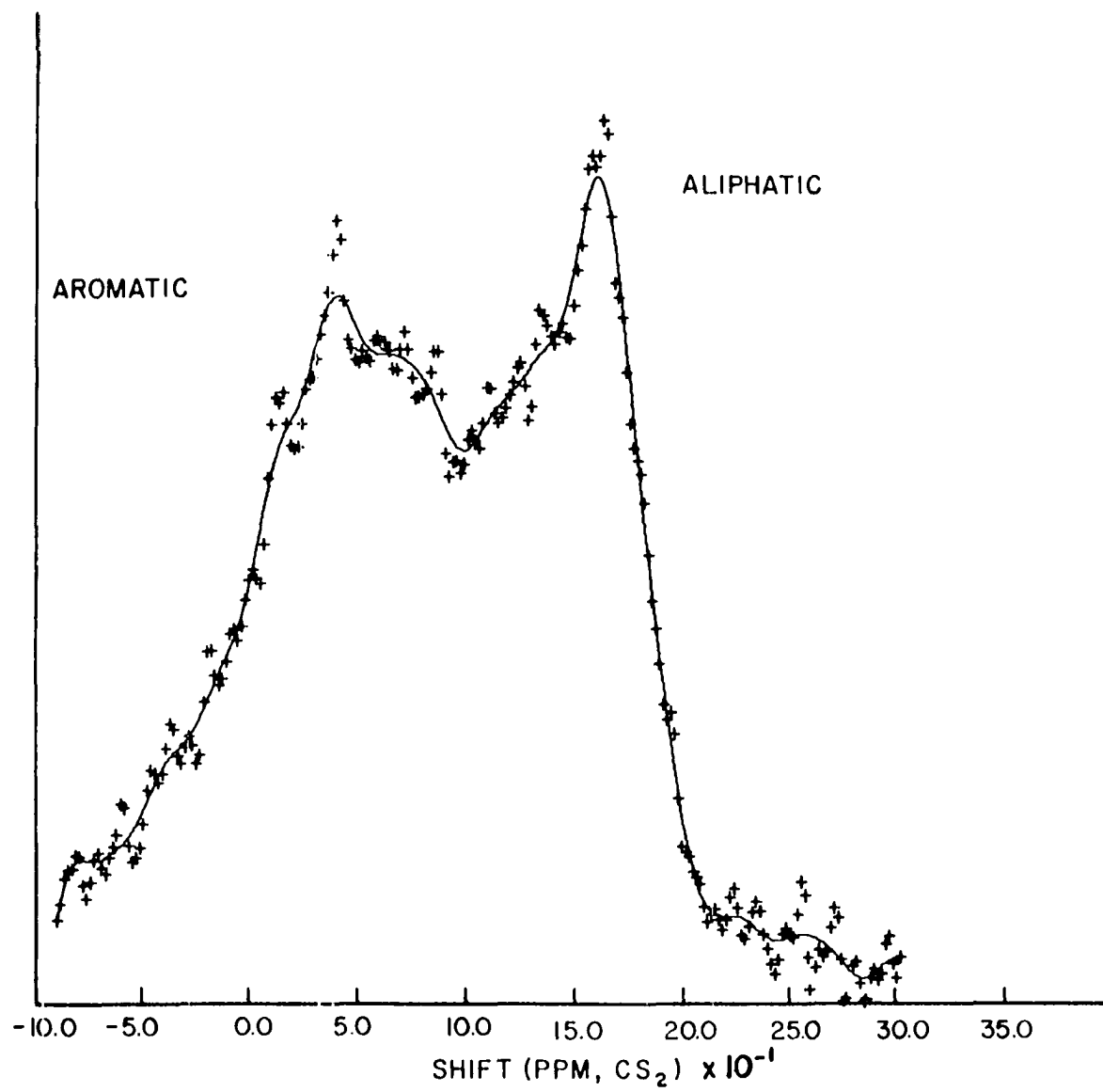
Figure 42. Dipolar decoupled ^{13}C NMR spectrum of Star vitrain.

AROMATIC

ALIPHATIC

SHIFT (PPM, CS_2) x 10^{-1}
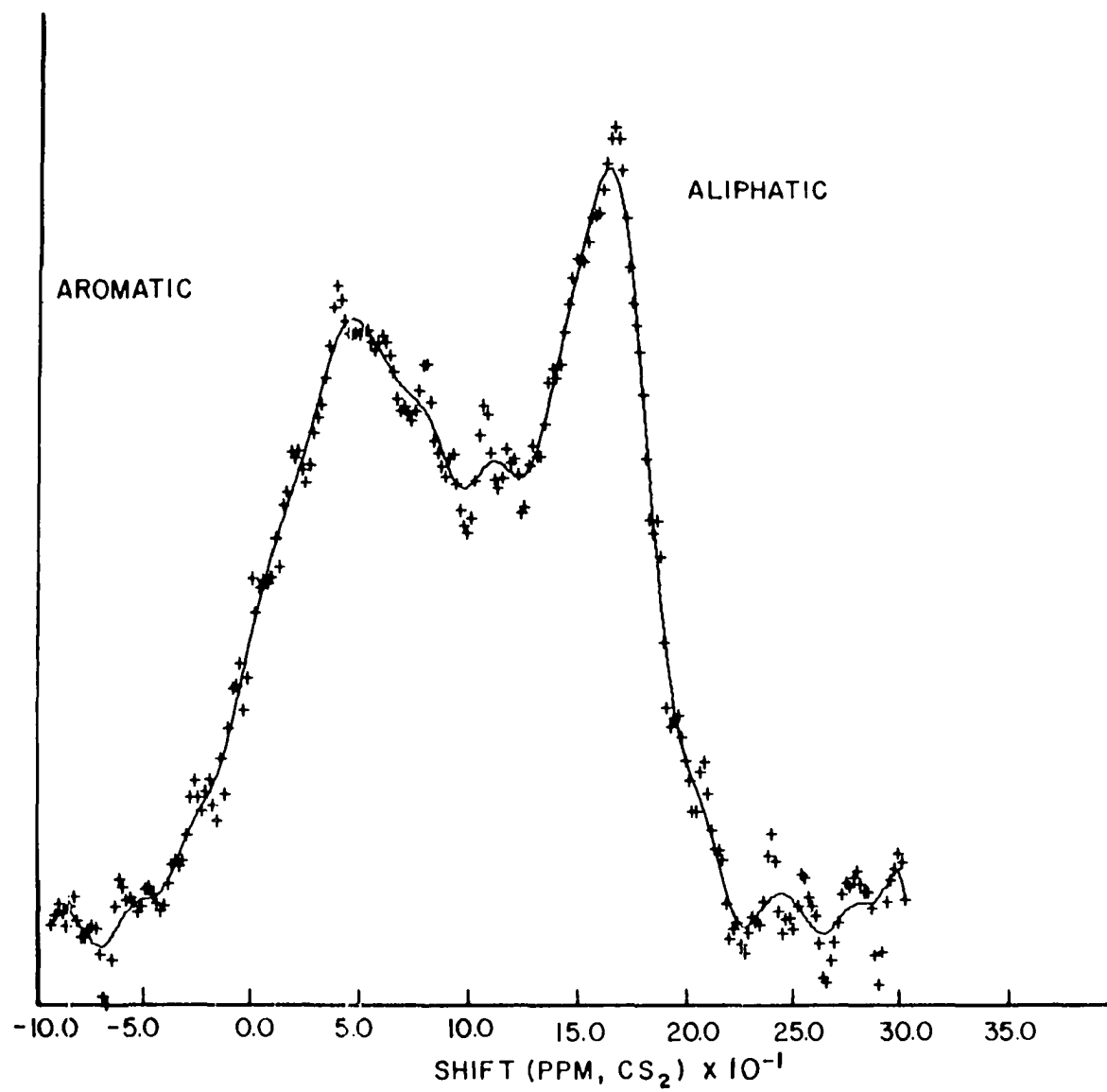
Figure 43. Dipolar decoupled ^{13}C NMR spectrum of Lovilia vitrain.

AROMATIC

ALIPHATIC

SHIFT (PPM, CS$_2$) x 10^{-1}
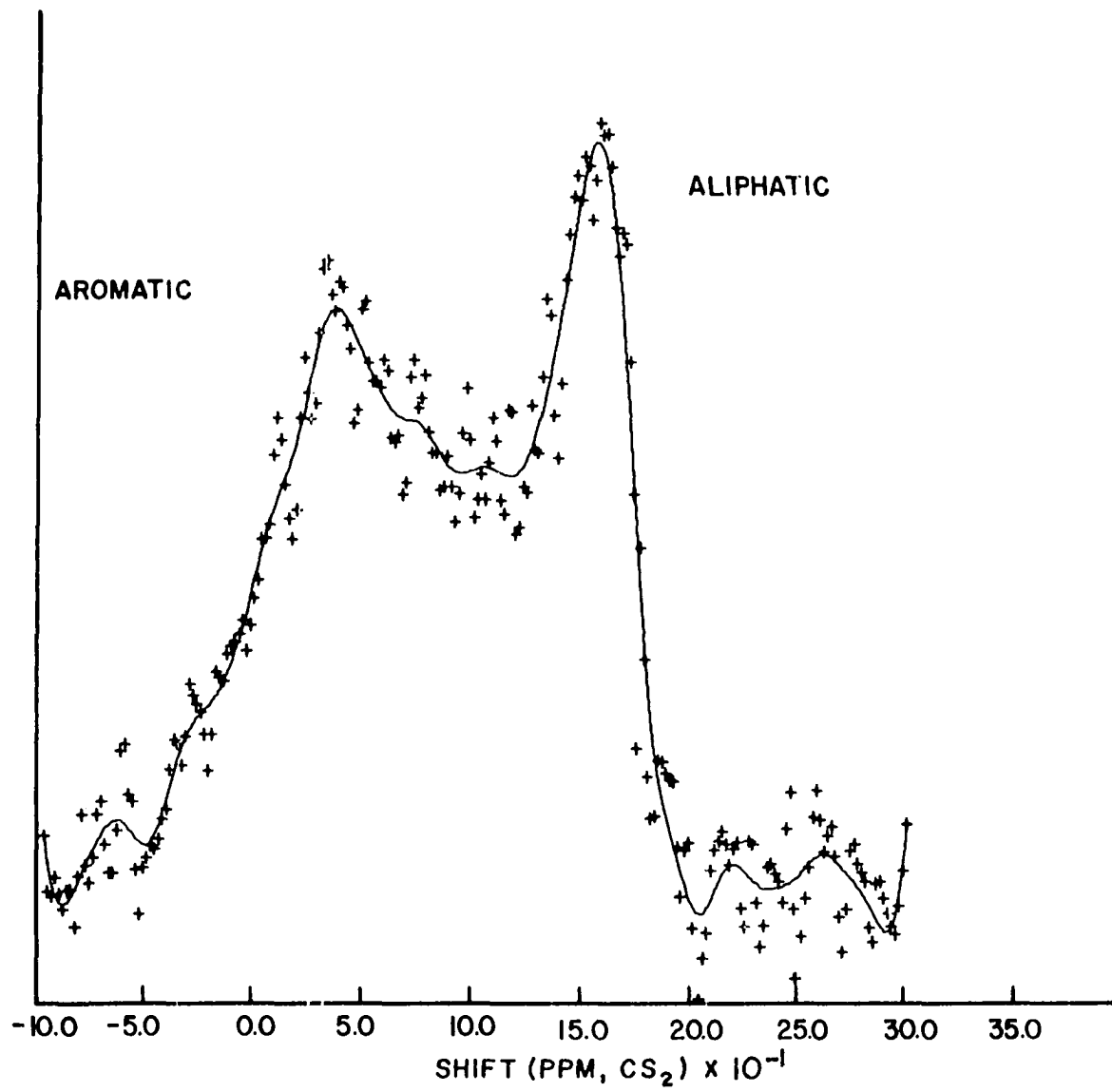
cross polarization time in each case was 2 msec. The spectra are dominated by chemical shift anisotropies resulting in an overlapping of the aromatic and nonaromatic components, as found by Vanderhart and Retcofsky (59). The fraction of aromatic carbon can be estimated by assuming an arbitrary straight line continuation of the aromatic ^{13}C NMR chemical shift tensor to higher field as previously reported (58,59). We have performed this type of analysis and obtained the fraction aromatic values shown in Table VI. Dr. D. L. Vanderhart has obtained 0.89 and 0.81 for Pocahontas No. 4 and Powellton vitrains, respectively (114), using this method.

The spectra obtained by combined dipolar decoupling and magic angle spinning at 1.5 KHz are shown in Figures 44-48. The removal of chemical shift anisotropies has improved the spectral resolution to the extent that there is a complete separation of the aromatic and nonaromatic regions. It is now possible to determine the percentage of aromatic components by a direct numerical integration of the areas under the peaks, with no assumptions necessary concerning spectral lineshapes and/or overlap. The results of such an integration are also given in Table VI. No appreciable difference was found between percentages determined using experimental points or the smooth curves drawn through them.

Table VI. Aromaticity as inferred from the ^{13}C NMR spectra both with and without magic angle spinning

	%C (by weight)	f_a (spinning)	f_a (nonspinning)
Pocahontas No. 4	90.3	.65	.86
Powellton	85.1	.65	.80
Upper Mich	81.0	.54	.75
Star	77.0	.54	.74
Lovilia	75.0	.52	.68

In Table VI is shown the typical direct relation between percent carbon in coals and percent aromatic component. The results obtained in this study indicate that the coals studied may be less aromatic than previously estimated. In particular, the aromatic fraction of ^{13}C in Pocahontas No. 4 and Powellton determined utilizing magic angle spinning is significantly less than that estimated by Vanderhart and Retcofsky. It might be argued that because effective cross polarization depends on heteronuclear dipolar interactions, magic angle spinning could average weak interactions between protons and isolated ^{13}C spins, leading to an artificial decrease in the aromatic component

Figure 44.   Magic angle spinning-dipolar decoupled ^{13}C NMR
spectrum of Pocahontas No. 4 vitrain.
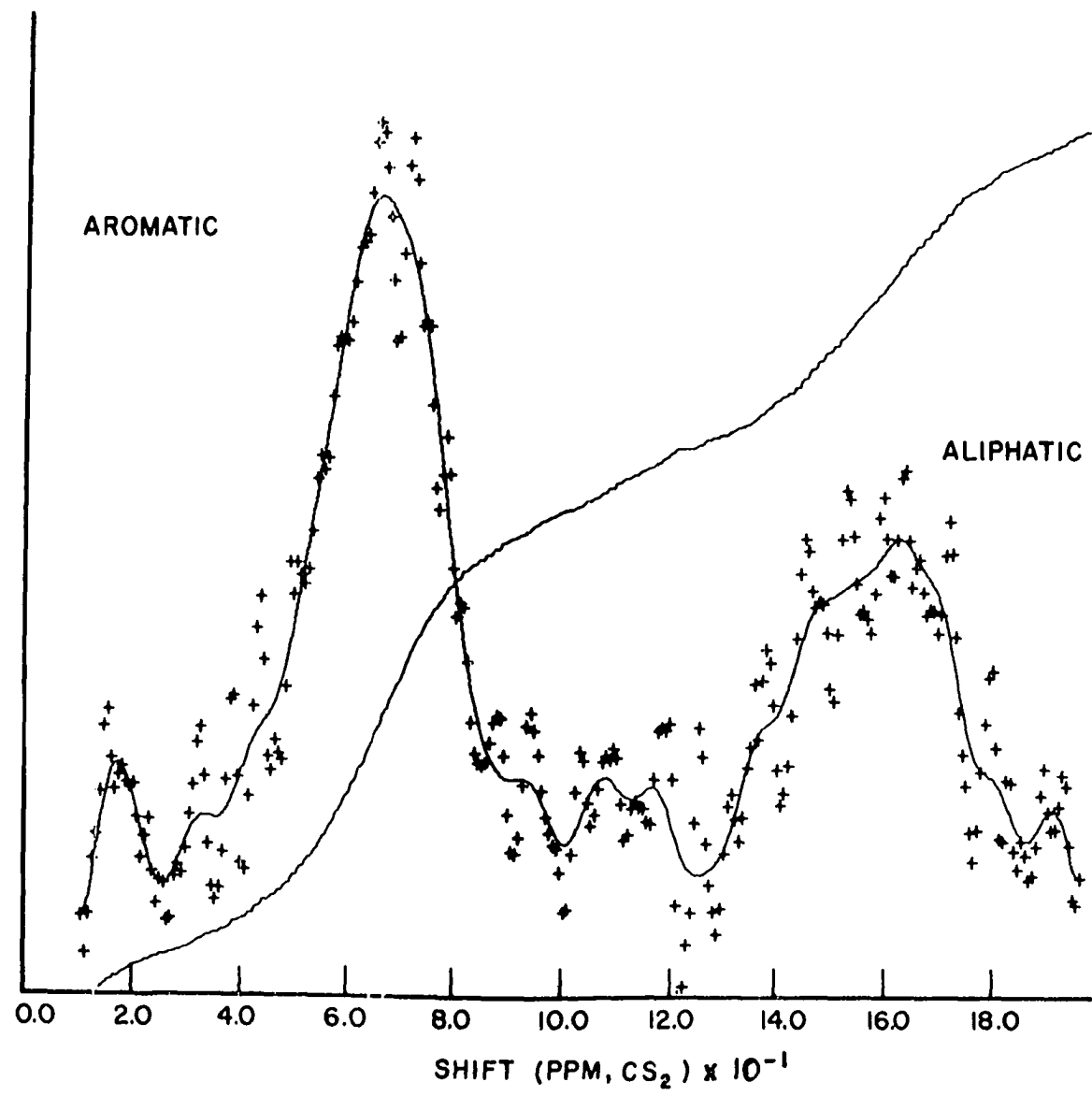
Figure 45. Magic angle spinning-dipolar decoupled ^{13}C NMR spectrum of Powellton vitrain.

AROMATIC

ALIPHATIC

SHIFT (PPM, CS_2) $\times 10^{-1}$
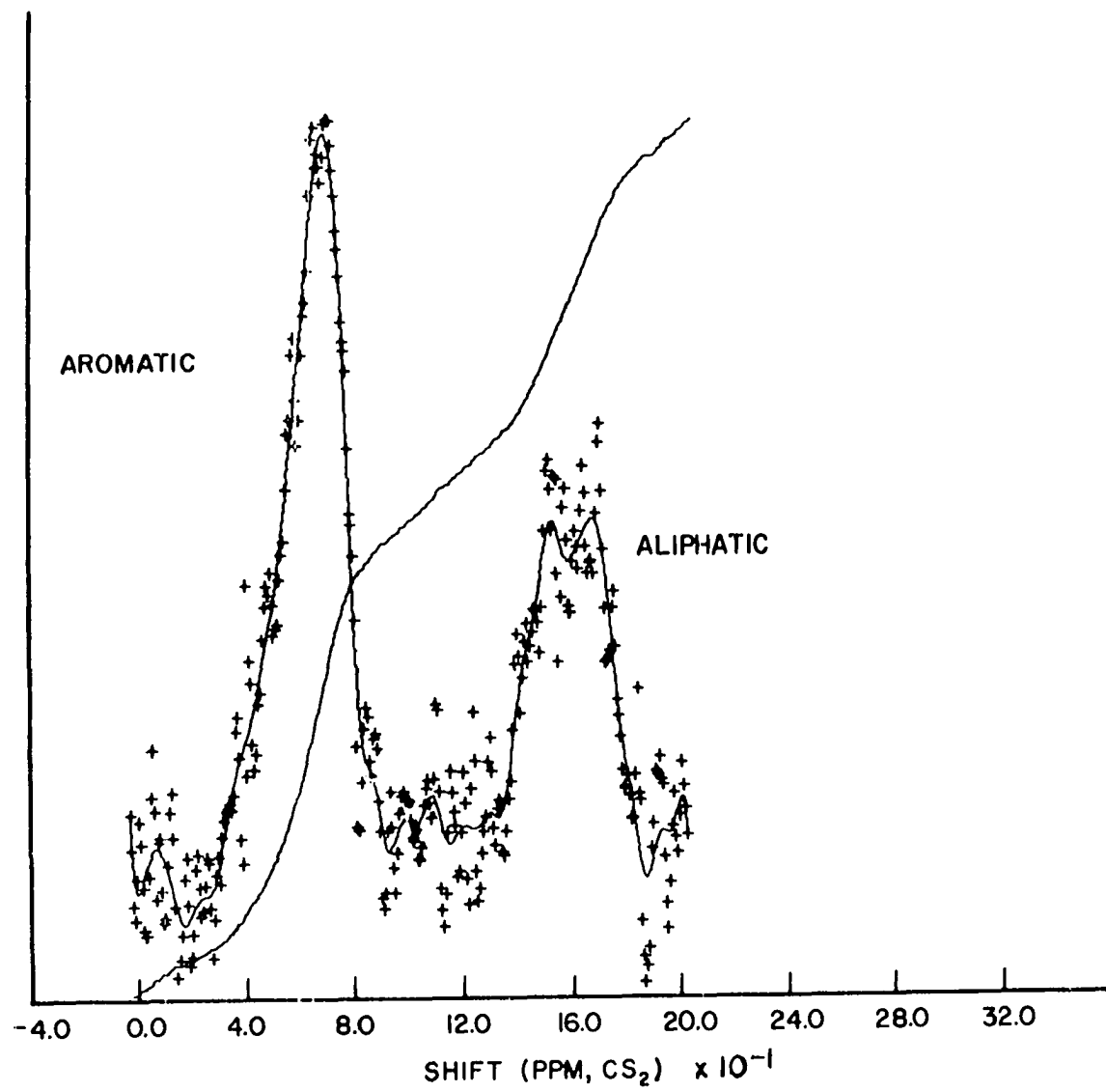
Figure 46. Magic angle spinning-dipolar decoupled ^{13}C NMR spectrum of Upper Mich vitrain.

AROMATIC

ALIPHATIC

SHIFT (PPM, CS$_2$) x 10^{-1}
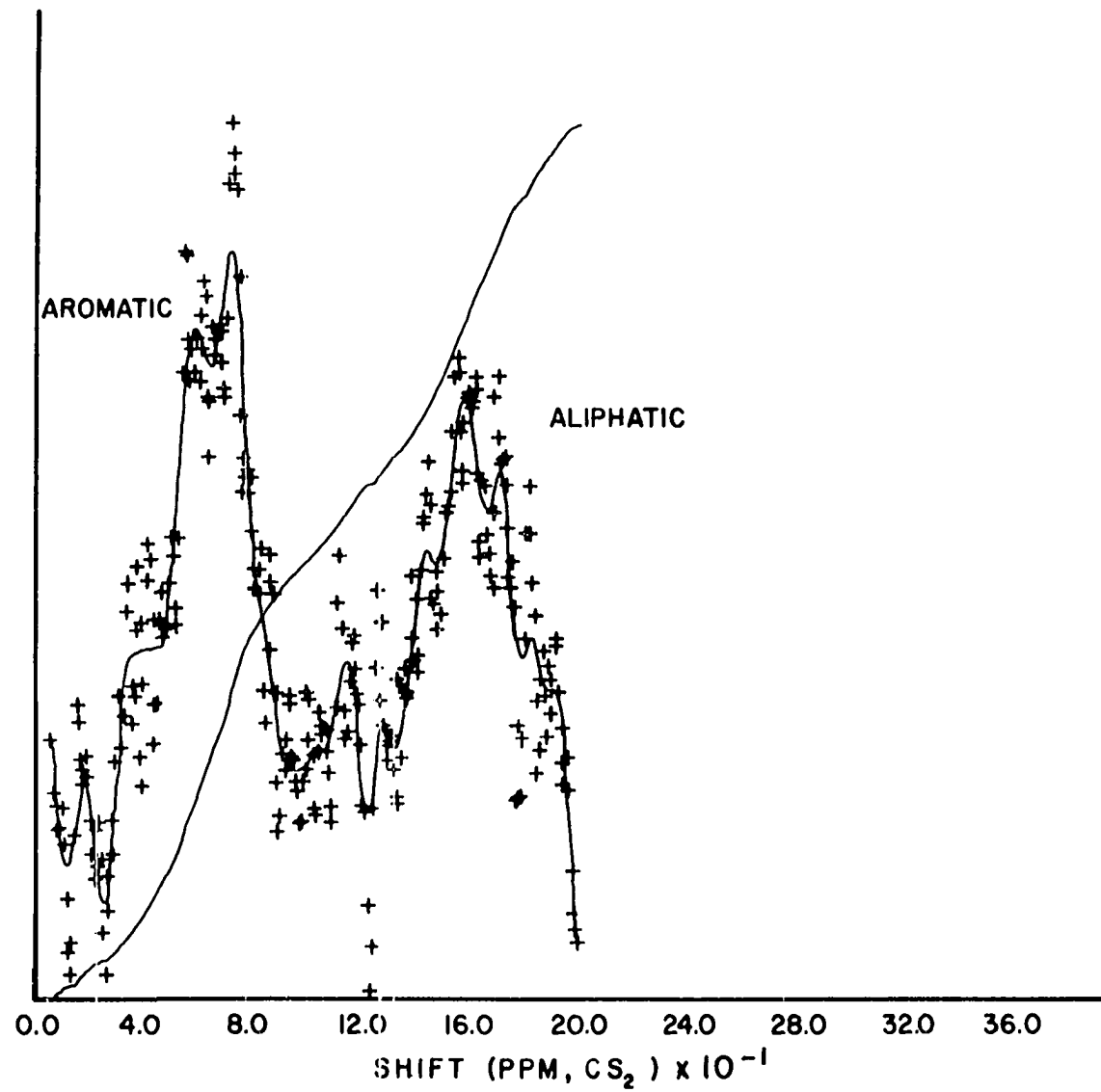
Figure 47.   Magic angle spinning-dipolar decoupled ^{13}C NMR
spectrum of Stai vitrain.

AROMATIC

ALIPHATIC

SHIFT (PPM, CS₂) ×10⁻¹

-4.0   0.0   4.0   8.0   12.0   16.0   20.0   24.0   28.0   32.0
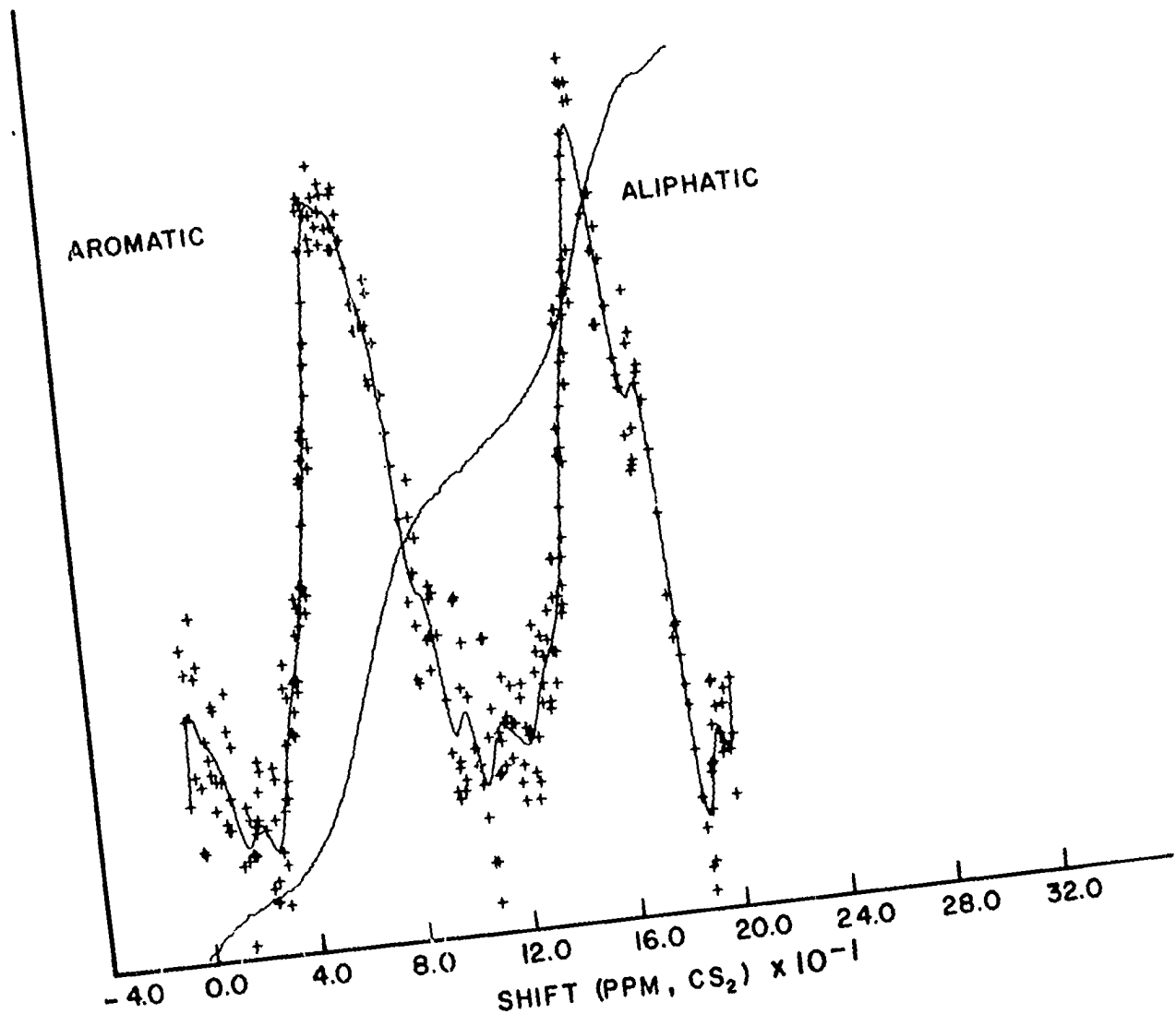
Figure 48. Magic angle spinning-dipolar decoupled ^{13}C NMR spectrum of Lovilia vitrain.

AROMATIC ALIPHATIC

SHIFT (PPM, CS$_2$) x10^{-1}
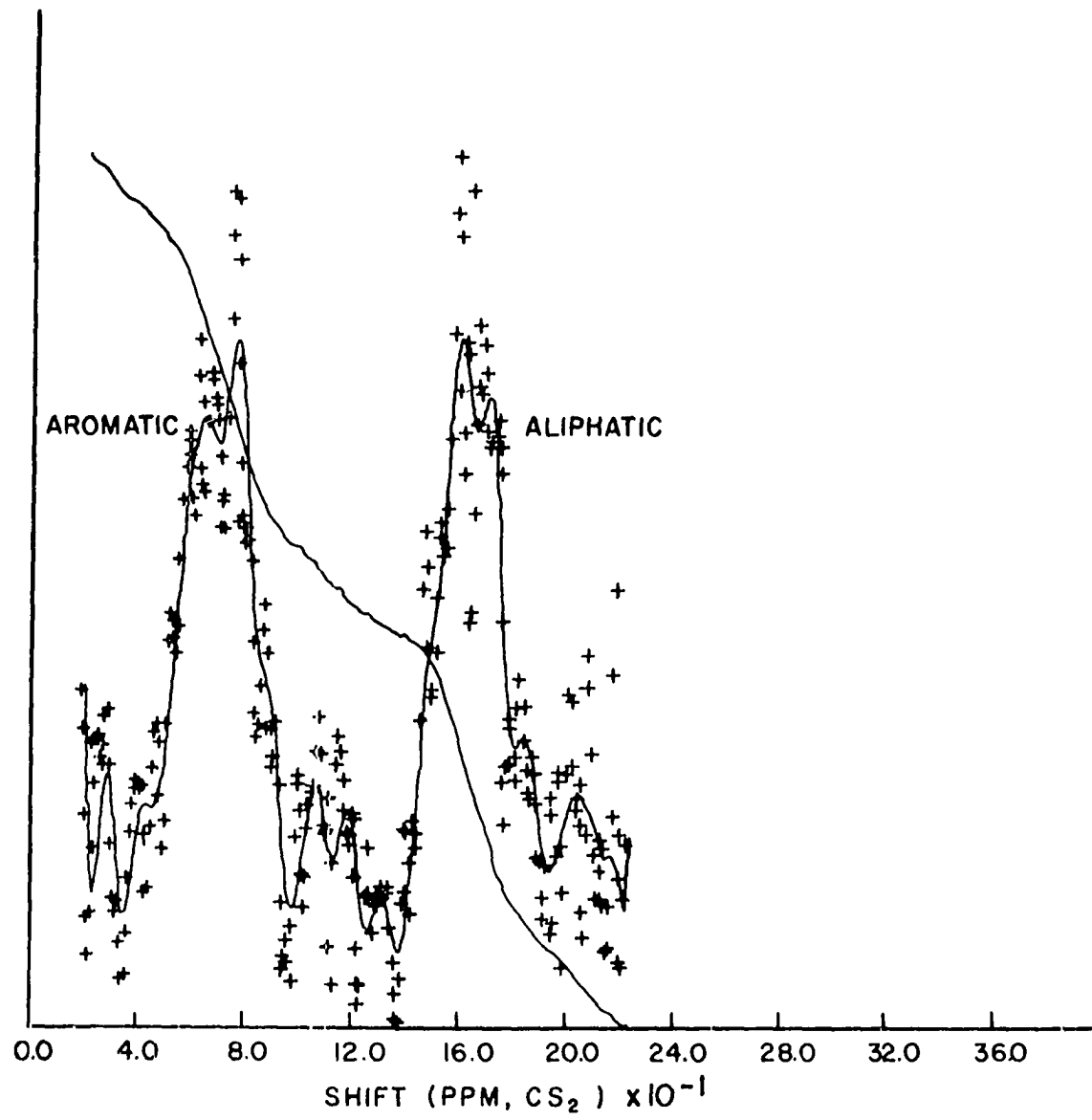
of the spectra. We have compared the initial amplitudes of the free induction decays (which are proportional to the number of ^{13}C spins being detected in the sample) for the spinning and nonspinning experiments, and found no difference in the number of spins detected within an experimental error of 2%. Also, the integrated areas of the two spectra were equivalent to the total carbon content obtained using initial amplitudes.

An additional problem which could cause spectral distortion and interfere with the integrated areas of the resonance peaks, would be the generation of spinning sidebands which overlap with the central peaks. Under such conditions, the center of gravity of the spinning and non-spinning spectra would differ. In the five coals studied no such distortion of the spectra were observed. The spectra of one coal, Pocahontas No. 4, was measured at a spinning speed of 2.2 kHz; assumed to be large enough to insure removal of sidebands from the area of spectral interest. The percentage of aromatic substituents did not differ from that determined at a spinning frequency of 1.5 kHz. If the ^{13}C aromaticities reported here are in error, it is probably due to insufficient spinning speeds to completely remove the spinning sidebands.

To insure that the present studies on these coals were made under conditions of maximum polarization transfer, the fraction of aromatic component in Pocahontas No. 4 was

studied at cross polarization times between 250 μsec and
3 msec. The fraction of aromatic carbon does not vary more
than 4% over this range, as shown in Table VII. Longer
contact times resulted in severe signal attenuation due to
the proton $T_{1\rho}$, which was determined to be 5 msec.

Table VII. Aromaticity of Pocahontas No. 4 vitrain as a
function of cross polarization contact time

Contact time (msec)	f_a
0.250	.62
0.500	.66
1.000	.65
1.500	.65
2.000	.63
3.000	.63

As a final test of the spinning experiment's quanti-
tative reliability, the ^{13}C spectrum of polystyrene was
determined, as is shown in Figure 49. The cross polarization
contact time was 500 μsec. The calculated aromaticity is
.76, compared to the expected value of 0.75.

In summary, the technique of combined magic angle
spinning-proton decoupling appears to be a powerful tool

Figure 49. Magic angle spinning-dipolar decoupled ^{13}C NMR spectrum of polystyrene. The integrated area yields 76% aromatic carbon.

POLYSTYRENE

AROMATIC

ALIPHATIC

SHIFT (PPM, CS$_2$) X10^{-1}
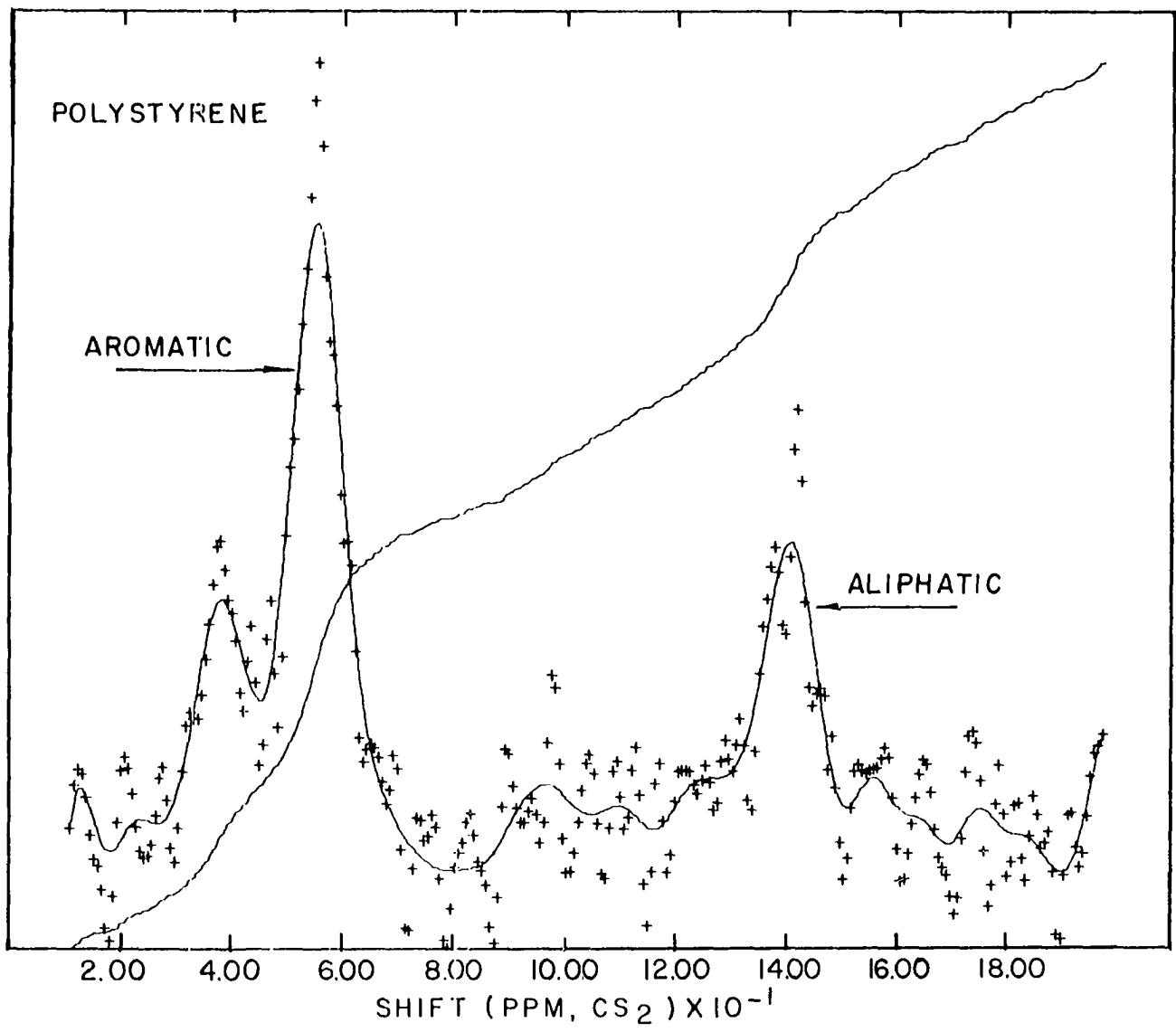
for the study of fossil fuels, as has already been indicated

by the results of Bartuska et al. (57). With this enhanced

spectral resolution, it may now be possible to follow

processes such as hydrogenation of solid coals under

relatively mild treatment utilizing ^{13}C NMR.

Dipolar-Narrowed Carr-Purcell Measurement of
Rotating Frame Spin Lattice Parameters in Polymers[1]

The measurement of proton NMR spin-lattice parameters

has proven useful in the description of orientational motions

of proton-containing molecules (115,44). In particular, the

measurement of $T_{1\rho}$ in systems in which reorientational

motions on the order of 10-100 kHz occur has been useful in

elucidating the nature of these motions, because this time

constant is sensitive to motions in this range. Elastomers

are examples of systems of ordered fluids in which

substantial low frequency motion provides a mechanism for

effective $T_{1\rho}$ relaxation and the often complicated frequency

dependence of $T_{1\rho}$ has provided insight into the motion of

elastomer segments. Residual dipolar interactions often

dominate the FID lineshape in these bulk polymers, but are

_____

[1]The material in this section consists of an article
co-authored with C. R. Dybowski of the University of Delaware
that has been submitted for publication to the Journal of
Chemical Physics.

reduced from the rigid lattice value by motion. Line narrowing multiple pulse NMR techniques reduce the static dipole-dipole contribution to the lineshape to reveal chemical shift and spin-lattice contributions. However, unlike solids, where $T_{1\rho}$ is long, both the spin-lattice relaxation and the chemical shift dispersion make sizeable contributions to the multiple pulse lineshape of a polymer sample (106). In this work we wish to describe a technique which allows the separation of these two lineshape factors - the dipolar-narrowed Carr-Purcell (DNCP) technique. It retains the efficacy of the MREV-8 sequence (23) in decreasing the static dipolar interactions and also cancels the chemical shift contribution to the lineshape, allowing independent measurement of the spin-lattice contribution. The decay is governed by a time constant, T_{1y}, which measures reorientational motions in the range of frequencies sampled by the spin-lock $T_{1\rho}$ experiment and may thus serve as an alternative means of determining these motional properties of polymers.

Sequences of pulses have been used to estimate spin-lattice relaxation in polymer systems before. The earliest reports on damping under multiple pulse sequences showed that the Ostroff-Waugh sequence (116) could be used to obtain data on orientational correlation times in polymer systems (117). Recently, a phase modification of the MREV-8 sequence was used to estimate the spin-lattice contribution to multiple pulse lineshapes in polymer substances (106). Very recently,

Rhim et al. (118), have shown that pulse sequences of the Ostroff-Waugh type with pulse nutation angles less than 90° can be used to produce effective spin-locking. This method can be used to measure $T_{1\rho}$ in dipolar solids like CaF_2.

Experimental

The rf modulation sequence used in these experiments is shown in Figure 50a. A preparation pulse places the magnetization along the y-axis in the rotating frame, after which the 17-pulse DNCP sequence is applied repetitively to the sample. Sampling occurs at the end of each 17 pulse cycle. The sequence in Figure 50b is a version of the DNCP which is derived from that in Figure 50a by a phase shift. Many such equivalent sequences are possible but they are interrelated by cyclic interchange of phases. The general sequence may be thought of as two subcycles, each consisting of a MREV-8 sequence which diminishes dipole-dipole interactions among the protons during each half of the cycle. Were it not for the 180° inverting pulse applied at $t=12\tau$, the detected magnetization at $t=24\tau$ would be modulated by the average chemical shift interaction, just as it is for the MREV-8 sequence. The inverting pulse, however, causes a refocussing of the chemical shift Hamiltonian's effect such that at $t=24\tau$, the magnetization is independent of this interaction. This action is quite analogous to the effect of the 180° pulse in the Carr-Purcell experiment (25,105,119) and has the same effect as a

Figure 50. Schematic diagram of the DNCP sequence. The sequence
in a) was used. b) is a version of the sequence
obtained by symmetric interchange of pulse phases.
The version in a) has a preparation pulse along x;
that in b) has a preparation pulse along y. There
are many versions of the DNCP related by symmetric
interchange of phases.
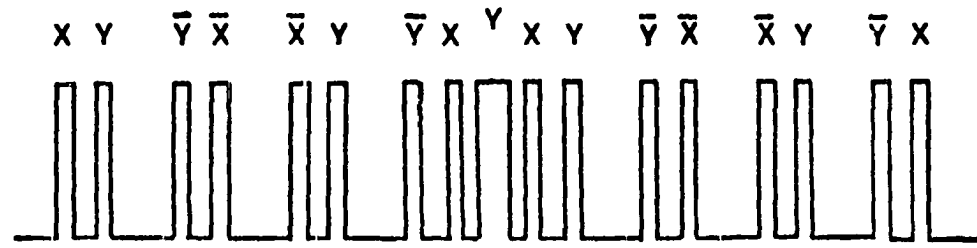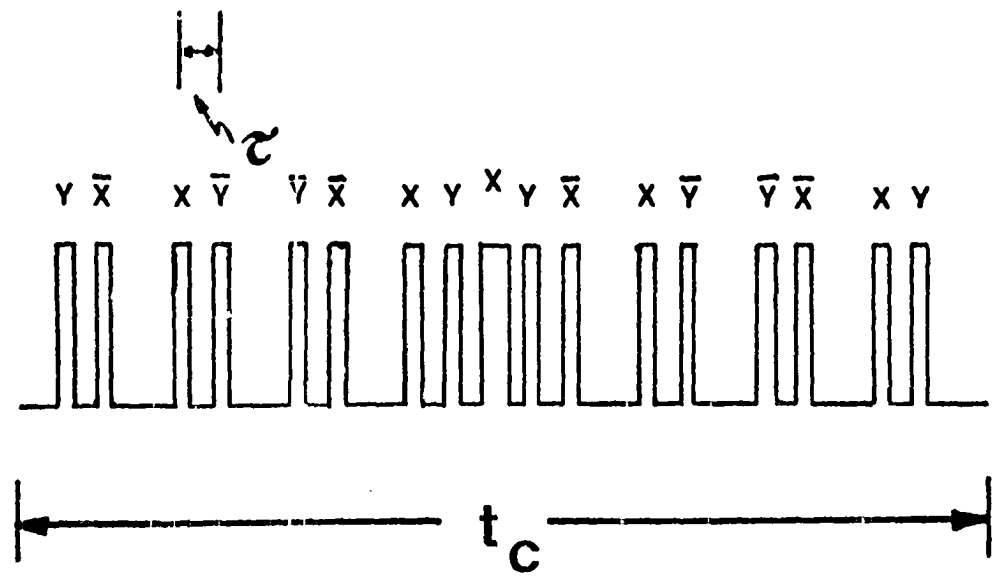
deliberate phase error introduced into the MREV-8 (106).
Hence, one might consider the sequence of Figure 50, a
dipolar-narrowed Carr-Purcell (DNCP) sequence.

The experiments were carried out on a spectrometer
described previously (112) and employed a microprocessor
based pulse sequencer which allows the experimenter to set
any pulse width or delay interval with a precision of 3 nano-
seconds. The seventeen pulse cycle time (= 24τ) was varied
between 72 microseconds and 480 microseconds and the ambient
temperature was 25°C. The spectrometer was carefully
adjusted so that the effects of instrumental artifacts were
minimized (25). With the same spectrometer, $T_{1\rho}$ for the
sample was also measured. The field strength was monitored
by determining the length of the 90° pulse for protons in a
liquid sample. This time was used to estimate the effective
field strength during the locking pulse.

Average Hamiltonian treatment of DNCP damping

It has been known that the limit of resolution of such
sequences as the WAHUHA-4 (21) and the MREV-8 should be
produced by spin-lattice relaxation similar to $T_{1\rho}$ processes
(120) in a carefully adjusted spectrometer (25). Recently,
Vega and Vaughan (121) have shown that the damping under the
MREV-8 sequence will be exponential after an initial
transient. For exponential correlations, the damping
constant for this decay, T_{1y}, is related to $T_{1\rho}$ as measured

with the usual spin-lock sequence. In this section we calculate the effect of motion in the DNCP sequence.

The spins attached to the reorienting segments of the polymer molecule are subject to several time dependent Hamiltonians, the time average values of which may not be zero. We consider here only the Hamiltonians corresponding to the dipolar chemical shift and rf field interactions:

$$H = H_D(t) + H_C(t) + H_{rf}(t) \tag{52}$$

where the $H_i(t)$ are given by Eqn. (6).

The chemical shift and dipolar Hamiltonians are time dependent because of molecular reorientation. One may formally separate out the static and time dependent parts of these two Hamiltonians:

$$H_D(t) = H_D^o + (H_D(t) - H_D^o) \tag{53}$$

$$H_C(t) = H_C^o + (H_C(t) - H_C^o) \tag{54}$$

and lump the time dependent parts into a general fluctuating term, $H_1(t)$ whose mean value averaged over time is zero:

$$H_1(t) = (H_D(t) - H_D^o) + (H_C(t) - H_C^o) \tag{55}$$

Hence, the total Hamiltonian has the form:

$$H = H_D^o + H_C^o + H_{rf}(t) + H_1(t) \tag{56}$$

The observable in the DNCP is the normalized signal:

$$S(t) = \frac{T\hbar I_y(t)I_y}{T\hbar I_y^2} \tag{57}$$

where

$$I_y(t) = U(t)I_y U^{-1}(t)$$

$$= U_{rf}(t)U_{int}(t)I_y U_{int}^{-1}(t)U_{rf}^{-1}(t) \tag{58}$$

For times, t, which are integral multiples of the rf cycle time, then,

$$I_y(t) = U_{int}(t)I_y U_{int}^{-1}(t) \tag{59}$$

Use of the Magnus expansion allows one to express the evolution operator as given by Eqn. (20) where the average internal Hamiltonians, through first order, are given by Eqns. (21) and (22).

Neglecting the average value of the time dependent fluctuation, the components of the zero order term, averaged over one rf cycle, are found from average Hamiltonian theory to be:

$$\overline{H}_D^{(0)} = 0 \tag{60}$$

$$\overline{H}_C^{(0)} = 0 \tag{61}$$

The fact that these terms are zero is in accord with the analogy suggested above between the Carr-Purcell experiment and the DNCP.

The first order terms among the static parts of the internal Hamiltonian need also to be considered. Applying the average Hamiltonian theory, these are evaluated to be:

$$\bar{H}_{DD}^{(1)} = 0 \tag{62}$$

$$\bar{H}_{CC}^{(1)} = 0 \tag{63}$$

$$\bar{H}_{DC}^{(1)} = 0 \tag{64}$$

Therefore, these first order static terms do not contribute to the damping of the magnetization. Assuming that the cross terms between H_1 and the static parts of H_{int} are negligible, the remaining first order terms are the autocorrelations of H_1. Thus, it would appear that terms of the form

$$\bar{H}_1^{(1)} = \frac{-i}{2t} \int_0^t dt' \int_0^{t'} dt'' [\tilde{H}_1(t'), \tilde{H}_1(t'')] \tag{65}$$

are responsible for the damping under the DNCP. Substitution into Eqn. (58) and then into Eqn. (57) produces a form for the signal, assuming that all higher order terms are negligible:

$$S(t) \cong T\hbar (e^{i\bar{H}_1^{(1)}t} I_y \, e^{-i\bar{H}_1^{(1)}t} I_y)/T\hbar I_y^2 \tag{66}$$

These are the terms whose effects have been previously calculated by Vega and Vaughan (121). These terms predict an exponential damping of the signal, the damping being

characterized by a time constant, T_{1y}:

$$S(t) = S(0)\exp(-t/T_{1y}) \tag{67}$$

and

$$\frac{1}{T_{1y}} = \frac{2}{3} \Delta m_2 \tau_c \{1 - \frac{1 - e + e^{-3\alpha} - e^{-4\alpha}}{2\alpha(1 + e^{-2\alpha} + e^{-4\alpha})}\} \tag{68}$$

where $\alpha = \dfrac{\tau}{\tau_c}$ and Δm_2 is the difference between the rigid

lattice and motionally averaged second moment.

Results

The results of a DNCP experiment performed on a poly-isoprene sample previously examined by the phase-altered MREV-8 method (106) are shown in Figure 51a. The total scan time on the oscilloscope trace is 197 milliseconds, the 17 pulse cycle time being 96 microseconds. In Figure 51b is shown for comparison the _off-resonance_ response of polyisoprene to a MREV-8 cycle. The scan time is the same as for Figure 51a, and the MREV-8 cycle time is matched to the 17 pulse cycle time. It is clear from comparison of Figure 51a with 51b that the DNCP sequence does suppress the chemical shift interaction, eliminating the beat pattern characteristic of the chemical shift between the two kinds of proton distinguishable (106) by multiple pulse NMR which is evident in 51b. The signal also persists longer and decays exponentially, following the initial transient behavior. To display the exponential behavior of the signal decay, the data for a DNCP experiment is plotted in Figure 52 on a semilogarithmic graph. The characteristic

Figure 51. a) Oscilloscope trace of the response to
a DNCP sequence from the polyisoprene sample.
Total scan time is 197 milliseconds. The
DNCP cycle time is 96 microseconds.

b) Time response to the REV-8 sequence from
the same polymer as in 2a). The scan time
is the same as in 2a. The decay was
monitored off-resonance. Note the beat
pattern, demonstrating the resolution of
two distinct types of protons in polyisoprene.
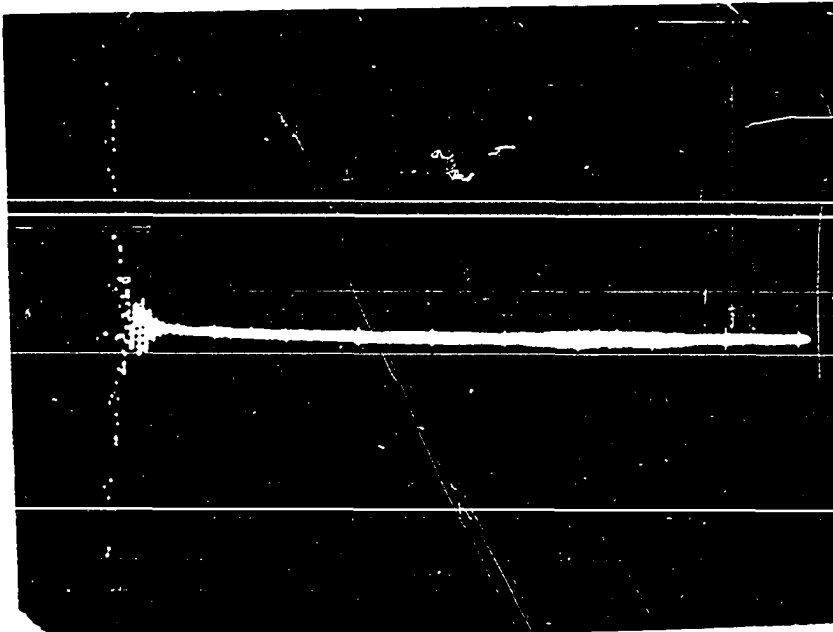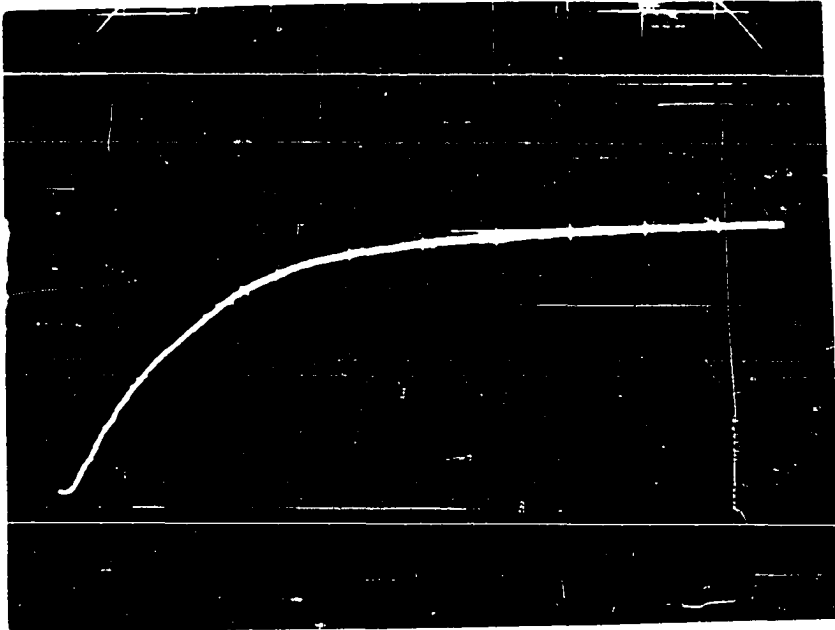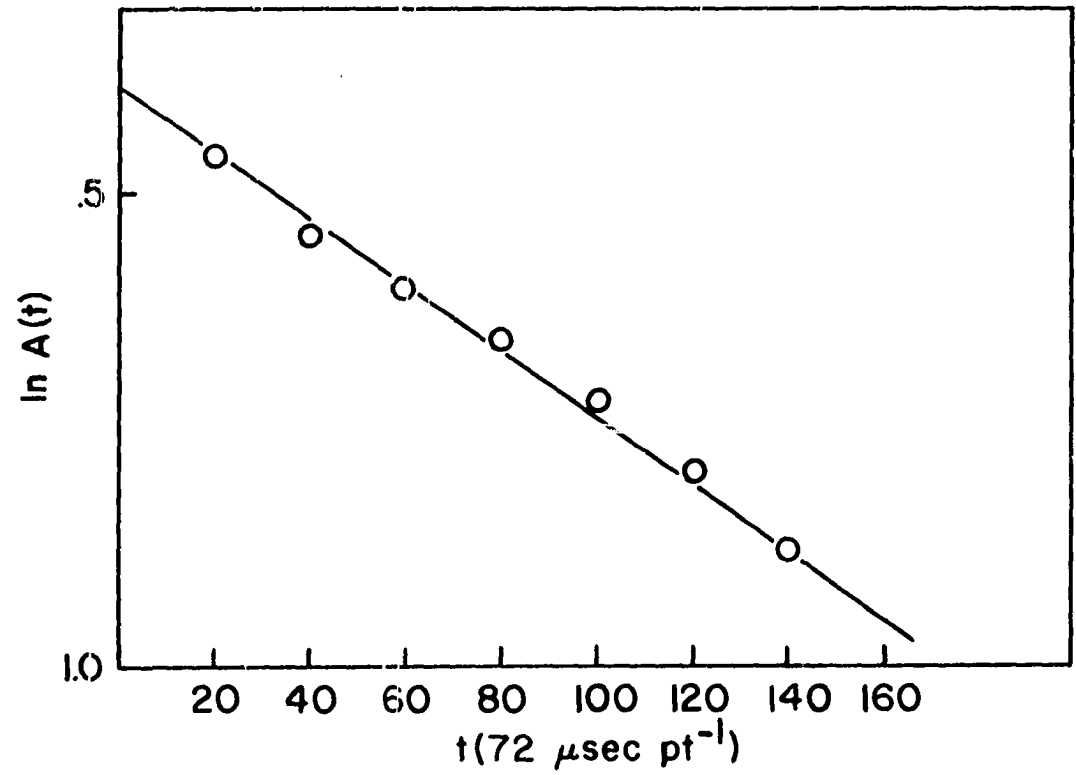
Figure 52. Semilogarithmic plot of the data from a DNCP experiment.

time constants, T_{1y}, for the polymer sample were determined from the slopes of such plots. We have measured T_{1y} as a function of the cycle time of the DNCP sequence (i.e., as a function of the pulse spacing, τ) and these results are displayed in Figure 53. It is clear that, for this polymer sample, the dependence of T_{1y} on τ is not simple.

It has been shown (117,120,121) that T_{1y} is related to the familiar $T_{1\rho}$, measured by the usual spin-lock procedure. In particular, Vega and Vaughan (121) give the following limiting expressions for T_{1y} if the motion is _exponentially_ correlated with correlation time, τ_C:

$$T_{1y}^{-1} = \frac{2}{3} \Delta M_2 \tau_C \qquad \text{(fast motion limit)} \qquad (69a)$$

$$T_{1y}^{-1} = \frac{5}{9} \Delta M_2 \tau^2 / \tau_C \qquad \text{(slow motion limit)} \qquad (69b)$$

where ΔM_2 is the difference between the rigid-lattice second moment and the motionally averaged residual second moment. Under the same assumptions, it can be shown that the spin-lock relaxation time depends on spin-lock amplitude as:

$$T_{1\rho}^{-1} = \Delta M_2 \tau_C \left\{ \frac{1}{1 + 4(\gamma H_1)^2 \tau_C^2} \right\} \qquad (70)$$

The inverse of the pulse spacing, τ^{-1}, plays a role in determining the DNCP damping constant, T_{1y}, similar to that which γH_1 does in the spin-lock sequence. If one, for example, compares the value of T_{1y} determined for a pulse spacing, τ, with the value of $T_{1\rho}$ from a spin-lock

Figure 53. T_{1y}^{-1} versus τ for the polymer at room temperature. $(T_{1y}^C)^{-1}$ is the predicted dependence for an exponentially correlated fluctuation. $\Delta\nu_{FID}$ for the polymer is shown above to indicate the extent of dipolar decoupling.
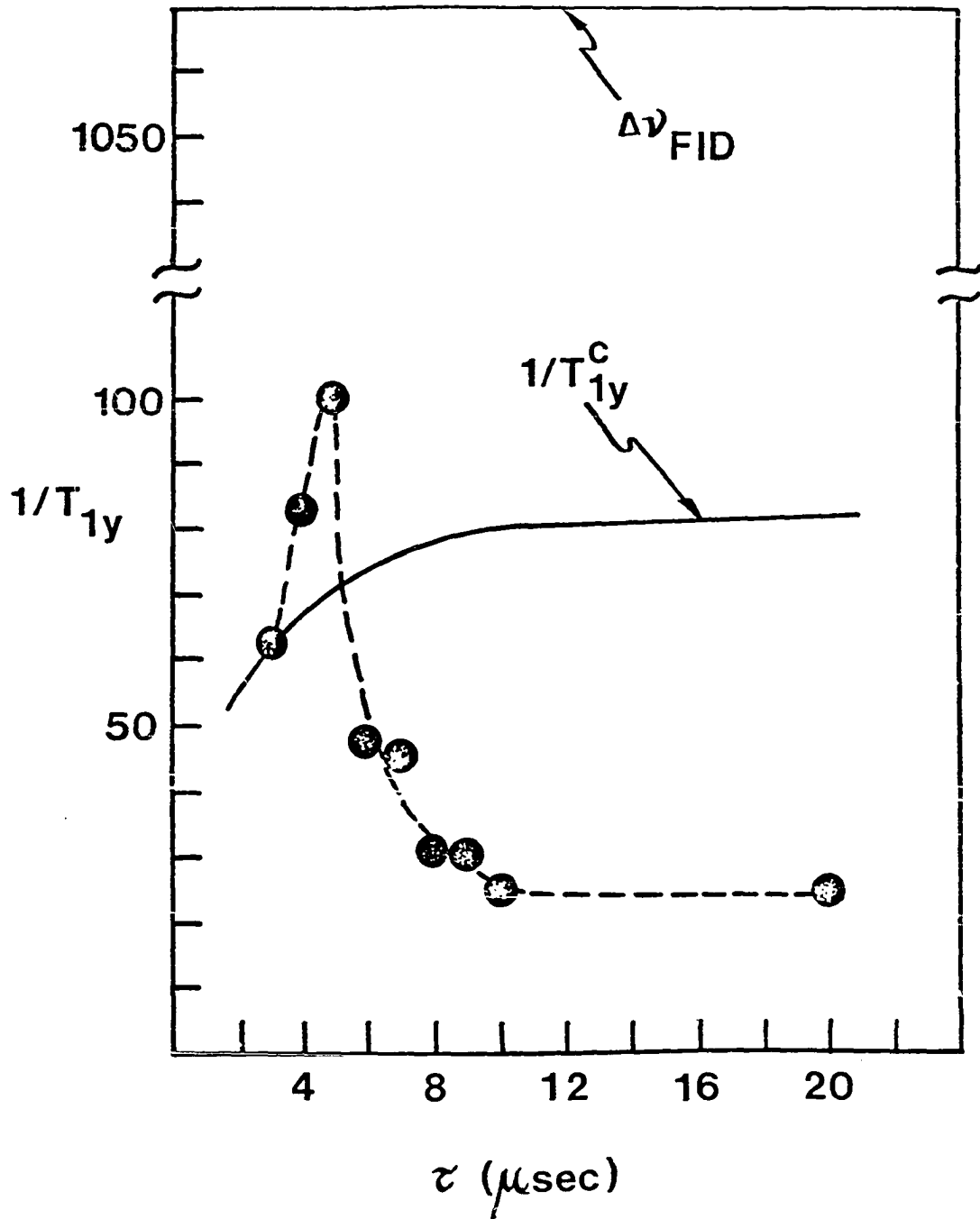
experiment with locking field, $H_1 = (\gamma\tau)^{-1}$, an estimate of the value of the ratio, $T_{1y}/T_{1\rho}$ can be made for that particular value of τ. In the extreme limits this ratio has the values

$$T_{1y}/T_{1\rho} = 9/20 \qquad \text{(slow motion limit)} \qquad \text{(71a)}$$

$$T_{1y}/T_{1\rho} = 3/2 \qquad \text{(fast motion limit)} \qquad \text{(71b)}$$

for exponential correlations. For a cycle time of 72.0 microseconds ($\tau = 3.0$ microseconds), the value of T_{1y} is 16.0±0.5 milliseconds. This pulse spacing corresponds to an effective spin-lock amplitude of 12.46 Gauss in a $T_{1\rho}$ experiment. For comparison we have measured $T_{1\rho}$ at this locking field strength and find it to be 16.0±0.8 milliseconds. Hence, within experimental error, the value of the ratio $T_{1y}/T_{1\rho}$ is 1.0. At these values we are neither in the fast nor the slow motion limit. Using the general relations (121) one can estimate the ratio of τ to τ_C. This ratio is approximately 1.95. Hence, if the exponential correlation model is valid for the polymer, the correlation time characterizing the motion producing the relaxation can be evaluated to be $\tau_C = 1.5$ microseconds. Whether the model is valid or not, it is clear that the experiment is sampling rather low frequency motions. We attribute this to non-localized motion of the polymer network as a whole. An additional observation in support of that view is that,

despite the fact that polyisoprene has protons in several

chemical and physical environments which can be observed in

the Fourier transform MREV-8 experiment, we see exponential

decay of the response to the DNCP sequence. The fact that

the MREV-8 suppresses the dipolar interaction, and thereby

spin diffusion, should result in a nonexponential decay if

the power spectra of the motions are different for the

different chemical and physical environments. One manner

in which the power spectra would be the same for all

physically and chemically distinct protons is if they

originate in motion of the polymer network as a whole. Then

all protons would have similar power spectra in this range.

The exponential mode. for the correlation function for

the motion producing damping of the DNCP signal is seen to

be too simple from the following considerations: knowing

the values of τ_C and ΔM_2 by the calculation above, one may

calculate, using Eqn. (77) of Reference (121), the values

of $1/T_{1y}$ for all values of the parameter τ. A plot of this

calculation is shown in Figure 53. Clearly this calculation

does not fit the experimental results. An interesting result

of this exercise is that, although the exponential

correlation model would predict that better resolution of

the MREV-8 spectrum will be achieved for shorter cycles, the

experiments indicate that there is an optimum range of cycle

time for resolution enhancement in the multiple pulse

experiment, which depends rather critically on the relaxation processes in the polymer, as suggested some time ago (120).

To understand the mechanism of relaxation in this polymer system, we must return to a consideration of the fundamentals of relaxation of spin systems. The multiple pulse experiments are sensitive to random modulation in the range of the inverse of the spacing between pulses (120). For these experiments, this time ranges from 3 microseconds to 20 microseconds. The dominant contributor to H_1 is dipolar correlations, the magnitude of the dipolar interaction being many times larger than that of the chemical shift. Hence, the fluctuations which are important in determining the lifetime, T_{1y}, are orientational correlations.

A calculation of the damping constant for the case in which H_1 is assumed to be dominated by the fluctuations of the dipolar Hamiltonian between 2 nearest neighbor protons gives

$$\frac{1}{T_{1y}} = \frac{9}{8} \frac{\gamma^4 h^2}{R^6} \sum_{n=1} J(n/\tau) a_n \tag{72}$$

where $J(\omega)$ is the frequency spectrum of the second order spherical harmonic:

$$J(\omega) = \int_{-\infty}^{+\infty} e^{-i\omega t} < (Y_{20}(t) - \overline{Y}_{20})(Y_{20}(0)$$

$$- \overline{Y}_{20}) > d\tau \tag{73}$$

and the a_n are factors characteristic of the sequence (120, 121). If one neglects all but the n=1 term, it is seen that $1/T_{1y}$ α $J(1/\tau)$. These same dynamic processes are sampled by other forms of spectroscopy; in particular mechanical retardation spectra (122) are sensitive to this overall network motion. A comparison of the retardation time spectra of polyisoprene (122) with the DNCP results shows that they both have maxima in the same region between τ = 1 µsec and τ = 10 µsec and have the same general dependence on frequency. This correspondence would seem to support our presumption that the DNCP measurements are sensitive to the longer range motions of the polymer network. A more comprehensive explanation would require one to model the dynamic processes in more detail and calculate the effect on T_{1y} via equation (68).

Conclusions

The utility of a technique for measuring low frequency relaxation in bulk elastomeric polymers has been demonstrated, which relies on the ability of multiple pulse cycles to remove simultaneously the effects of dipole-dipole broadening and chemical shift dispersion. Use of the cycle time dependence of the damping constant has allowed a measurement of the spectral density in the range 50-300 kHz. Based on the exponential character of the damping and comparison of the results with mechanical retardation

spectra of polyisoprene, we infer that the predominant character of the motion producing relaxation is nonlocal motion of the overall polymer network. We have borne out the prediction that substantial low frequency motion may in fact destroy the resolution of multiple pulse line narrowing experiments. However, by careful study of the resulting broadening of the spectrum, one may infer information on the type of motional processes present. The utility of the DNCP is not limited to the measurement of relaxation under the multiple pulse experiments. In principle it should be possible to synchronize the DNCP with bursts of magnetic field gradient (123) to allow the measurement of diffusion constants in ordered fluids in which the presence of dipolar interactions obviates the possibility of determining these parameters by the usual means (124,125).

BIBLIOGRAPHY

1. E. M. Purcell, H. C. Torrey and R. V. Pounds, Phys. Rev. 69, 37 (1946).

2. F. Bloch, W. W. Hansen and M. E. Packard, Phys. Rev. 69, 127 (1946).

3. W. G. Proctor and F. C. Yu, Phys. Rev. 81, 20 (1951).

4. J. T. Arnold, S. S. Dharmatti and M. E. Packard, J. Chem. Phys. 19, 507 (1951).

5. A. Abragam, _Principles of Nuclear Magnetism_ (Clarendon Press, Oxford, 1961).

6. See for example, J. W. Emsley, J. Feeney and L. H. Sutcliffe, _High Resolution Nuclear Magnetic Resonance Spectroscopy_ (pergamon Press, New York, 1965).

7. Charles P. Slichter, _Principles of Magnetic Resonance_ (Harper and Row, New York, 1963).

8. T. C. Farrar and E. D. Becker, _Pulse and Fourier Transform NMR_ (Academic Press, New York, 1971).

9. E. R. Andrew, A. Bradbury and R. G. Eades, Arch. Sci. (Geneva) 11, 223 (1958).

10. E. R. Andrew, A. Bradbury and R. G. Eades, Nature 182, 1659 (1958).

11. E. R. Andrew, Arch. Sci. (Geneva) 12, 103 (1959).

12. E. R. Andrew, A. Bradbury and R. G. Eades, Nature 183, 1802 (1959).

13. E. R. Andrew and R. G. Eades, Discuss. Faraday Soc. 34, 38 (1962).

14. E. R. Andrew and L. F. Furnell, Mol. Phys. 15, 157 (1968).

15. E. R. Andrew and V. T. Wynn, Proc. Roy. Soc. 291A, 257 (1966).

16. I. Lowe, Phys. Rev. Letters 2, 285 (1959).

17. B. Schnabel and T. Taplick, Phys. Letters <u>27A</u>, 310 (1968).

18. U. Haeterlen and J. S. Waugh, Phys. Rev. <u>175</u>, 453 (1968).

19. I. Lowe and R. E. Norberg, Phys. Rev. <u>107</u>, 46 (1957).

20. J. S. Waugh, C. H. Wang, L. M. Huber and R. L. Vold, J. Chem. Phys. <u>48</u>, 662 (1968).

21. J. S. Waugh, L. M. Huber and U. Haeberlen, Phys. Rev. Letters <u>20</u>, 180 (1968).

22. U. Haeberlen, J. D. Ellett, Jr. and J. S. Waugh, J. Chem. Phys. <u>55</u>, 53 (1971).

23. W.-K. Rhim, D. D. Elleman and R. W. Vaughan, J. Chem. Phys. <u>58</u>, 1772 (1973).

24. W.-K. Rhim, D. D. Elleman and R. W. Vaughan, J. Chem. Phys. <u>59</u>, 3740 (1973).

25. W.-K. Rhim, D. D. Elleman, L. B. Schreiber and R. W. Vaughan, J. Chem. Phys. <u>60</u>, 4595 (1974).

26. P. Mansfield, J. Phys. C. <u>4</u>, 1444 (1971).

27. P. Mansfield, M. J. Orchard, D. C. Stalker and K. H. B. Richards, Phys. Rev. B <u>7</u>, 90 (1973).

28. A. Pines, D. J. Ruben, S. Vega and M. Mehring, Phys. Rev. Letters <u>36</u>, 110 (1976).

29. S. Vega, T. W. Shattuck and A. Pines, Phys. Rev. Letters <u>37</u>, 43 (1976).

30. George C. Levy and Gordon L. Nelson, <u>Carbon-13 Nuclear Magnetic Resonance for Organic Chemists</u> (Wiley-Interscience, New York, 1972).

31. S. R. Hartman and E. L. Hahn, Phys. Rev. <u>128</u>, 2042 (1962).

32. D. A. McArthur, E. L. Hahn and R. Walstedt, Phys. Rev. <u>188</u>, 609 (1969).

33. E. P. Jones and S. R. Hartman, Phys. Rev. <u>36</u>, 757 (1972).

34. M. Mehring, A. Pines, W.-K. Rhim and W. S. Waugh, J. Chem. Phys. $\underline{54}$, 3239 (1971).

35. A. Carrington and A. D. McLachlan, Introduction to Magnetic Resonance (Harper and Row, New York, 1967).

36. L. R. Soules and R. M. Cotts, Phys. Rev. $\underline{111}$, 853 (1958).

37. A. Pines, M. G. Gibby and J. S. Waugh, J. Chem. Phys. $\underline{59}$, 569 (1973).

38. A. Pines, M. G. Gibby and J. S. Waugh, J. Chem. Phys. $\underline{56}$, 1776 (1972).

39. A. Pines, M. G. Gibby and J. S. Waugh, Phys. Letters $\underline{15}$, 569 (1973).

40. U. Haeberlen, High Resolution NMR in Solids. Selective Averaging (Academic Press, New York, 1976).

41. M. Mehring, "High Resolution NMR Spectroscopy in Solids", Vol. 11 of NMR Basic Principles and Progress Grundlagen and Fortschritte, edited by P. Diehl, E. Fluck and R. Kosfeld (Springer-Verlag, New York, 1976).

42. J. Schaefer, E. O. Stejskal and R. Buchdahl, Macromolecules $\underline{8}$, 291 (1975).

43. J. Schaefer and E. O. Stejskal, J. Am. Chem. Soc. $\underline{98}$, 1031 (1976).

44. J. Schaefer, E. O. Stejskal and R. Buchdahl, Macromolecules $\underline{10}$, 384 (1977).

45. H. L. Retcofsky and R. A. Friedel, Adv. Chem. Ser., NO. 55, 503 (1966).

46. H. L. Retcofsky and R. A. Friedel, Fuel $\underline{47}$, 391 (1968).

47. H. L. Retcofsky and R. A. Friedel, "Spectra of Coals and Coal Extracts: Proton Magnetic Resonance Spectra of Pyridine and Carbon Disulfide Extracts" in Spectroscopy of Fuels, edited by R. A. Friedel (Plenum Press, New York, 1970) Chap. 6, p. 70.

48. J. K. Brown, W. R. Ladner and N. Sheppard, Fuel $\underline{39}$, 79 (1960).

49. J. K. Brown and W. R. Ladner, Fuel <u>39</u>, 87 (1960).

50. W. R. Ladner and A. E. Stacey, Fuel <u>40</u>, 295 (1961).

51. J. F. M. Oth and H. Tschamler, Fuel <u>42</u>, 467 (1963).

52. R. A. Durie, Y. Schlwchyk and S. Sternhill, Fuel <u>45</u>, 99 (1966).

53. H. L. Retcofsky and R. A. Friedel, Fuel <u>55</u>, 363 (1976).

54. H. L. Retcofsky and R. A. Friedel, J. Phys. Chem. <u>77</u>, 68 (1973).

55. F. K. Schweighardt, R. A. Friedel and H. L. Retcofsky, Applied Spectroscopy <u>30</u>, 291 (1976).

56. H. L. Retcofsky, F. K. Schweighardt and M. Hough, Anal. Chem. <u>49</u>, 585 (1977).

57. Victor Bartuska, Gary E. Maciel, Jacob Schaefer and Edward O. Stejskal, Fuel <u>56</u>, 353 (1977).

58. H. L. Retcofsky, Applied Spectroscopy <u>31</u>, 116 (1977).

59. David L. Vanderhart and H. L. Retcofsky, Fuel <u>55</u>, 202 (1977).

60. H. L. Retcofsky, paper presented at the Institute of Scientific Problems Relevant to Coal Utilization, May 1977.

61. F. A. Bovey, <u>Nuclear Magnetic Resonance Spectroscopy</u> (Academic Press, New York, 1969).

62. F. A. Bovey, <u>High Resolution NMR of Macromolecules</u> (Academic Press, New York, 1972).

63. I. Ya. Slonim and A. N. Lyubimov, <u>The NMR of Polymers</u> (Plenum Press, New York, 1970).

64. E. Hunter and W. G. Oaks, Trans. Faraday Soc. <u>41</u>, 49 (1945).

65. H. C. Haines, R. B. Richards and H. Byer, Trans. Faraday Soc. <u>41</u>, 56 (1945).

66. J. B. Nichols, J. Appl. Phys. <u>25</u>, 840 (1954).

67. W. P. Slichter, J. Appl. Phys. <u>31</u>, 1865 (1966).

68. D. W. McCall and W. P. Slichter, J. Polym. Sci. 26, 171 (1957).

69. C. W. Wilson and G. E. Pake, J. Polym. Sci. 10, 503 (1953).

70. F. Bloch, Phys. Rev. 70, 460 (1946).

71. F. Bloch, W. W. Hansen and M. Packard, Phys. Rev. 70, 474 (1946).

72. D. Barnall and I. J. Lowe, Phys. Rev. Letters 11, 258 (1963).

73. D. E. Barnaal and I. J. Lowe, Phys. Rev. 148, 328 (1966).

74. E. R. Andrew, Progress in Nuclear Magnetic Resonance, Vol. 8, edited by J. W. Emsley, J. Feeney and L. H. Sutcliffe (Pergamon Press, New York, 1971), p. 1.

75. B. C. Gerstein and C. R. Dybowski, An Introduction to the Theory and Practice of Pulse Techniques in Nuclear Magnetic Resonance (in preparation).

76. W. A. B. Evans and J. G. Powles, Proc. Phys. Soc. London 93, 1046 (1967).

77. a) W. Magnus, Commun. Pure Appl. Math 7, 649 (1954); b) R. M. Wilcox, J. Math. Phys. 8, 962 (1967).

78. M. Mehring, R. G. Griffin and J. S. Waugh, J. Chem. Phys. 58, 746 (1971).

79. L. M. Ryan, R. C. Wilson and B. C. Gerstein, J. Chem. Phys. 67, 4310 (1977).

80. L. M. Ryan, R. C. Wilson and B. C. Gerstein, Chem. Phys. Letters 52, 341 (1977).

81. S. R. Hartman and E. P. Jones, Phys. Rev. 36, 757 (1972).

82. C. P. Slichter and W. C. Holton, Phys. Rev. 122, 1701 (1961).

83. M. Goldman, Spin Temperature and Nuclear Magnetic Resonance in Solids (Oxford University Press, London, 1961).

84. I. Solomon, C. R. Acad. Sci. Paris <u>248</u>, 92 (1959).

85. J. Jeener, R. DuBois and P. Broekaert, Phys. Rev. <u>139A</u>, 1959 (1965).

86. J. Jeener and P. Broekaert, Phys. Rev. <u>157</u>, 232 (1967).

87. A. G. Anderson and S. R. Hartmann, Phys. Rev. <u>128</u>, 2023 (1960).

88. J. D. Ellett, Jr., M. G. Gibby, U. Haeberlen, L. M. Huber, M. Nehring, A. Pines and J. S. Waugh, Advan. Magnetic Resonance <u>5</u>, 117 (1971).

89. R. W. Vaughan, D. D. Elleman, L. M. Stacey, W.-K. Rhim and J. W. Lee, Rev. Sci. Instrum. <u>43</u>, 1356 (1972).

90. Radio Amateur's Handbook (The American Radio Relay League Inc., Newington, CT, 1972), p. 49.

91. R. G. Pembleton, R. C. Wilson and B. C. Gerstein, J. Chem. Phys. <u>66</u>, 5133 (1977).

92. E. R. Andrew, L. F. Fornell, M. Firth, T. D. Gledhill and I. Roberts, J. Mag. Res. <u>1</u>, 27 (1969).

93. B. C. Gerstein, R. G. Pembleton, R. C. Wilson and L. M. Ryan, J. Chem. Phys. <u>66</u>, 361 (1977).

94. A. Pines, J. J. Chang and R. G. Griffin, J. Chem. Phys. <u>61</u>, 1021 (1974).

95. M. E. Stoll, A. J. Vega and R. W. Vaughan, Rev. Sci. Instrum. <u>48</u>, 800 (1977).

96. P. Murphy, IS-4310, Ames Laboratory, Ames, Iowa.

97. E. O. Stejskal and J. Schaefer, J. Mag. Res. <u>18</u>, 560 (1975).

98. B. C. Gerstein and R. G. Pembleton, Anal. Chem. <u>49</u>, 75 (1977).

99. The f_{XTL} from density and heat of fusion were determined by A. F. Burmester of Dow Chemical Co., Midland, MI.

100. Z. Mencik, J. Pol. Sci., Polym. Phys. Ed. <u>11</u>, 1585 (1973).

101. G. U. D. Tiers and F. A. Bovey, J. Polym. Sci. Part A 1, 833 (1963).

102. E. Lippma, M. Alla and T. Tuhern, paper presented at the 19th Congress ampere, Heidelberg, September, 1976.

103. E. O. Stejskal, Jacob Schaefer and R. A. McKay, J. Mag. Res. 25, 569 (1977).

104. J. S. Waugh and Matti Maricq, Chem. Phys. Letters 47, 327 (1977).

105. S. Meiboom and D. Gill, Rev. Sci. Instrum. 29, 688 (1958).

106. C. R. Dybowski and R. W. Vaughan, Macromolecules 8, 50 (1975).

107. M. Bishop and D. L. Ward, Fuel (London) 37, 191 (1950).

108. ESR measurements were carried out by Dr. R. C. Wilson.

109. H. L. Retcofsky, J. M. Start and R. A. Friedel, Anal. Chem. 40, 1966 (1968).

110. R. Greer, Working Paper No. 4, Iowa Coal Project, Documents Library, Ames Laboratory-ERDA, Iowa State University, Ames, Iowa.

111. L. B. Schreiber and R. W. Vaughan, J. Catal. 40, 226 (1975).

112. B. C. Gerstein, C. Chow, R. G. Pembleton and R. C. Wilson, J. Phys. Chem. 81, 565 (1977).

113. Dr. C. R. Dybowski, private communication.

114. D. L. Vanderhart, private communication.

115. D. McCall, Acc. Chem. Res. 4, 223 (1971).

116. a) E. Ostroff and J. Waugh, Phys. Rev. Letters 16, 1097 (1966); b) P. Mansfield and D. Ware, Phys. Letters 22, 133 (1966).

117. W. Gruender, D. Freude and H. Schmiedel, Ann. Physik 7, 409 (1971).

118. W. Rhim, D. Burum and D. Elleman, Phys. Rev. Letters 37, 1764 (1976).

119. H. Carr and E. Purcell, Phys. Rev. $\underline{94}$, 630 (1954).

120. U. Haeberlen and J. Waugh, Phys. Rev. $\underline{185}$, 420 (1969).

121. A. Vega and R. Vaughan, J. Chem. Phys. $\underline{68}$, 1958 (1978).

122. a) F. Bueche, Physical Properties of Polymers (Wiley, New York, 1962); b) A. P. Payne, in The Rheology of Elastomers, edited by P. Mason and N. Wookey (Pergamon, New York, 1958).

123. E. Stejskal and J. Tanner, J. Chem. Phys. $\underline{42}$, 288 (1965).

124. R. Blinc, J. Pirs and I. Zupancic, Phys. Rev. Letters $\underline{30}$, 546 (1973).

125. a) E. Samulski, B. Smith and C. Wade, Chem. Phys. Letters $\underline{20}$, 167 (1973); b) S. Roeder, E. Burnell, A. Kuo and C. Wade, J. Chem. Phys. $\underline{64}$, 1848 (1976).

ACKNOWLEDGEMENTS

APPENDIX. THE DIPOLAR HAMILTONIAN

IN THE CRAMPS FRAME

To determine the effect combined "magic angle" spinning-multiple pulse has on the time development of a spin system a time dependent form of H_D^{II} must be considered. This time dependence is built into the spacial part, $(3 \cos^2\theta_{ij}-1)$, and is given by Eqn. (21). It is the purpose of this Appendix to develop the time dependent term, $b_{ij}(t)$.

The "sample spinning" coordinate system (c.s.), X',Y', Z' is related to the lab c.s., X,Y,Z, by a negative rotation about the Y axis by an angle γ. At any time, t, $\theta(t)$ is described by

$$\cos \theta_{ij}(t) = \hat{k} \cdot \frac{\bar{r}_{ij}}{|r_{ij}|} \tag{1}$$

The unit vector $\hat{k}$ in the primed c.s. is

$$\hat{k} = \hat{k}^i \cos\gamma + i^i \sin\gamma \tag{2}$$

and

$$\frac{\bar{r}_{ij}}{|r_{ij}|} = \frac{x'(t)\hat{i} + y'(t)\hat{j} + z'(t)\hat{k}'}{|r_{ij}|} \tag{3}$$

In the primed c.s. a rotation about Z' by an angle $\omega_r t$ will correspond to the transformation.

$$\begin{pmatrix} X'(t) \\ Y'(t) \\ Z'(t) \end{pmatrix} = \begin{pmatrix} \cos \omega_r t & - \sin \omega_r t & 0 \\ \sin \omega_r t & \cos \omega_r t & 0 \\ 0 & 0 & 1 \end{pmatrix} \begin{pmatrix} X'(o) \\ Y'(o) \\ Z'(o) \end{pmatrix} \tag{4}$$

Substituting Eqn. (2-4) into Eqn. (1) where we consider just one pair of spins

$$\cos\theta(t) = \frac{Z'(o)\cos\gamma}{|r|} + \frac{\sin\gamma}{|r|} (X'(o)\cos\omega_r t$$

$$- Y'(o)\sin\omega_r t) \qquad (5)$$

Expressing the primed c.s. in terms of polar coordinates Eqn. (5) becomes

$$\cos\theta(t) = \cos\gamma\cos\alpha + \sin\gamma\sin\alpha\cos(\omega_r t + \beta) \qquad (6)$$

where α and β are the angles relating $\bar{r}$ to the primed system at t=0. For $\gamma = \tan^{-1}\sqrt{2}$, e.g., the "magic angle"

$$\cos\theta(t) = \frac{\cos\alpha}{\sqrt{3}} + \frac{\sqrt{2}}{3} \sin\alpha\cos(\beta + \omega_r t) \qquad (7)$$

With Eqn. (7) we obtain the time dependent form of $(3\cos^2\theta(t) - 1)$ as

$$b(t) = (3\cos\theta_{ij}(t)-1) = \sqrt{2} \sin2\alpha \cos(\beta+\omega_r t)$$

$$+ \sin^2\alpha\cos2(\beta+\omega_r t) \qquad (8)$$

This may be written in a form more amiable for calculations using

$$\cos(A+B) = \cos A\cos B - \sin A\sin B \qquad (9)$$

as

$$b(t) = A\cos\omega_r t - B\sin\omega_r t + C\cos2\omega_r t - D\sin2\omega_r t \qquad (10)$$

where

$$A = \sqrt{2}\ \sin2\alpha\cos\beta$$

$$B = \sqrt{2}\ \sin2\alpha\sin\beta$$

$$C = \sin^2\alpha\cos2\beta \qquad\qquad (11)$$

$$D = \sin^2\alpha\sin2\beta$$